

# Improvement of stability and speed in liquid-environment atomic force microscopy

メタデータ	言語: eng 出版者: 公開日: 2017-10-05 キーワード (Ja): キーワード (En): 作成者: メールアドレス: 所属:
URL	<a href="http://hdl.handle.net/2297/42380">http://hdl.handle.net/2297/42380</a>

This work is licensed under a Creative Commons Attribution-NonCommercial-ShareAlike 3.0 International License.



Dissertation

**Improvement of stability and speed in liquid-environment atomic  
force microscopy**

Graduate School of  
Natural Science & Technology  
Kanazawa University

Division of Electrical Engineering and Computer Science

Student ID Number: 1223112001

Name: Akrami Seyed Mohammad Reza

Chief advisor: Prof. Takeshi Fukuma

January 9<sup>th</sup>, 2015

# Contents

<b>1</b>	<b>Introduction</b>	<b>2</b>
1.1	General remarks . . . . .	2
1.2	High-speed AFM . . . . .	3
1.3	Purpose . . . . .	4
1.4	Structure of Thesis . . . . .	5
<b>2</b>	<b>Atomic force microscopy</b>	<b>8</b>
2.1	Scanning Electron Microscopy (SEM) . . . . .	8
2.2	Transmission electron microscopy (TEM) . . . . .	9
2.3	Scanning tunneling microscopy (STM) . . . . .	10
2.4	Atomic force microscopy (AFM) . . . . .	11
2.4.1	Review of literature . . . . .	11
2.4.2	Roll of AFM in Nanotechnology . . . . .	12
2.4.3	Atomic Force Microscopy components . . . . .	13
2.5	Cantilever Equations . . . . .	14
2.6	Tip-sample interaction force . . . . .	19
2.7	Force curve measurement . . . . .	23
2.8	AFM operating modes . . . . .	24
2.8.1	Contact mode . . . . .	25
2.8.2	Semi contact or tapping mode . . . . .	27
2.8.3	Non contact mode . . . . .	28
2.8.4	Lateral force microscopy (LFM) . . . . .	29
2.9	Frequency modulation (FM-AFM) . . . . .	29
2.10	Amplitude modulation (AM-AFM) . . . . .	30
<b>3</b>	<b>High-speed Z tip scanner for atomic-resolution atomic force microscopy</b>	<b>33</b>
3.1	Introduction . . . . .	33
3.2	Screw type Z tip scanner . . . . .	34
3.2.1	Basic Designs . . . . .	34
3.2.2	Effect of using Sic and SUS316 as a different material on performance of Z tip scanner . . . . .	35
3.2.3	Triangular shape stage . . . . .	36
3.2.4	Calibration of the inputs data in COMSOL software . . . . .	36
3.2.5	Preparation of Phosphate Buffer Saline(PBS) . . . . .	38
3.2.6	Experimental details . . . . .	39
3.2.7	Results and Discussion . . . . .	40

3.3	Counterbalance Z tip scanner . . . . .	46
3.3.1	Basic design . . . . .	46
3.3.2	Experimental detail . . . . .	46
3.3.3	Simulation of Counterbalance Z tip scanner . . . . .	46
3.3.4	Effect of changing the plate thickness on the performance of the counterbalance structure . . . . .	47
3.3.5	Effect of changing the type of piezo on the performance of the counterbalance structure . . . . .	49
3.3.6	Effect of changing the piezo position on the performance of the counterbalance structure . . . . .	49
3.3.7	Asymmetric actuating system . . . . .	49
3.4	Summary . . . . .	53
<b>4</b>	<b>Capacitive sensor</b>	<b>58</b>
4.1	Introduction . . . . .	58
4.2	Theory . . . . .	59
4.3	Experiment . . . . .	63
<b>5</b>	<b>Stability and reproducibility improvement of atomic force microscopy in liquid</b>	<b>71</b>
5.1	Introduction . . . . .	71
5.2	Experimental details . . . . .	73
5.2.1	Tip treatment methods . . . . .	73
5.2.2	AFM measurements . . . . .	74
5.2.3	Other evaluation methods . . . . .	74
5.3	Results and Discussions . . . . .	75
5.3.1	SEM imaging . . . . .	75
5.3.2	Atomic-resolution imaging . . . . .	76
5.3.3	$\Delta f$ curve measurements . . . . .	77
5.3.4	Origin of the fouling resistance . . . . .	83
5.3.5	Origin of the improved stability and reproducibility . . . . .	84
5.4	Summary . . . . .	88
<b>6</b>	<b>Conclusions</b>	<b>93</b>

# Chapter 1

## Introduction

### 1.1 General remarks

There are fictional stories about amazing electro mechanical products in micro or nano scale. The nature surrounds us consists of atoms. Different combinations of these atoms create molecules. Each of them has a specific chemical and physical property. These molecules bond to each other with attractive or repulsive forces caused different physical phase like solid, liquid and gas. These molecular interaction forces kept the materials steady, known as van der waals force which is playing the major role in nanotechnology. The fantasy of engineering in nano scale or atomic level made the scientists to discover molecular space conditions. The physical and mechanical characteristics in nano space must be investigated. This new field of science requires precise metrology, positioning and microscopy methods in atomic scale level. Human being always wanted to see small features as deep as perceivable. Invention of optical microscope by van Leeuwenhoek in 17<sup>th</sup> century opened new criteria of knowledge. First optical microscope was a simple hand held glass lens made of silver or copper.<sup>1,2</sup> Optical high school microscopes which are familiar to all of us can magnify objects around one micron like red blood cells ( $7 \mu\text{m}$ ). Investigating far through features progressed ceaselessly to obtain more resolution and visibility. Microscopy is categorized in three main branches known as optical, charged particle (electron and ion) and scanning probe microscopy. Optical and charged particle microscopy, as their name proposed, collect data from specimen by diffracting, reflecting, and refraction of electromagnetic wave or electron/ion with sample surface while the scanning probe microscopy investigates by different interaction of scanning probe and sample surface. Scanning probe microscope includes the technologies provides high resolution imaging for not only quantitative measurements but also physical and chemical properties at the nano scale level.<sup>3,4</sup> This microscopy particularly provides sample morphology so it is playing a main role in

thin film physics, nanometrology or any structural base science. The SPM scanning developments provide dominant achievements in different fields of science and engineering. The system instrumentation based on a quit sharp tip (about 10 nm) mounted on a flexible cantilever travels across the sample surface. During tip moving over the sample, the intermolecular forces between them effects on cantilever deflection. These influenced movements could be detected by various sensors. According to interaction types this microscopy includes three main methods. Atomic force microscopy (AFM),<sup>8</sup> scanning tunneling microscopy (STM) and near field scanning optical microscopy operated based on molecular interaction force, weak electrical current flow and tiny light source respectively. For many SPM scanners like AFM and MFM, the cantilever and integrated probe are made by acid etching of silicon nitride ( $\text{Si}_3\text{N}_4$ ).<sup>6</sup> There are many different types of SPMs operated based on various physical quantitative like magnetic, electrostatic, electrical capacitance, optical and thermal creates different set ups. Each instrument could be operated in all three modes of contact, noncontact and semi-contact.

## 1.2 High-speed AFM

Clearly the slow scanning speed of a conventional AFM around minutes per frame limits the dynamic visualization of macromolecules behavior. Scanning individual biological cell and its behavior in buffered solution of ions in physiological concentrations could be mentioned as a good example in this case.<sup>7,8</sup> This ability persuade us to expand this imaging to record dynamic behavior of such molecules. Practically only slow processes could be recorded by commercial AFMs however the amazing biological interactions occur at higher rate.<sup>9-11</sup> The suitable imaging mode for biological samples is tapping mode because the cantilever oscillates near its resonance frequency decreases lateral force between tip-sample.<sup>12</sup> There are several limitations such as force sensor response time, macromolecules dynamic behavior and feedback loop bandwidth controlling the tip sample interaction force and data acquisition rate of system. By enhancing the mechanical design of the AFM and applying smaller and faster force sensors, speed up imaging is not seems difficult.<sup>13</sup> To develop the image bandwidth the feedback loop elements should be optimized. One of the main parts of this loop is cantilever. A high resonance frequency is needed to provide high tapping frequency and also needed a low spring constant to reduce tip-sample interaction forces. These two conflicted conditions are satisfied only with small cantilevers.<sup>14,15</sup> Another part of this loop must have a wide bandwidth is z scanner made of piezo actuator with high resonance frequency .

Biological AFMs scanning rate improved in recent years. The main parameter in

this case is disturbance and aggressiveness reduction while the probe faces the sample. Ando developed the data acquisition rate significantly to more than 10 frames per seconds for scan area of  $240 \times 240 \text{ nm}^2$  with  $100 \times 100$  pixels.<sup>2</sup> By novel High-speed AFM methods, dynamic behavior and structural altering of macromolecules like proteins have been visualized. For example DNA targeting enzymes procedure, nucleosome and DNA structural altering have been achieved also. As a literature it could be mentioned that Vaint et al have applied the small cantilevers and resonance frequencies around 150 KHz to image DNA and GroELGroES complexes on mica, in liquid.<sup>17,18</sup> Sulchek et al applied a type of cantilever with an integrated zinc oxide piezo actuator resulted an imaging bandwidth of 38 kHz and frame rate of 4/sec.<sup>19,20</sup>

These days this is the only technique with sub second time frame and nano meter resolution to single molecule tracing in macromolecules dynamics. Currently high-speed type of AFM consists of a held z piezo scanner and a movable sample along vertical axis to control a constant force in x-y scanning plane. The main disadvantage of these systems is their small sample stage which is necessary for high resonance frequency. This property limits the sample size for visualization purpose.

### 1.3 Purpose

There are some potential research area in AFM, in which we can classify in 3 groups. First group is new technologies that cover 3D-AFM and surface potential measurements. Second group is improvement of performance including the high-speed AFM , high sensitivity and mechanical design of AFM. The last group covers applications of AFM in biology , chemistry, industry and so on. Our aim through this research is to improve the mechanical design of AFM. In ordet to do,I will focus on improving accuracy , usability and stability of AFM. During this study , we try to introduce new designs for advancing the imaging speed. We introduced two type of precisely machined plate with screw holding mechanism Ztip scanner and its performance by imaging of the calcite crystal. In addition, counterbalance Z tip scanner with two arrangement and those performance and effect of them on the imaging speed was admitted. The affect of improvement explained in detail in chapter 3. There are three parameters that affect the accuracy of scanner. First of all Non-linearity of our system;second, Hysteresis phenomena, and the last one is creeping. To solving this problems,we have to use closed loop feedback controller. Although there are several types of closed loop feedback controller, but we want to use capacitive detection system. In recent years, one of the main major improvements of Atomic force microscopy in aqueous environments have been achieving of high atomic scale resolution in various interfacial phenomena studies. During this analysis, instabil-

ities and poor data reproducibility made systematic studies impossible. To solve this problem, the effect of various tip treatment methods for atomic scale imaging and force measurements in liquid environments is investigated during the following research. The tested methods, examined in Si coating, Ar plasma, Ar sputtering and UV/O<sub>3</sub> cleaning tips. The experiments demonstrated that, all of these methods provide remarkable progress in both the imaging and force measurements even though the tip is transferred through the air.

## 1.4 Structure of Thesis

This study is organized in 6 chapters which can be description shortly as follows: In chapter 1, we provide brief explanation of the general remarks, purpose and structure of the thesis. In this part, importance of high demand in nanotechnology shall be presented. Moreover, I carry out improvement of the previous research in AFM in some main aspects.

Chapter 2 deals with the fundamental methods and instrumentation of scanning probe microscopy. In this chapter AFM component and its related issues is described. In addition, tip-sample interaction force, force distance curve and AFM operating modes will be admitted.

In chapter 3,  $Z$  tip scanner for high-speed atomic force microscopy is introduced. High-speed scanner has much attention due to its unique capability of visualizing nanoscale dynamic processes at a solid/liquid interface. I introduce high-speed  $Z$  tip scanner with screw holding mechanism and counterbalance structure  $Z$  tip scanner. By using both of them the usability of the AFM system is improved.

Chapter 4 is related to the capacitance sensor. As described in previous section, accuracy of the AFM system has very important role in the performance of imaging. So, in this chapter we develop the capacitance sensor as a displacement sensor.

In Chapter 5, we discuss achieving high atomic scale resolution in various interfacial phenomena studies as one of the main major improvements of Atomic force microscopy in aqueous environments. During this analysis, the effect of various tip treatment methods for atomic scale imaging and force measurements in liquid environments have been investigated.

In Chapter 6, conclusions and some suggestions for future work are presented.

# Bibliography

- [1] Brian J. Ford *From Dilettante to Diligent Experimenter: a Reappraisal of Leeuwenhoek as microscopist and investigator*, 1992.
- [2] Leeuwenhoek V. *How he made his tiny microscopes*, 2013.
- [3] Meyer E, Hug H J, Bennewitz R *Scanning probe microscopy: the lab on a tip*, 2003.
- [4] Weisendanger R *Scanning probe microscopy and spectroscopy: methods and applications*, 1994.
- [5] Binnig G, Quate C F, Gerber C. *Phys Rev Lett.*, 1986;56:930933.
- [6] Akamine, S.; Barrett, R. C. and Quate, C. F. *Improved atomic force microscope images using microcantilevers with sharp tips*, Applied Physics Letters 57, 1990.
- [7] Drake B, Prater C B, Weisenhorn A L, Gould S A, Albrecht T R, Quate C F, Cannell D S, Hansma H G, Hansma P K. *Science.*, 1989;243:15861589.
- [8] Bustamante C, Rivetti C, Keller D J. *Curr Opin Struct Biol.*, 1997;7:709716.
- [9] Guthold M, Bezanilla M, Eire D A, Jenkins B, Hansma H G, Bustamante C. *Proc Natl Acad Sci USA.*, 1994;91:1292712931.
- [10] Kassas S, Thomson N H, Smith B L, Hansma H G, Zhu X, Guthold M, Bustamante C, Kool E T, Kashlev M, Hansma P K. *Biochemistry*, 1997;36:461468.
- [11] Oberleithner H, Schneider S, Bustamante J-O. Pflgers *Arch Eur J Physiol.*, 1996;432:839844.
- [12] Sulchek T, Hsieh R, Adams J D, Minne S C, Quate C F, Adderton D M. *Rev Sci Instrum.*, 2000;71:20972009
- [13] G. Schitter . *Design and Modeling of a High-Speed AFM-Scanner.*, Member, IEEE, 2007.

- [14] Schffer T E, Viani M, Walters D A, Drake B, Runge E K, Cleveland J P, Wendman M A, Hansma P K. *Proc SPIE.*, 1997;3009:4852.
- [15] Walters D A, Viani M, Paloczi G T, Schffer T E, Cleveland J P, Wendman M A, Gurley G, Elings V, Hansma P K. *Proc SPIE.*, 3009:4347, 1999.
- [16] T. Ando, N. Kodera, E. Takai, D. Maruyama, K. Saito, and A. Toda. *Proc. Natl. Acad. Sci. USA*, 98:12468, 2001.
- [17] Viani M B, Schffer T E, Paloczi G T, Pietrasanta L I, Smith B L, Thompson J B, Richter M, Rief M, Gaub H E, Plaxco K W *Rev Sci Instrum.*, 70:43004303, 1999.
- [18] Viani M B, Pietrasanta L I, Thompson J B, Chand A, Gebeshuber I C, Kindt J H, Richter M, Hansma H G, Hansma P K. *Nat Struct Biol.*,7:644647, 2000.
- [19] Sulchek T, Hsieh R, Adams J D, Minne S C, Quate C F, Adderton D M. *Rev Sci Instrum.*, 71:20972009,2000.
- [20] Minne S C, Manalis S R, Quate C F. *Appl Phys Lett.*, 67:39183920, 1995.

# Chapter 2

## Atomic force microscopy

### 2.1 Scanning Electron Microscopy (SEM)

Scanning Electron Microscopy (SEM) is a scanning topography method that investigates the sample with high energy focused electron beam at the surface of solid specimen. These primary electrons excited target surface atom electrons. By these interactions secondary electrons produced and emitted through the surface. These electron bombardments continue all over the sample. Reflected and diffracted electrons involved surface topography data. Scattered electrons (secondary electrons, back-scattered electrons and X-ray) was collected in cathode to amplify and evaluate. This signal examination ends in the creation of high quality image. Particularly SEM image provided the magnification over range of 10 to 400,000 times. Resolution of SEM, in contrary of optical microscopy, did not depend on objective lenses power. Its the function of residual magnetic fields in scan coils and distance between the target and the lens. Schematic of this instrument is shown in Figure 2.1. The particular resolution of SEM depends on electron wave length produced in through scanning. According to instrument type, resolution of system varies between 1 nm and 20 nm. Focused dept increases remarkable in SEM scanning rather than optical microscopy.<sup>1</sup> Comparison of these two is presented in table 2.1.

SEM image achieves sample topography, texture morphology, roughness measurement, physical dimensions and corrosion measurement. Scanning electron microscopy has the ability of imaging electrical conductive samples. So to scanning insulating materials, like biological features, the sample must be coated with electrical conductive thin film. These presses could be done in chemical vapor deposition of metals such as: gold (Au), platinum (Pt), Osmium (Os), iridium (Ir), tungsten (W) and chromium (Cr).<sup>2</sup>

Typical SEM scans the sample under vacuum conditions. So the sample which sublimate easily is not proper for this scanning because gaseous molecules may react

Table 2.1: Comparison dept of focused in optical and SEM microscopy

Image magnification	Depth of focused	
	Optical	SEM
10	60 $\mu\text{m}$	1000 $\mu\text{m}$
100	8 $\mu\text{m}$	100 $\mu\text{m}$
1000	0.2 $\mu\text{m}$	10 $\mu\text{m}$
10000	—	1 $\mu\text{m}$

with scattered electrons. SEM can supply 2D image of samples analyzed by computer. A particular way of obtaining higher resolution is to use focused ion beam (FIB) instead of electrons. These ions produced two to eight secondary electrons through these interactions. These extra electrons increase the image resolution. One of the disadvantages of using nano particles instead of electrons is that they may harm the sample surface through investigation. Helium ( $2\text{He}^+$ ) ion is one of the most popular beam for this issue provided a high resolution scanning system.

## 2.2 Transmission electron microscopy (TEM)

Transmission electron microscopy (TEM) operates based on optical microscopy principles, however in this case the electrons play the photon roles. When an electromagnetic wave passes through an aperture, it is diffracted by aperture edges. This diffracting is a function of hole size and wavelength so the greater aperture size or the shorter wavelength causes the better resolution.

Since the electron wavelength is much lower than light, resolution of these microscopy increases remarkable (Eq. 2.1 and Table 2.2). In this method a beam of energetic electron focused and passed through a thin film specimen. These interacted electrons carried on texture data converged to an imaging system like fluorescent screen or photographic film to magnify in CCD camera. (Figure 2.3) The whole set up is under vacuum which increases mean free path of electron gas scattering. TEM consist of vacuum system, an electron gun to produce energetic electron beam, a series of electromagnetic lenses to converge the electron radiation, removal of specimen and imaging device sensor. TEM scanning has a wide application in medical and material science, nanotechnology and nano electronics.<sup>3</sup> Resolution of imaging system calculates as below (Figure 2.2):

$$\rho = \frac{0.6\lambda}{\eta \sin \alpha} \quad (2.1)$$

Where:

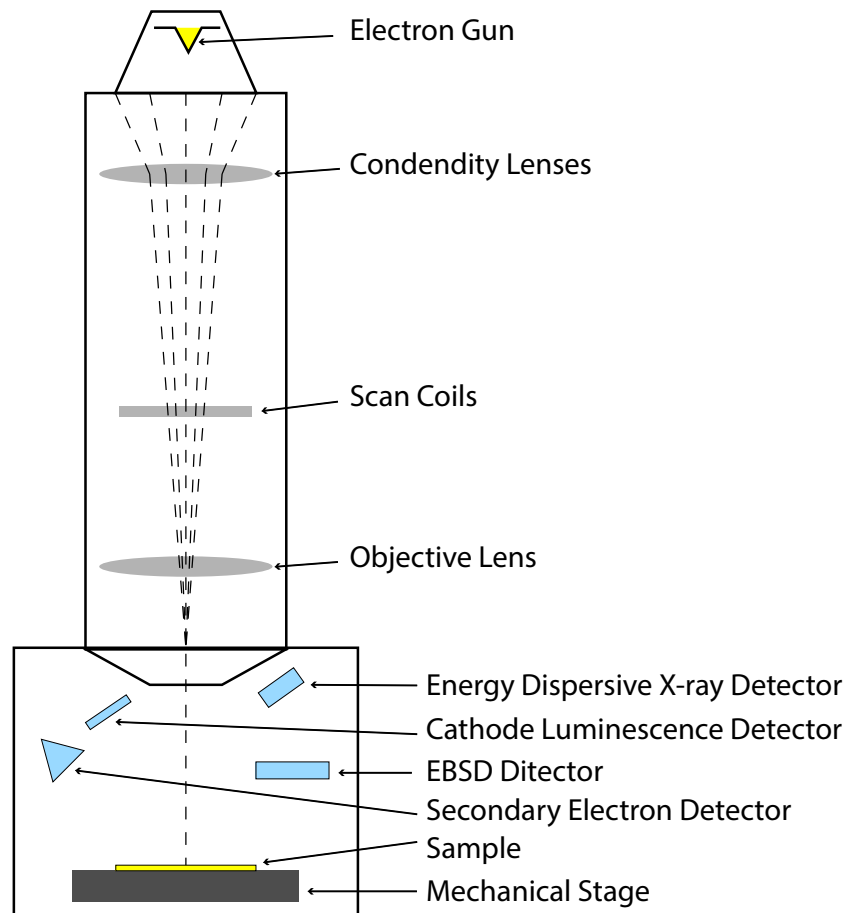


Figure 2.1: Schematic of scanning electron microscopy (SEM)

$\lambda$ = wavelength of the image radiation

$\eta$ = lens refraction index

$\alpha$ =illumination semi angle

$\eta \sin \alpha$ =Numerical aperture

Table 2.2 shows a comparison between optical and electrical microscopy resolution.

## 2.3 Scanning tunneling microscopy (STM)

Scanning tunneling microscopy (STM) works based on quantum mechanics concept of electron tunneling. Applying bias voltage between conductive scanner tip and conductive or semi- conductive sample made the free electrons tunneling through the vacuum gap. Also the tip and sample surface through scanning stayed away from each other this current produced based on quantum mechanics concept. This electrons carry the surface information and must be monitored to achieve a high res-

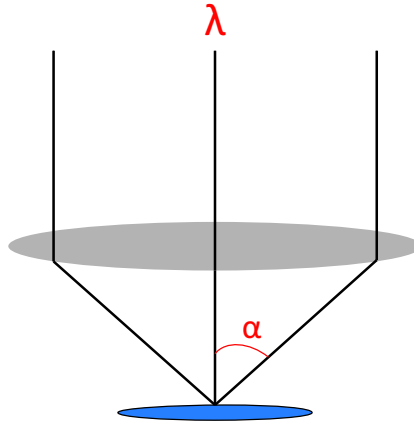


Figure 2.2: Schematic of simple imaging system

olution sample image. This microscopy method can provide 2D image of specimen.

## 2.4 Atomic force microscopy (AFM)

### 2.4.1 Review of literature

One of the major limitations of STM is electrical conductivity conditions. So non-conductive samples couldnt be scanned with this method. To overcome this weakness a novel idea of measuring force instead of electrical current was recommended in 1986. The first idea of atomic force microscopy (AFM) was conceived by Gerd Bening,Calvine Quate and Christoph Gerber. Bening and Quate demonstrated that adding a quit small sharp tip at the end of the AFM cantilever can improve the image quality magnificently. They also proposed cantilever vibration over the sample has the same impressive effects. However the practical pattern was illustrated by Wickramasinghe in 1987.<sup>4</sup> Also the cantilever vibration amplitude was monitored by interferometer methods. AFM has many advantages over other microscopy methods for example organic and mineral materials can be investigated under it. Electron microscopes can scan samples in 2D space while AFM has both in plane and out of plane scanners that provide 3D images. In AFM, samples dont need any specific preparation before scanning. The scanning is possible in the air, vacuum or liquid environments. Figure 2.4 shows schematics of SEM and AFM. Atomic interaction between end of the tip and target causes attractive or repulsive forces bends the cantilever. This bending was detected by laser beam divergence in photo detector. Table 2.3 shows a comparison between electron microscopes and AFM.

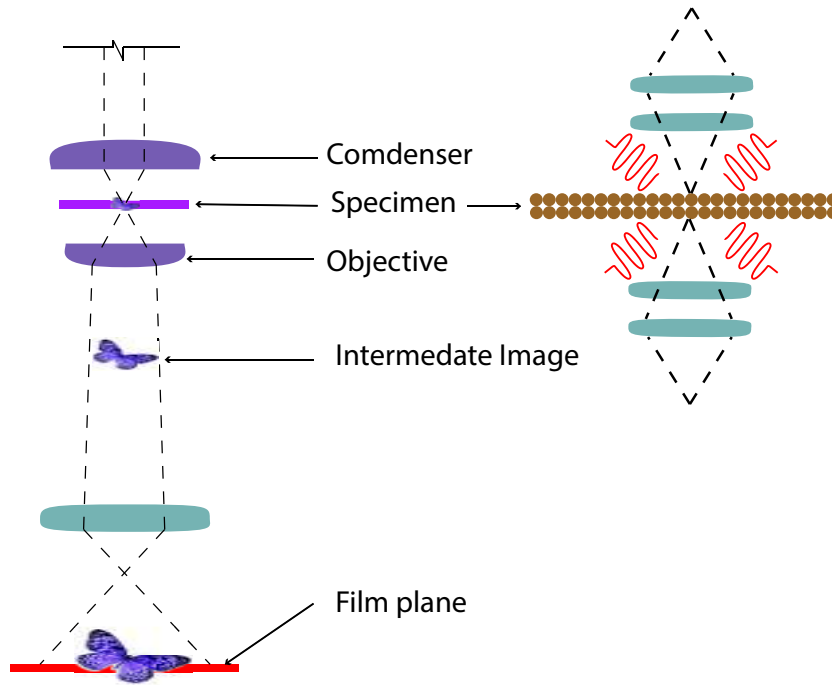


Figure 2.3: TEM deals directly with specimen molecular lattice

Table 2.2: Light versus electron microscopy resolution

Optical microscopy	Electron microscopy
$\lambda=0.5 \mu\text{m}$	$\lambda=0.068 \text{ \AA}$
$\eta=1.5(\text{glass})$	$\eta=1(\text{vacuum})$
$\alpha \sim 70^\circ$	$\alpha \leq 1^\circ$
$\rho=0.21 \mu\text{m} = 2100 \text{ \AA}$	$\rho= 4.1 \text{ \AA}$

## 2.4.2 Roll of AFM in Nanotechnology

The science, engineering and application in molecular size can be used in all other fields such as physics, chemistry and biology known as nanotechnology. In atomic scale dimension control plays the major role in system outputs. Engineering in nano scale needs an accurate nanometrology device. An atomic force microscopy prepare 3D image in nano scale resolution so we can measure dimensions of atomic features and visualize ultra small objects. In addition to measuring distance by pushing the tip over a surface and measuring repulsive force hardness of surface can be measured so sample stiffness could be calculated. Other physical properties like elasticity and friction could be measured. Another implementation of atomic force microscope is nano scale lithography with AFM tip. In this new method we can change the surface by rasping the underlying sample. This changing is happen in molecular deposition scale. With AFM tip manipulating features over a sample surface is attainable. Holding, pushing, pulling, gathering the features is possible with AFM probes so

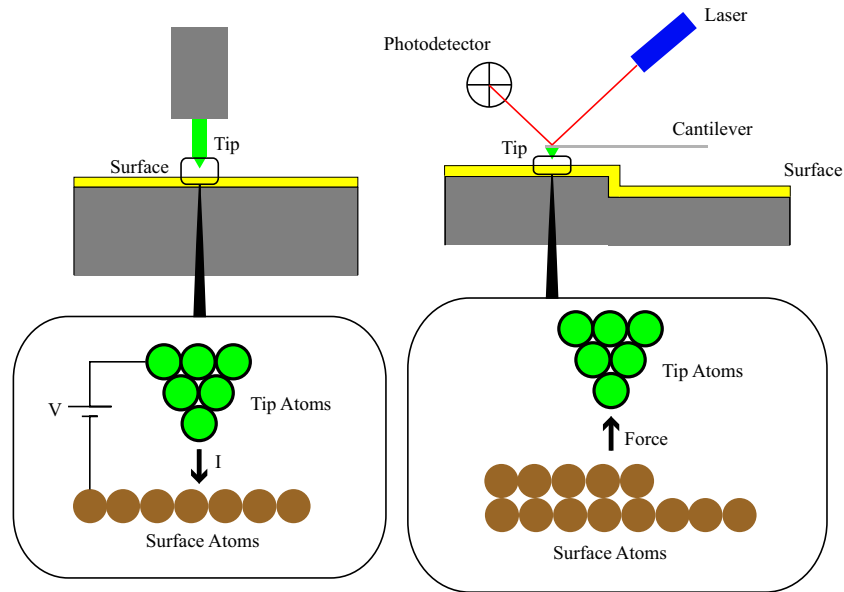


Figure 2.4: Schematics of SEM and AFM

creating nanometer size patterns are achievable.

### 2.4.3 Atomic Force Microscopy components

#### Piezoelectric XYZ scanner

The piezoelectric effect is the reversible material properties of generating electrical current due to mechanical stress. Solid materials such as crystals or ceramics have this worth. Piezoelectric ceramics may be soft, amorphous or hard according to chemical formulation. The most common material used in AFM build up is amorphous  $\text{PdBaTiO}_3$ . When voltage applied to different sides of these materials the geometry of the material is changed.(Figure 2.5) In AFM the movement of probe or samples could be controlled by piezocrystal scanner. It could be used under the samples or attaching to cantilever. In most AFM s the x-y plane range of motion is  $80 \times 80 \mu\text{m}$  and maximum z displacement of  $5 \mu\text{m}$ .

#### Probe

An AFM probe is a micrometer cantilever with sharp tip smoothly fluctuating over samples. The tip diameter is in nano scale range. The AFM probe is the main part of this scanner which is made by MEMS technology. Most of the cantilevers are typically made from silicon (Si) or silicon nitride ( $\text{Si}_3\text{N}_4$ ).The tip of AFM is fluctuating very close to sample surface. It is made molecular interaction forces causes cantilever bending ends in image production. There are different types of

scanning. According the type of scanning and interaction forces between the Tip and underlying surface, Tip needs to qualified by appropriate coating. For instance investigating covalence interaction in biological molecules, gold or platinum coating is suitable. Most of these coating are applied on silicon tips because with silicon as a tip substrate, coating has less effect on bending of probes than silicon nitride. The information collected from scanning depends on tip geometry like size, angles and shape. Based on investigation type each probe has different designation and geometry. One of the most famous of them is V- shape probes which have low mechanical resistance to vertical bending and high one to laterals. Figure 2.6 shows a V-shape cantilever.

## 2.5 Cantilever Equations

In V-shape cantilever, vertical, torsional and bending force are constants. Besides resonance frequency is calculated by the following equations:

$$K_{ver} = w \times \frac{E}{4} \times \left(\frac{t}{l}\right)^3 \quad (2.2)$$

$$K_{lat} = t \times \frac{E}{4} \times \left(\frac{w}{l}\right)^3 \quad (2.3)$$

$$K_{tor} = w \times \frac{G}{3} \times \frac{t^3}{l} \times \frac{1}{(H + 0.5)^2} \quad (2.4)$$

Where:

$E$ =Youngs modulus;

$t$ = Cantilever thickness;

$l$ =Cantilever length;

$t$ =Cantilever thickness;

$K_{ver}$ =Vertical force constant;

$K_{lat}$ = Lateral force constant;

$K_{tor}$ =Torsional force constant;

$G$ = Modulus of rigidity;

$m_0$ = Effective mass;

$f_0$ = Resonance frequency;

$$f_0 = \frac{1}{2} \left( \frac{K_{ver}}{m_0} \right)^{1/2} \quad (2.5)$$

Different Aspect	SEM/TEM	AFM
Samples electrical conductivity	Conductive	Insulation or Conductive
Image Type	2 Dimensional	3 Dimensional
Scanning environment	Vacuum	Vacuum, Air and Liquid
Time for imaging	0.1-1 minute	1-5 minute
Horizontal Resolution	0.2 nm(TEM) ; 5 nm(FE-SEM)	0.2 nm
Vertical Resolution	N/A	0.05 nm
Image range	100 nm(TEM) ; 1 mm(SEM)	100 $\mu\text{m}$
Depth of Field	Good	Poor
Contrast on flat samples	Poor	Good

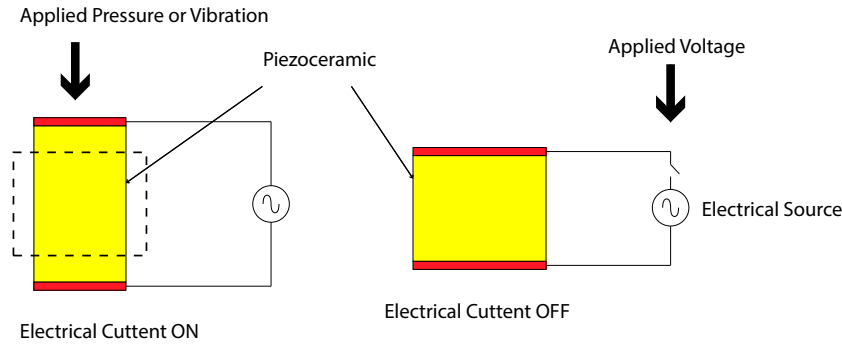


Figure 2.5: Piezoelectric effect due to applied voltage

The following table demonstrate standard properties of different cantilevers used in different operating modes.

One of the improving probe methods is putting a sphere at the end of the AFM tip, made the cantilever more controllable.(Figure 2.7) Another type of probe geometry is ultra sharp tip which is providing a certain horizontal resolution. Sharpening the tip needs micro fabrication process like chemical vapor deposition of  $\text{Si}_3\text{N}_4$  over a sharpened substrate. It could also be oxide sharpened to qualify the aspect ratio and decrease the radius low to 5 nm. Silicon tips could be sharpened by chemical etching methods or focused ion beam instruments.

These typical tips have the cone radius of 5 nm and half cone angle of  $35^\circ$ . Sharpened silicon tips by electro chemical etching can improve cone smaller the tip to diameter of 2-5 nm and half cone angle of  $10^\circ$ . Large cones have the less accuracy in imaging through ultra tight and deep structures. So the smaller cones angle

Table 2.4: Standard cantilever properties in different imaging mode in different environments<sup>5</sup>

Operating mode (environment)	K(N/m)	F (kHz) (in air)	Descriptions
Contact mode (Air/liquid)	< 1	10-30	Using soft cantilever V-shape cantilever is used to decrease friction force and rectangular one is used to measure it.
Intermediate mode (Air)	1.5-3	25-70	To overcome capillary and adhesion forces Large K is needed
Intermediate mode (liquids)	< 0.1		Without capillary and adhesion, softer cantilever could be used than in air
Dynamic modes (Air)	15-60	130-350	To overcome capillary and adhesion force large k is needed in air Moderate amplitude oscillation(> 5nm)
Dynamic modes (liquid)	< 0.1	30-50	Small amplitude oscillation(< 5nm)

the better resolution. The ideal probe is a conical tip with zero angles. This idea is possible if we attach a cylindrical nano structure with powerful mechanical and chemical qualification cause it remains constant during the imaging through gas or liquid environments. The satisfactory example for this nano cylindrical structure is carbon nanotube tip. A carbon nanotubes (CNTs) is allotrope of carbon with  $SP^2$  chemical hybridization just like graphite. These structures have conductive properties because of free carbon electrons. Nano tubes are classified as single wall nanotubes (SWNTs) and multi walled nanotubes (MWNTs). Clearly SWNTs is an individual tube of graphene structure while MWNTs consist multi centered carbon nanotubes with radius scale around 3 to 50 nm. Figure 2.8 show SWNT and MWNT.<sup>6</sup>

By attaching a carbon nanotube at the end of AFM tip, microscopic mapping can be improved. Some of exceptional dominance properties of such probes are as follows:

- High Young's modulus and ability to tolerate under high buckling, compressive, torsion and bending forces. Hollow structure of SWNTs and MWNTs exhibit Young's modulus of 1.8 and 1.3 TPa respectively.
- High aspect ratio made the investigation possible through deep and tight features.
- Low adhesion force between nanotube tip and samples
- SWNT probes have the resolution of sub 0.5 nm.<sup>7</sup>

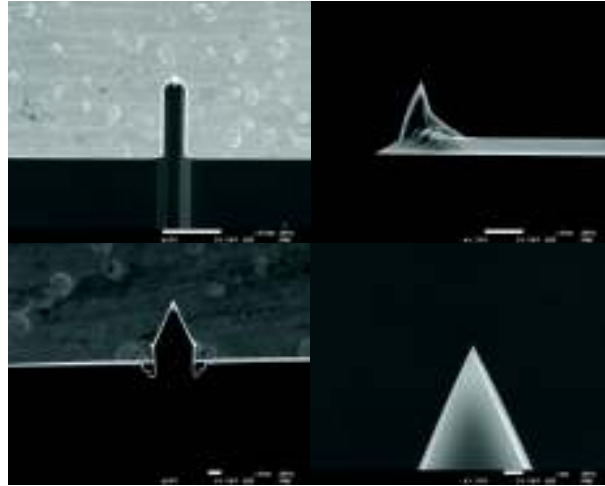


Figure 2.6: SEM image of AC55 and NCHAuD cantilever

### Force sensors

AFM's sensors must have the ability to measuring very minor interaction forces. These minor interaction forces utilize between tip and sample. This is because low pressure keeps the small probe safe from damage. There are different force sensors to measure the cantilever bending examined in AFM systems. Some of them are as follows:

- Scanning tunneling microscopy: Initial AFM was invented in 1985 by Binnig, Quate and Gerber. In that design scanning tunneling microscopy tip was applied to measure AFM probe displacement. The AFM set up consists of diamond tip glued to gold foil for scanning the sample, when the tip displacement is calibrated with second tip (STM tip) employed above it. (Figure 2.9) Matching and fixing these two are difficult despite combination of them is probable.

- Crystal oscillator: A crystal oscillator is an electrical oscillator made by piezo-electric crystal like quartz, which causes electrical definite frequencies due to mechanical resonance input. If a probe attached to this crystal oscillator, the tip vibration over a sample changes the oscillator frequency which is another calibration method. (Figure 2.10)

- Michelson and Twyman-Green interferometer: Optical interferometer plays a main role in nanometrology and Michelson interferometer is a common type of it. By applying this set up over the AFM cantilever, displacement could be measured. (Figure 2.11) This calibration is not accurate because the tip may shift between interference fringes.<sup>8</sup>

- Piezo-resistive Cantilevers: Piezo resistive materials exhibit a change in electrical resistance by applying strain. The electrical resistance of sensor with  $l$  length

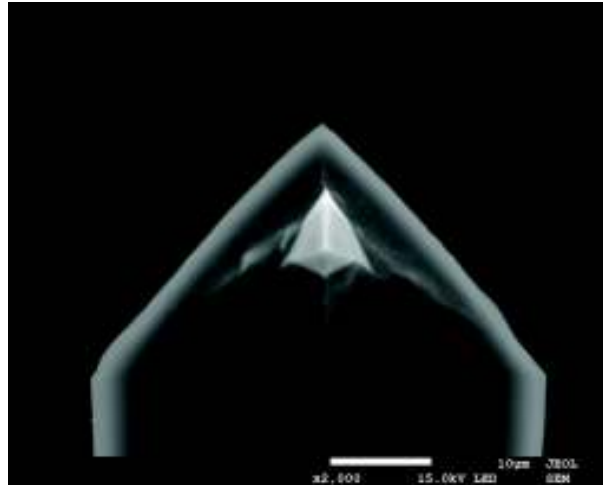


Figure 2.7: SEM image of NCHAuD cantilever and its apex

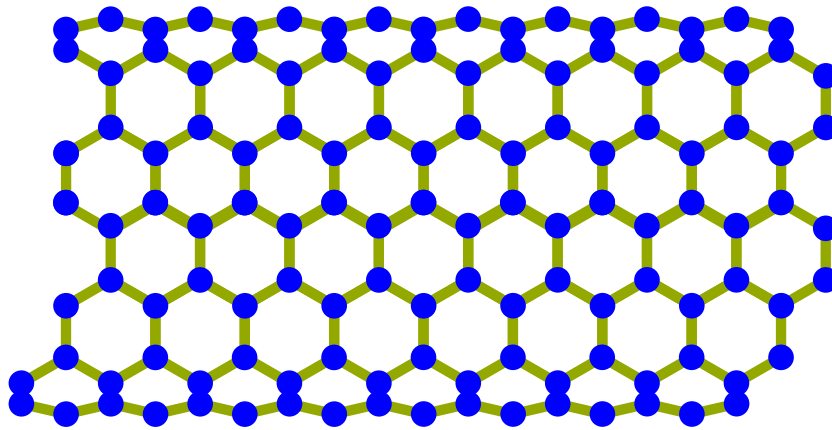


Figure 2.8: Single wall carbon nanotube

and cross section area  $A$  is calculated by:

$$Q = \rho \frac{l}{A} \quad (2.6)$$

AFM cantilever could be fabricated by piezo-resistive material so vertical bending pressure altered the electrical resistance of it.(Figure 2.12) Manufacturing this kind of piezo resistive cantilevers is difficult.<sup>9</sup>

- Fiber optic sensor: Fiber optic sensor is a kind of thin waveguide glass or fiber for sensing physical quantities like temperature, strain, force, acceleration and rotation by using optical gyroscopes. By applying sending and receiving fiber set up over a cantilever while lightening a diode laser light source, the quantity of waves reflected and collected from the back side of cantilever depends on distance from the fiber to the cantilever.(Figure 2.13)

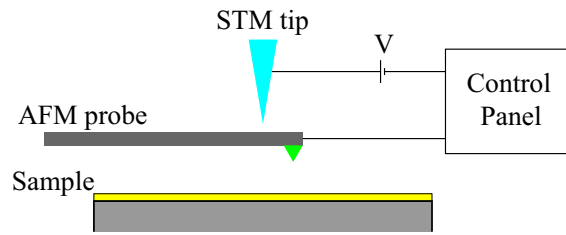


Figure 2.9: STM method for measuring AFM cantilever deflection

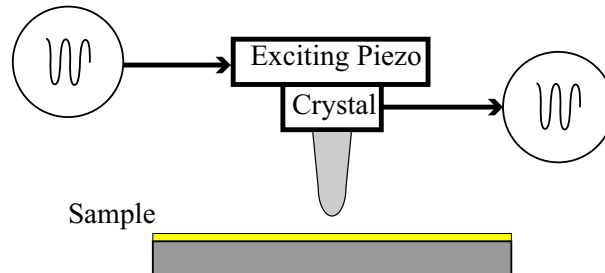


Figure 2.10: STM method for measuring AFM cantilever deflection

- Light lever sensors (LL-AFM) Light lever sensor is one of the optical displacement measuring instruments established in 1988 uses an optical lever technique. This sensor plays a major role in most AFMs fabricated by MEMS technology. The cantilever needs a probe attached to the end for investigation. It has a longitude between  $50$  and  $300\mu m$ , wideness between  $20$  and  $60$  microns and thickness of  $0.2$  to  $1$  microns. In this case a light reflected from the back side of cantilever to four quadrant photo detector. When cantilever is vibrating over a sample, the interaction between reflecting light of the cantilever will change. This light moves to the detector and this altering would be monitored.(Figure 2.14)<sup>10</sup>

### X-Y stage

AFMs typically have X-Y position stage for moving the samples under the probe. This stage could be both manual and motorized. The resolution and accuracy of stage motion is 10 percent of the probe scanning.

## 2.6 Tip-sample interaction force

- Short and long range force:

When AFM Tip became too close to sample surface, intermolecular forces bond them to each other. Without electrostatic forces, the force between exterior sample atoms and tip is calculated by the following equation:

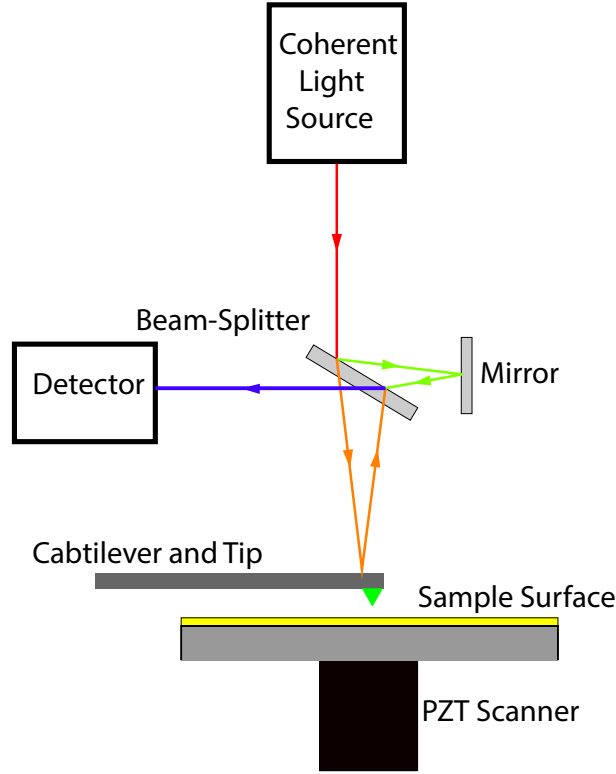


Figure 2.11: Michelson interferometer for measuring cantilever displacement

$$F = -\frac{C}{r^n} \quad n < 7 \quad (2.7)$$

Where negative sign shows attractive forces and  $C$  is a constant. Interaction force is categorized in short and long range forces. For short range forces  $n=9-16$  and for long range forces  $n=7$ . Short range forces appear when inter atomic distance became less than 1 nanometer. In small inter atomic distance, atomic electron shells overlap. Based on Pauli Exclusion quantum mechanics Principle, two identical fermions cant occupy the same quantum state simultaneously. So overlapping electron shells causes extremely repulsive force. Short range forces also can be attractive when two overlap atoms chemically binned to each others. This combination is useless for probe investigation. Long range forces appear in inter molecular distance based on materials chemistry known as permanent dipole interaction, permanent and induced dipole interaction and London forces.<sup>11</sup> If the tip has conical geometry, force applying to the sample surface is calculated by the following formula:

$$F = -\frac{-HR\tan^2\theta}{d^2} \quad (2.8)$$

Where:

$H$  = Hamaker constant (van der walls body- body interaction)  $=\pi^2 \times C \times \rho_1 \times \rho_2$

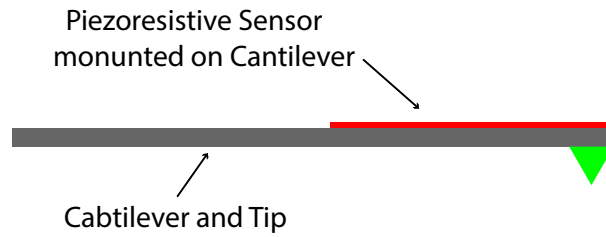


Figure 2.12: Piezoresistive AFM cantilever

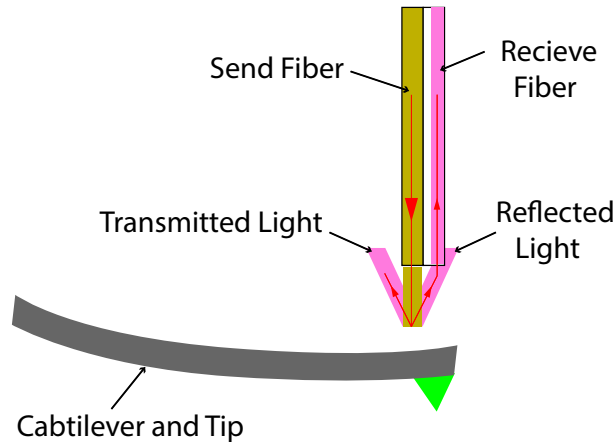


Figure 2.13: Fiber optic interferometer for AFM<sup>9</sup>

$\rho_1$  and  $\rho_2$ = The number of atoms per unit volume in two contacting bodies and  $C$  is the constant

$R$ =Radius of the AFM tip

$d$  =tip-sample displacement

Interaction forces between the tip and sample surface can be modeled by Lennard-Jones potential.

$$V(r) = 4\epsilon\left[\left(\frac{\sigma}{r}\right)^{12} - (\sigma r)^6\right] \quad (2.9)$$

And

$\epsilon$ = Dept of potential

$\sigma$ = Atom diameter

$r$ = inter atomic distance

The following figures(Fig 2.17 and 2.18) describe a proper force interaction demonstration dependent to distance in different operating modes of AFM.

- Friction force:

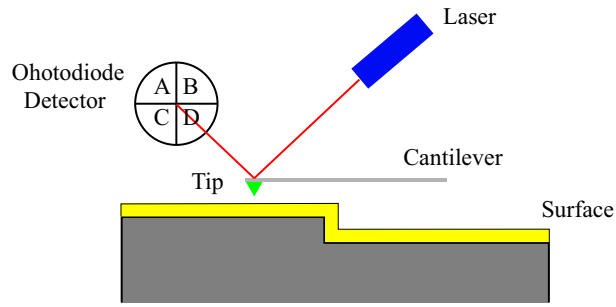


Figure 2.14: Illustration of LL-AFM sensor

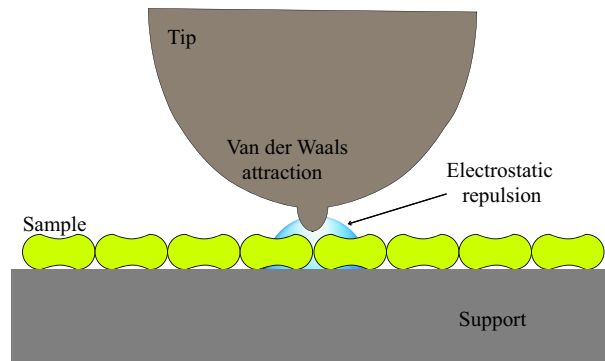


Figure 2.15: Schematic of Tip-sample interaction

Friction is a resisting force to relative motion of objects depends on normal applied force. Friction force is one of the main phenomena plays a major role in tribology science just like adhesion. Indeed friction rise from inter atomic forces between surface harshness, elastic and plastic altering which clarifying topography and stress distribution of objects moving against each other.<sup>12,13</sup> Guillaume Amontons proposed two following famous friction laws in French Royal science academy.<sup>14</sup> After that, Coulomb completed these laws with third one.

First law: The friction force is proportional to the normal load.

$$F_f = \mu F_N \quad (2.10)$$

Where  $\mu$  is expressed the friction coefficient.

Second law: The friction force is independent of the apparent area of contact.

Third law: The friction force is independent of sliding velocity

In microtribology:

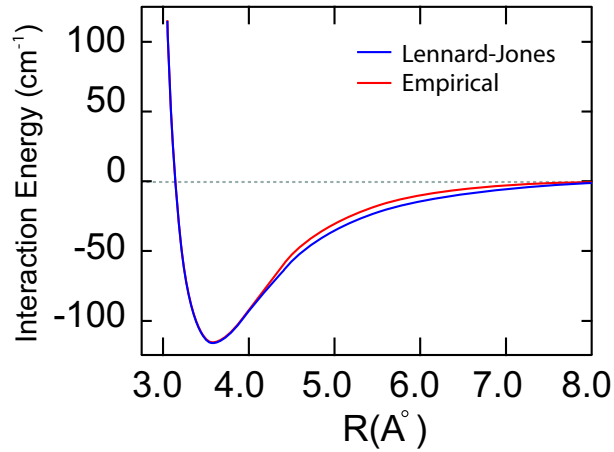


Figure 2.16: Lennard jones potential for Ar

$$F_f = \tau A \quad (2.11)$$

Where:

$\tau$  = Shear stress;

$A$  = Real contact area;

According to Tabor theory and by assuming the radius type tip, friction force is proportional to real contact challenging area of tip-sample and normal load force:

$$F_f \propto F_N^{2/3} \quad (2.12)$$

- Capillary force: An important attractive force in interacting between two surfaces is capillary adhesion. This force appears in aqueous samples through imaging in air. By closing two surfaces in existence of aqueous materials, liquids condense to meniscus form between two surfaces.<sup>15</sup> The force caused by Laplace pressure of ellipse liquid made it bob up called capillary force. This force is estimated to be something around 100 nN or stronger. When scanning completely done through liquids, meniscus couldnt create so this force doesn't exist. This force affected on two surface connections by altering adhesion and friction forces especially in static frictions.<sup>16</sup> the following figure shows strong capillary force between tip-sample during imaging.

## 2.7 Force curve measurement

Beside topographic analysis, AFM can also measure long range attractive or repulsive forces between tip and the sample surface. This method of investigation known

as force distance curves presented in 1989. By this method physical properties like adhesion, elasticity, friction and molecular adsorption could be measured. The clarification of force curves AFM is based on force laws as a function of tip-sample separation distance.<sup>17</sup> Force versus distance curve AFM consists of a cantilever with micro tip deflects through surface interacting. This deflection could be measured in different methods to create the sample topography. This scanning is applicable by applying triangle wave voltage arrangement to the  $Z$  scanner attached the cantilever. Controlling frequency and amplitude of input voltage, let us change the AFM tip separation distance or speed during the force measurement. However the similar AFM oscillating measuring methods like tapping mode or non contact mode can support force measurement, actually force curve method can provide surface magnetic and electric fields and sample surface viscoelastic properties moreover. This method is applicable for all types of samples in all environmental conditions. It has the high lateral, vertical and force resolution of 25 nm, 0.1Å and 1 pN respectively.<sup>18</sup>

An AFM force distance curve is a graph demonstrated with the tip-sample interaction force versus the separation distance of them. To obtain this graph, tip or sample vibrated along  $z$  axis so the cantilever deflection is achieved. Tip-sample interaction force obeys the HOOKs law:

$$F = -k \times d_c \quad (2.13)$$

$k$  shows the cantilever spring constant. Force measurement has a wide application in living cell investigations. These measurements provide information of atomic or molecular adhesive and elastic interaction forces. These data illuminate the chemical, biological and physical world surrounding us.

## 2.8 AFM operating modes

Typical AFM has four types of operation modes: (1) contact mode (2) intermediate mode (3) noncontact mode (4)lateral force microscopy (LFM) .Intermediate and noncontact modes are dynamics or vibrating modes. In contact mode, tip deflection is measured to image the specimen. While in oscillating mode frequency or amplitude is the scanner input. Contact mode operation is suitable for hard solid samples and provided the resolution of more than 50 nm while the vibrating mode is proper for creamy samples and provided less resolution.

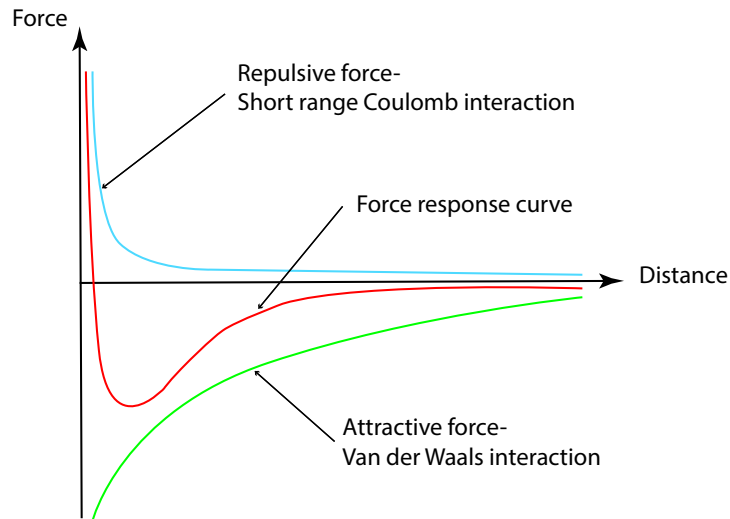


Figure 2.17: short range and long range forces

### 2.8.1 Contact mode

In this mode cantilever investigates the sample surface with constant height (few angstrom) and constant tip deflection. (Fig 2.20) Because of atomic scale displacement between tip and exterior sample molecules, interaction force is repulsive. The force applies from tip to surface in this mode obeys the Hooks law. This method is operating either at force constant or distance constant depends on the scanning situation.

$$F = -k \times D \quad (2.14)$$

Where:

$F$ = Force constant;

$K$ = Stiffness;

$D$ = Deflection displacement;

In this mode cantilever stiffness must be small to improve scanning sensitivity and avoid scratching sample surface. This parameter could be calculated by cantilever dimensions and material properties. One of the benefits of this operating mode is high scan speed with nanometer (atomic) resolution. Also scanning of fluctuated surface samples is easily possible. As a disadvantage of this mode, it could be mentioned that friction forces may change the image. Extreme normal forces could damage soft biological sample so decrease the resolution.

#### Constant height mode

Obviously in constant height mode operation, the end of microscopy probe slides over a sample surface with fixed height. The vertical cantilever deflection is detected

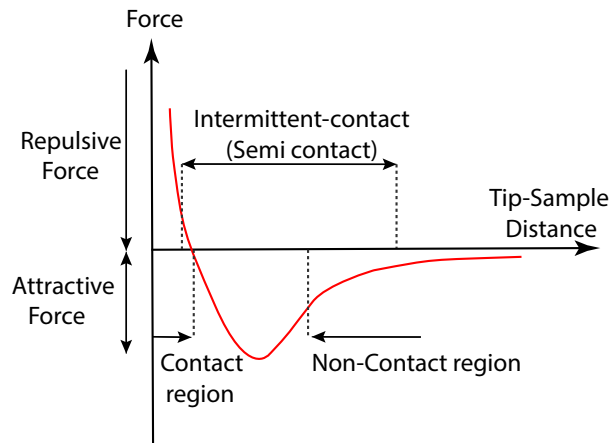


Figure 2.18: Force interaction between tip-sample in different modes

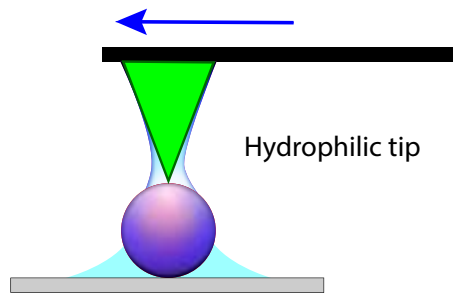


Figure 2.19: Illustration of creating liquid meniscus and strong capillary force between tip-sample during scanning

by optical systems converted to electrical DFL signals. These signals create sample topography and characterization. There is a linear relationship between the cantilever deflections and interaction force. The following figure (Fig. 2.21(a)) shows the schematic of this operating method.

A particular advantage of this mode is high scanning speed with nanometer resolution. So this is an appropriate method for recording real-time images of surface topography altering. Some of this method disadvantages, are more probable sample scratch and cantilever breakage meanwhile comfort fast scanning is done so samples must be smooth enough. Apparently this isn't a safe method for soft samples like biological cells or organic components because the tip is contact to samples. Also considerable capillary force in liquid layer made noises in topographic image.<sup>19</sup>

### Constant force mode

Through constant mode investigation a feedback system controls cantilever bending at a constant point. Tip surface interaction forces affect on cantilever deflection. By

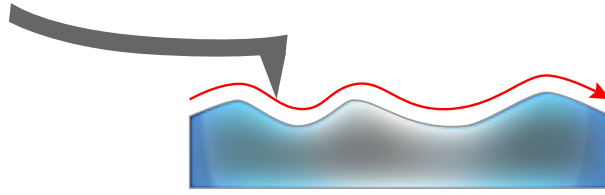


Figure 2.20: Schematic of scanning by contact AFM

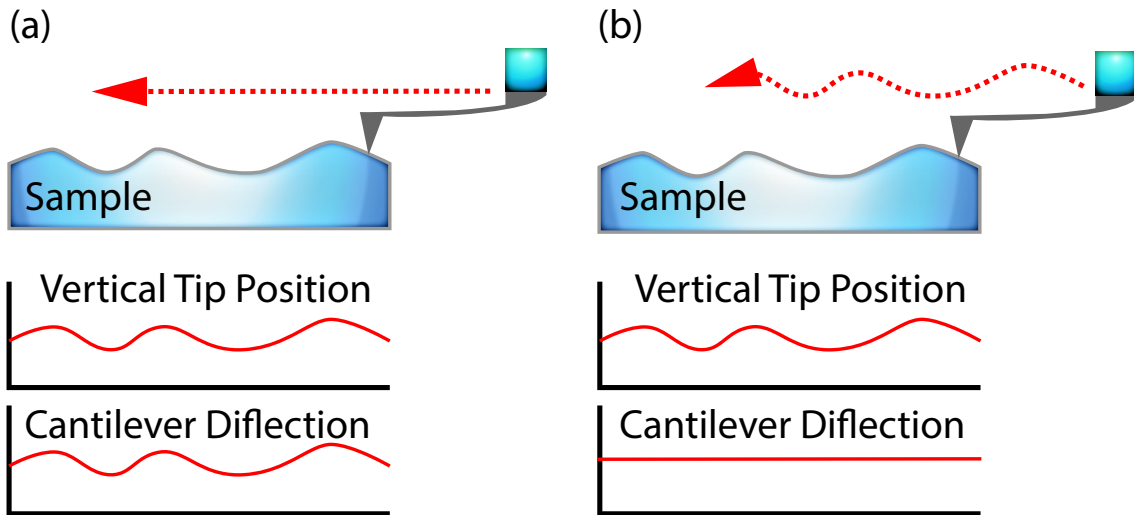


Figure 2.21: (a)Constant height operation mode ; (b)Constant force operating mode

fixing this deflection the feedback system changes input voltage applied to z-scanner. This voltage altering creates sample topography. Fig 2.21(b) shows schematic of this mode. This mode has the similar disadvantages of constant height mode however sample destroying probability is much lower. This is because the scanning is done under lower velocity to control the feedback system. The major benefit of this method is the ability to measure other physical properties like friction force and spreading resistance at the same time.

## 2.8.2 Semi contact or tapping mode

Another operation mode of scanning is known as vibrating or tapping mode. In this mode the tip sinusoidal touch the surface and cantilever vibrates around its resonance frequency. (Fig. 2.22(a)) This oscillation is supplied by piezoelectric. Amplitude of vibration usually changes between 10 to 100 nano meters. Cantilever frequency  $\omega_0$  is calculated by:

$$\omega_0 = C\sqrt{K} \quad (2.15)$$

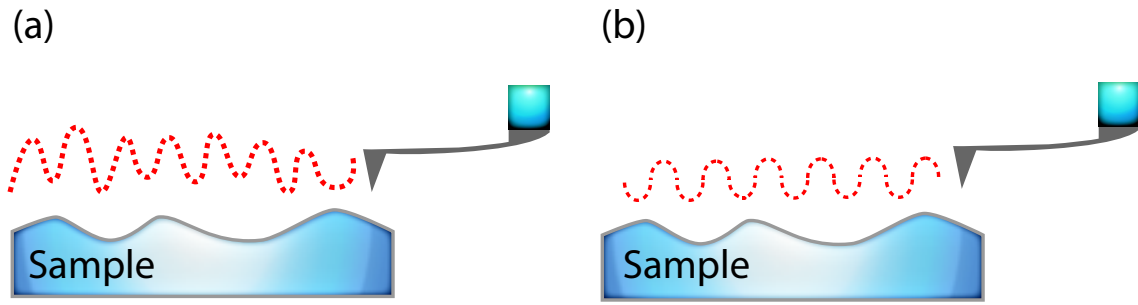


Figure 2.22: Schematic of scanning by (a)tapping mode AFM ; (b) non contact mode AFM

And  $C$ = proportionality constant;

$K$ = force constant;

By calculating the phase difference between input applying signals and measured cantilever oscillations (output phase) valuable surface structural data like chemical composition, frictions, elasticity, adhesion, and so on could be obtained. This method advantages are causing low forces made less influence on samples and almost no frictions. Slow speed scanning could be mentioned as a disadvantage of this mode.

### 2.8.3 Non contact mode

As its name proposed, in this mode the cantilever is oscillating above the sample surface. There are few force interactions between tip and exterior surface molecules in this case. These forces are attractive Van der Waals type (around  $10^{-12}$  N) measured to scan sample topography. Silicon (Si) cantilevers are proper in this case. Figure 2.22(b) shows schematic of non contact scanning mode. Scanning aquatic samples by contact mode AFM in ambient, is challenging with some difficulties. Presence of water layer on sample or tip caused the capillary effect between them. That effect made the tip cantilever attachment (jump to contact) so this method is not suitable for fluid layers. Surface characteristics let us to choose the best method and scanning conditions.

As an advantage of this operating mode it could be mentioned that low force interactions between tip and sample cause less influence and shape altering. Slow scan speed to prevent attaching the sample surface attachment, is a disadvantage of this method. The following is going to describe two major types of this operating mode known as frequency modulation and amplitude one.

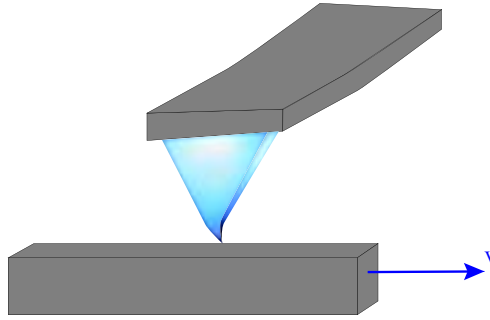


Figure 2.23: Schematic of lateral force microscopy

### 2.8.4 Lateral force microscopy (LFM)

Scanning thorough rough and fluctuated surface, in contact mode, generates the cantilever torsion. This twisting happens by changing in surface friction force. By considering friction forces as an input data of surface, this kind of scanning is known as a lateral or friction force microscopy. (LFM/FFM) Since the friction force depends on the normal force element, cantilever stiffness, and dimensions, it could be measured during the scanning to achieve surface topography.<sup>20</sup> LFM has a high resolution to determine molecular roughness of sample surface. Stiffness and elasticity measurement also could be done by this method. This is a proper method in dissimilar surface materials. Fig 2.23 shows the schematic of this operation.

## 2.9 Frequency modulation (FM-AFM)

Frequency modulation of atomic force microscopy (FM-AFM) is presented in magnetic force microscopy by Albercht and coworkers in 1991. During this type of scanning the cantilever consciously vibrated over the sample by its current resonance frequency. Actually there is a positive feedback loop of cantilever vibration with constant amplitude and eigenfrequency of  $f_0$ . There is a constant phase shifted deflection of 90 degrees between mechanical excitation and sensor response. Resonance frequency altering ( $\delta f$ ), the control signal of the automatic gain control unit as an interacting energy loss measurements and tunneling current creates between tip-sample in conductive cases, are three quantities could be recorded by this method.<sup>21</sup> Compared with amplitude modulation there is a remarkable enhancement in scanning rate and noise level. In 1994, high atomic resolution achieved in Si (111)-(7 × 7) surface which was a great progress in AFM scanning. AFM cantilevers with spring constant of  $k \approx 2000$  N/m can be carried on with  $\text{\AA}$  range amplitude.

## 2.10 Amplitude modulation (AM-AFM)

Amplitude modulation is one of the main operation branches of tapping mode presented by Binnig and Quate in 1986. A cantilever in this mode is driven by exciting the sensor with fixed amplitude ( $A$ ) just around its resonant frequency. Interaction forces could be monitored as an amplitude shifting ( $\delta A$ ). An attractive interaction force makes a fall in resonant frequency, so the driving frequency rises from resonance and amplitude falls. Repulsive forces create the conditions vice versa. This method provides clear imaging from rough or dynamically changing samples where typical tips couldnt tolerate during hard adhesion. If dissipative forces change during the scanning, resonant amplitude also changes so this method may fail. Both conservative and dissipative interaction forces can alter  $\delta A$  during the scanning which is end in topographic artifacts in taken images. An advantage of this method compared to FM-AFM is simpler mechanism which has just one feedback loop rather than three. AM-AFM faces limitations in vacuum because of its high  $Q$  factor. So the sensor oscillates too much before the amplitude settles to its new value which takes time and reduces the operation velocity compared to Air.

# Bibliography

- [1] J. Goldstrein. *Kluwer Academic/Plenum Publishers*, P. 689 , 2003.
- [2] E. Suzuki . "High-resolution scanning electron microscopy of immunogold-labelled cells by the use of thin plasma coating of osmium" ,*Journal of Microscopy*, 208 (3): P.153-157 , 2002.
- [3] D B. Williams and C. Barry Carter . *Transmission electron microscopy: a textbook for materials science. New York, Spinger*, 2009.
- [4] P.E. West. *Introduction to atomic force microscopy, Theory, practice, application*, 2009.
- [5] M. Baro and R.G. Reifenberger. *AFM in liquid .UAM, Madrid. Perdue University*, 2012.
- [6] J.H. Hafner and C.L. Cheunge. *Structural and functional imaging with carbon nanotube AFM probes. Department of Chemistry and Chemical Biology, Harvard University, Cambridge, MA 02138, USA*.
- [7] C. Cheung, J. H. Hafner and C. M. Lieber. *Carbon nanotube atomic force microscopy tips: Direct growth by chemical vapor deposition and application to high-resolution imaging, Department of Chemistry and Chemical Biology, Harvard University, Cambridge,1999*.
- [8] R.K. Leach . *Fundamental Principles of Engineering Nanometrology,1st edition, Elsevier Inc.,2010*.
- [9] Liu . *Piezoresistive sensors*, Ch 06, P. 207-218.
- [10] A. D. Kersey. *A review on recent developments in fiber optic sensor technology, Opt. Fiber Technol.*, 2,291,1996.
- [11] W.N. Sharp. *Handbook of experimental solid mechanics, Springer Science Business Media,2008*.

- [12] J.A. Greenwood. *Constriction resistance and the real area of contact. British Journal of Applied Physics*,1966.
- [13] J.A. Greenwood and J.B.P. Williamson. *Contact of Nominally Flat Surfaces. Proceedings of the Royal Society of London. Series A, Mathematical and Physical Sciences* ,1966.
- [14] D. Dowson. *History of tribology. London; New york, Longman.* ,1978.
- [15] J. Israelachvili. *Intermolecular and Surface Forces. Intermolecular and Surface Forces* ,1977.
- [16] M. Mser and V. L. Popov. *Contact Mechanics and Friction: Physical Principles and Applications.*
- [17] J.N. Israelashvili. *Intermolecular and Surface Forces, Academic Press.*,1992.
- [18] B. cappella and G. Dietler . *Force distance curves by atomic force microscopy, Elsevier.*,1999.
- [19] Magonov and N. Sergei *Surface Analysis with STM and AFM. Experimental and Theotetical Aspects of Image Analysis. VCH*,1996.
- [20] Lievonen and Jarkko *Force measurements and tip shape approximation with the atomic force microscope, Department of Physics, University of Jyväskylä*,2011.
- [21] B. Bhushan. *Handbook of Nanotechnology,2nd edition, Springer*,2007.

# Chapter 3

## High-speed Z tip scanner for atomic-resolution atomic force microscopy

### 3.1 Introduction

In the 1986, invention of atomic force microscopy (AFM)<sup>1</sup> impressed researchers in various field of nanotechnology such as material science, biological materials, physics and chemistry. Atomic force microscopy can be operated not only in liquid but also in air and vacuum. Moreover, it can be used for samples from organic to mineral, from insulated material to conductive one and from very soft material to harder ones. Owing of these unique capability, AFM can be used for wide range of samples. In contrast, AFM has some high potential fields of study for improvement. Typically the scan rate of AFM is approximately 1 Hz and for having of image by dimension of  $10nm \times 10nm$  takes 1 min for every frame. It would be advantageous to have a AFM with higher scan rate to image the dynamic process solid/liquid interfaces. High-speed AFM require creating the mechanical controlling system which has high first resonance frequency. Scan rate is limited by parameters such as: (1) first resonance frequency of *XY* Scanner, (2) force sensing system, (3) bandwidth of feedback control and (4) first resonance of the *Z* tip scanner. Scan rate is determined by the slowest responsiveness of these issues. Therefore, researchers focus on the enhancement of the resonance frequency of scanners and reducing the cross talk between *XY* and *Z* scanner. Based on the previous works, high-speed AFM has been developed. Tabak *et al.* introduce the micro electro mechanical system (MEMS) as a high-speed *Z* scanner to provide high-speed scanning motion. The introduced *Z* scanner has low mass (about  $10^{-11}$  Kg) and high resonance frequency (in order of several MHz). On the other hand they used separated *XY* and *Z* scanner to avoid the cross talk.<sup>10</sup> Ando *et al.* developed high-speed scanner by using the counterbalance structure.

This improvement was done by decreasing the cross talk of scanners.<sup>2</sup> Fukuma *et al.* developed resonance frequency of  $Z$  axis by inertia balance support and can get 540 kHz resonance frequency in  $Z$  axis. They supported cubic actuator at 4 sides perpendicular to excitation axis.<sup>11</sup> Hansma *et al.* represented scanning unit for AFM system 3 times faster than the conventional AFM. They used the parallel flexure stage for this purpose. Their design was developed more by other researchers.<sup>7</sup> Miyata *et al.* presented a design of separate-type high-speed scanner that consists of  $XY$  sample and  $Z$  tip scanners. In addition, they presented the design of a wide band and low noise HVAMP to achieve sufficient noise performance to allow high-speed and high-resolution imaging.<sup>6</sup> So, improving the first resonance frequency of  $Z$  tip scanner is one of the most important part that strongly influence the operation speed and usability of AFM. Though this chapter I focus on the improvement of the  $Z$  tip scanner and for this purpose I will introduce two kinds of developed  $Z$  tip scanner by the name of precisely machined plate with screw holding mechanism  $Z$  tip scanner and counterbalance  $Z$  tip scanner. Some experiment will be done to demonstrate the improvement on the following methods.

## 3.2 Screw type $Z$ tip scanner

### 3.2.1 Basic Designs

In the previous works,<sup>6</sup> different cantilever holding mechanisms using a screw, a plate spring and glue was compared. The result showed that the screw holding mechanism gives the best balance between the performance and the usability. However, the design for the  $Z$  tip scanner with a screw holding mechanism was not optimized for achieving the best performance. For example, the dependence of the performance on actuator size and screw arrangement has not been investigated. In figure 3.1 we introduce the new precisely machined plate with screw cantilever holding mechanism .we compare it with different cantilever holding mechanism(Figure 3.2). These designs are different in actuator size and screw arrangement. The screw is laterally displaced from the cantilever position in Figs. 3.2(a) and 3.2(b) while vertically displaced in Figs. 3.2(c) and 3.2(d). Here we refer to the former as Design I and the latter as Design II. The actuator in Figs. 3.2(a) and 3.2(b) has a smaller size ( $2 \times 2 \times 2 \text{ mm}^3$ ) while the one in Figs. 3.2(c) and 3.2(d) has a larger size ( $3 \times 3 \times 2 \text{ mm}^3$ ).

An actuator is fixed to a holder body with glue. Then, a cantilever stage is fixed on the actuator. A cantilever is sandwiched between the cantilever stage and a metal plate spring. The plate spring is fixed with a screw to the cantilever stage. All the metal parts are made of stainless steel (SS316).

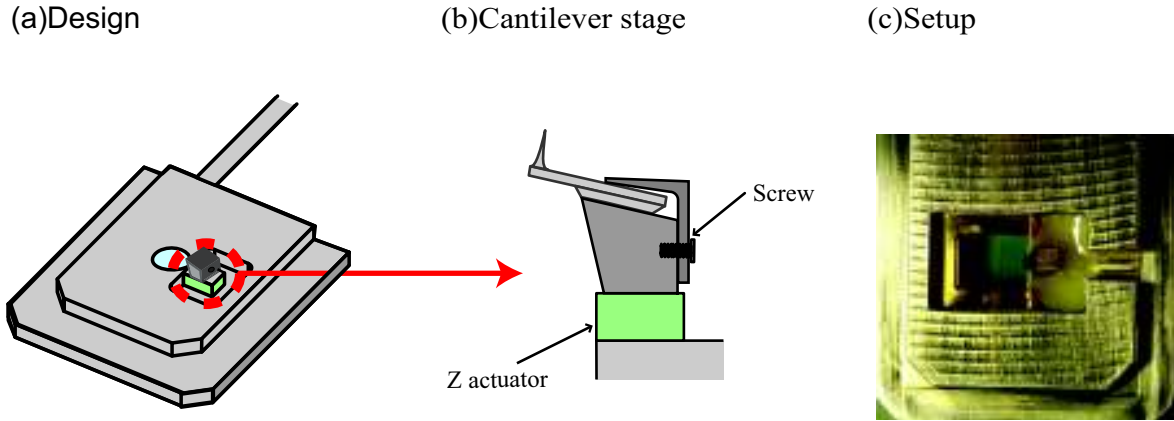


Figure 3.1: High-speed  $Z$  tip scanner with vertical arrangement screw cantilever holding mechanism ;(a)Design (b)Cantilever Stage (c)Setup

In Design II, we found that the design of the plate spring is important. If we use a plate spring manufactured by bending a metal plate with a uniform thickness, it is easily fatigued by repeated use. In addition, the holding force is insufficient so that spurious resonances appear in the low frequency range. We found that this problem can be solved by using a precisely machined metal plate with a variable thickness. This design gives a sufficient holding force and allows repeated exchange of cantilevers. Before making of new cantilever holding mechanism, we did some simulation for finding the effect of every design parameter on the performance of the scanner. FEA software (COMSOL Metaphysics, COMSOL) was used for theoretical analysis of the frequency response and vibration modes of the scanner. We used Young's Modulus of 193 GPa, Poisson's ratio of 0.25 and density of 7970 kg/m<sup>3</sup> for modeling the scanner bodies made of SS316. For modeling the stack piezoactuators, we used density of 7500 kg/m<sup>3</sup>.

### 3.2.2 Effect of using Sic and SUS316 as a different material on performance of $Z$ tip scanner

In the improvement of the resonance frequency, one of the most important parameter is decreasing the mass of  $Z$  scanner. In parallel of mass decreasing we want to figure on the sufficient mechanical strength and low contamination. There is wide range of the material with different mechanical and chemical properties to use as a cantilever stage. Beside of the SUS316, we can use the SiC. In comparison, SiC has lower mass than SUS316 while keeping the high mechanical strength and low chemical contamination with the same dimensions. During this part, we have simulation of both SiC and SUS316. (Figure 3.3) Simulation results shows that in the performance

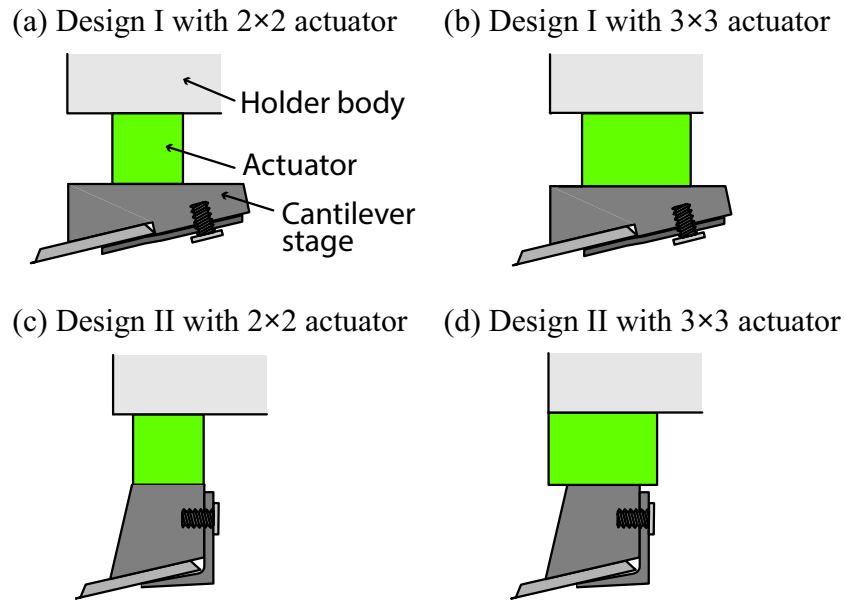


Figure 3.2: Schematic models of the  $Z$  tip scanners with different designs of a cantilever screw holding mechanism

SiC has resonance frequency around 180 kHz while for the SUS316 ,it is 110kHz.So, by using the Sic as a cantilever stage material,the performance of  $Z$  tip scanner will be improve. Although the resonance frequency was shifting based on the achieved result,but the manner of both material are the same.

### 3.2.3 Triangular shape stage

The mass of cantilever stage plays very important role in performance of the  $Z$  scanner. Based on the experiment reports,cantilever stage of  $Z$  scanner allow to support tilt in range of  $10^\circ \sim 15^\circ$  for cantilever .The best and optimized is  $13^\circ$  tilt.So, the simplest cantilever stage would be the triangular shape with  $13^\circ$  tilt. Although using of this kind of cantilever stage limits of the usability of system but we can attach the cantilever by glue. We checked the performance of this cantilever stage by simulation. the results shows that in resemblance with usability limitation ,it does not have very significant advantage (Figure3.4). These vibration modes correspond to the peaks indicated by the circles in Fig. 3.4.

### 3.2.4 Calibration of the inputs data in COMSOL software

Parameters of used piezo are unknown in material library of COMSOL software.For simulation the accurate manner of the piezo material ,we need two parameters; main resonance peak and displacement of real piezo should be same as the simulation ones.

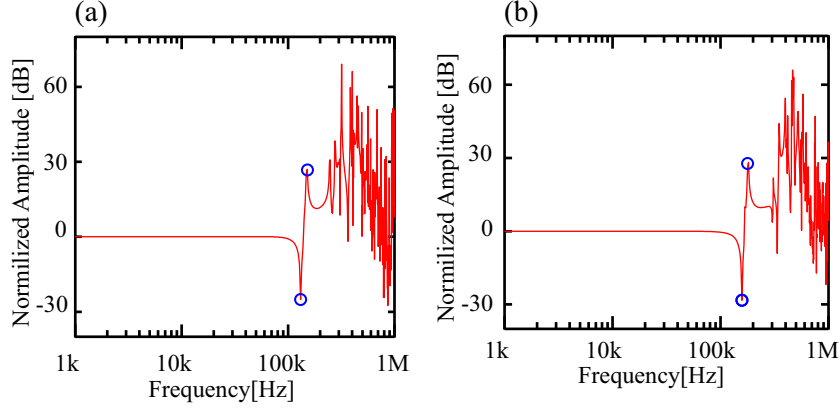


Figure 3.3: Effect of using (a)SUS316 and (b)SiC as a different material on performance of  $Z$  tip scanner

For calibration of parameters of piezo material in COMSOL, from material library the nearest piezo material in parameters with the piezo that we will use in experimental will be chosen and we will modify the parameters of this material. For this purpose the  $PZT - 5H$  has the similar parameters with our piezo and we chose it. Before modifying step, we should measure the performance of piezo material that attached by glue on the heavy body by frequency resonance analyzer(FRA5097,NF). By this experiment we can get the resonance frequency and maximum displacement of the real piezo. To modify the resonance frequency, we need to modify elasticity matrix parameters of  $PZT - 5H$  in COMSOL. By running the software with  $PZT - 5H$  as a piezo material, resonance frequency of simulation will be calculated. The simulation resonance frequency is 330 kHz whereas the experimental on with  $3 \times 3 \times 2 \text{ mm}^3$  is 150kHz. The modifying coefficient of elasticity matrix can be calculated by:

$$a = \left(\frac{f_2}{f_1}\right)^2 \quad (3.1)$$

where  $f_2$  and  $f_1$  are experimental and simulation resonance frequency respectively. Modifying coefficient should be multiply to all elasticity matrix parameters. In our case, this coefficient is 0.2066. As modifying the displacement parameters, coupling matrix should be modified. We will measure the experimental displacement of piezo on the 1kHz and compare it with corresponding value of simulation one. Modifying coefficient of the coupling matrix can be calculated by:

$$b = \frac{\Delta_2}{\Delta_1} \quad (3.2)$$

where  $\Delta_2$  and  $\Delta_1$  are experimental and simulation displacement. Modifying coefficient should be multiply to all coupling matrix parameters. In our case, this coefficient is  $37.4 \times 10^{-3}$ .

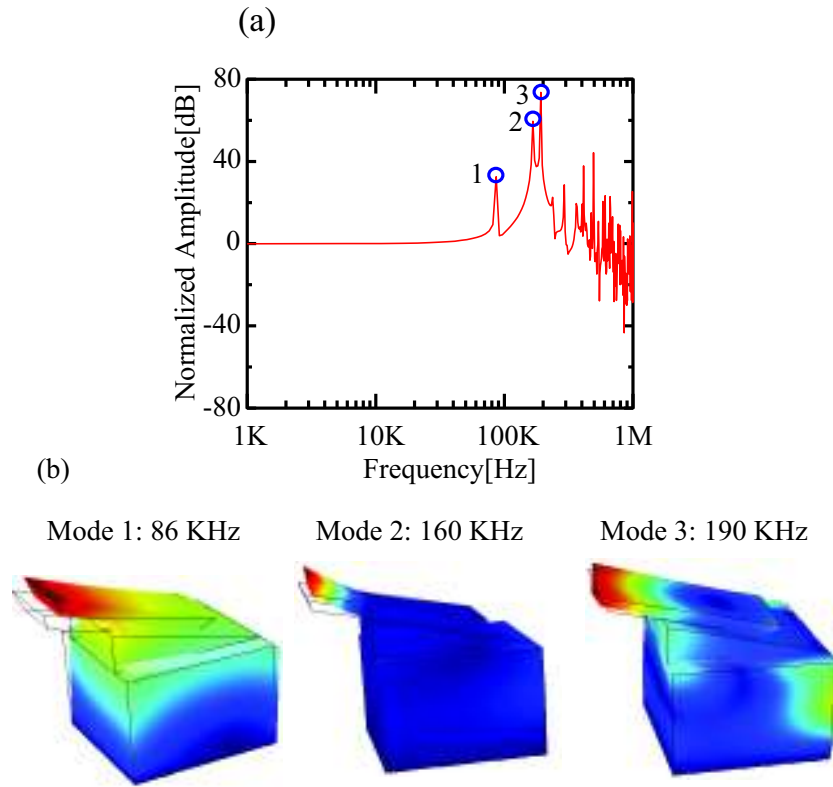


Figure 3.4: Simulation of rectangular shape cantilever stage as a simplest type of stage and its (a)Amplitude and (b)vibration modes

### 3.2.5 Preparation of Phosphate Buffer Saline(PBS)

A phosphate buffer saline is salty buffer to use especially in biological applications. This buffer can be prepared in the PH from 2 to 12. But it commonly was prepared in the PH around 7 and we prepared this solution by MilliQ water in our experiments(PH  $\approx$  5.5). To prepare this solution we will follow some steps. After washing the bottle,in which we want to use for storing this solution,to remove the possible contamination from the bottle, we will take 200 ml MilliQ water and use 1 tablet of phosphate buffered saline(SIGMA-ALDRCH)in which contains 1.9g of material. As dissolving of tablet takes long time,after slightly shaking the bottle, we will leave it in the refrigerator for a 24 hours.We can make a note on the bottle and explain the preparation date and solution name.This solution can be used for 6 months if we keep it in the refrigerator during this period. In addition before every use of this solution in experiment ,we have to use the filter and syringe to remove the contamination from solution.



Figure 3.5: Phosphate Buffered Saline(PBS) solution

### 3.2.6 Experimental details

FEA software (COMSOL Metaphysics, COMSOL) was used for theoretical analysis of the frequency response and vibration modes of the scanner. We used Young's Modulus of 193 GPa, Poisson's ratio of 0.25 and density of  $7970 \text{ kg/m}^3$  for modeling the scanner bodies made of SS316. For modeling the stack piezoactuators, we used density of  $7500 \text{ kg/m}^3$ .

We measured frequency response of the developed scanner by frequency response analyzer (FRA5097, NF). We measured displacement of the  $Z$  scanner by detecting the vibration of cantilever body attached to the cantilever stage using a heterodyne laser displacement sensor (ST-3761, IWATSU).

For AFM imaging, we used a home-built AFM system with an ultralow noise cantilever deflection sensor.<sup>28–30</sup>

To demonstrate the ability of new developed  $Z$  tip scanner to image in atomic resolution, we image the cleaved surface of the mica disc(= 12mm, Furuuchi chemical) by a cantilever with spring constant of  $\sim 85 \text{ N/m}$  (AC55) in phosphate buffered saline(PBS) solution and frequency mode AFM. For this experiment, we used a commercially available AFM controller (ARC2, Asylum Research).(Figure 3.6)

We performed contact-mode AFM imaging of a cleaved surface of a calcite crystal (Furuuchi Chemical) using a cantilever with a spring constant of  $\sim 2 \text{ N/m}$  (AC240, Olympus). We used the  $XY$  sample scanner and the HVAMP that previously developed.<sup>6</sup> This experiment was performed at room temperature in water.

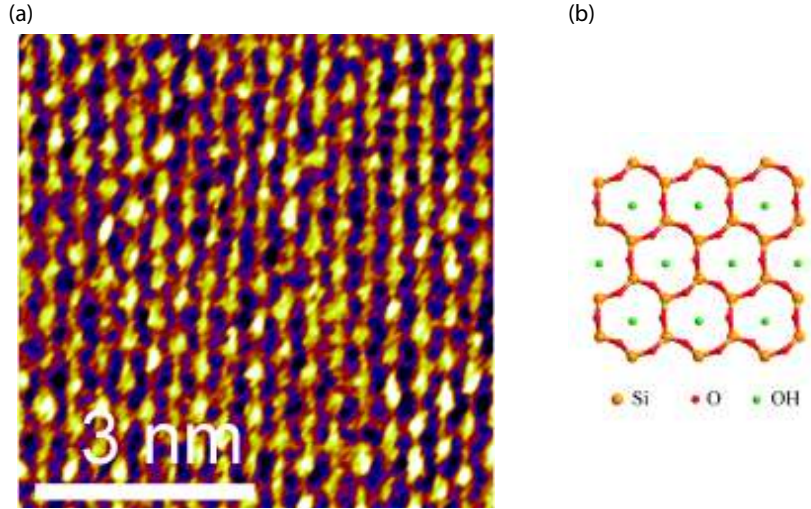


Figure 3.6: (a) Atomic resolution Imaging of mica surface with new  $Z$ tip scanner; (b) Model of mica surface

### 3.2.7 Results and Discussion

#### Simulation

Figure 3.7 shows frequency response of the  $Z$  scanners with different cantilever holding mechanisms calculated by FEA. These curves show several peaks corresponding to the vibration modes of the scanners. Figure 3.8 shows the first four vibration modes (Modes 1–4) of the  $Z$  scanners calculated by FEA. These vibration modes correspond to the peaks indicated by the circles in Fig. 3.7.

For all the designs, the lowest frequency peak (Mode 1) corresponds to the swinging motion of the actuator and the cantilever stage. Thus, the frequency of this vibration mode should determine the maximum frequency for driving the scanner. The results show that the frequency of Mode 1 obtained with the larger actuator (Figs. 3.2(a) and 3.2(b)) is higher than that with the smaller actuator (Figs. 3.2(c) and 3.2(d)). Due to the small width of the smaller actuator, the aspect ratio of the structure consisting of the actuator and the cantilever stage is relatively high. This should account for the lower frequency observed for the scanner with the smaller actuator.

The lowest frequency peaks of the curves in Figs. 3.7(b) and 3.7(d) are found at 47 kHz and 40 kHz, respectively. Although the result suggests that Design I provides slightly higher frequency, the difference is subtle. In contrast, the magnitude of the peak is significantly different between these two designs. The peak height in the curve obtained by Design II is much lower than that in the curve obtained by Design I. In Design I, the cantilever stage is laterally protruded from the side of

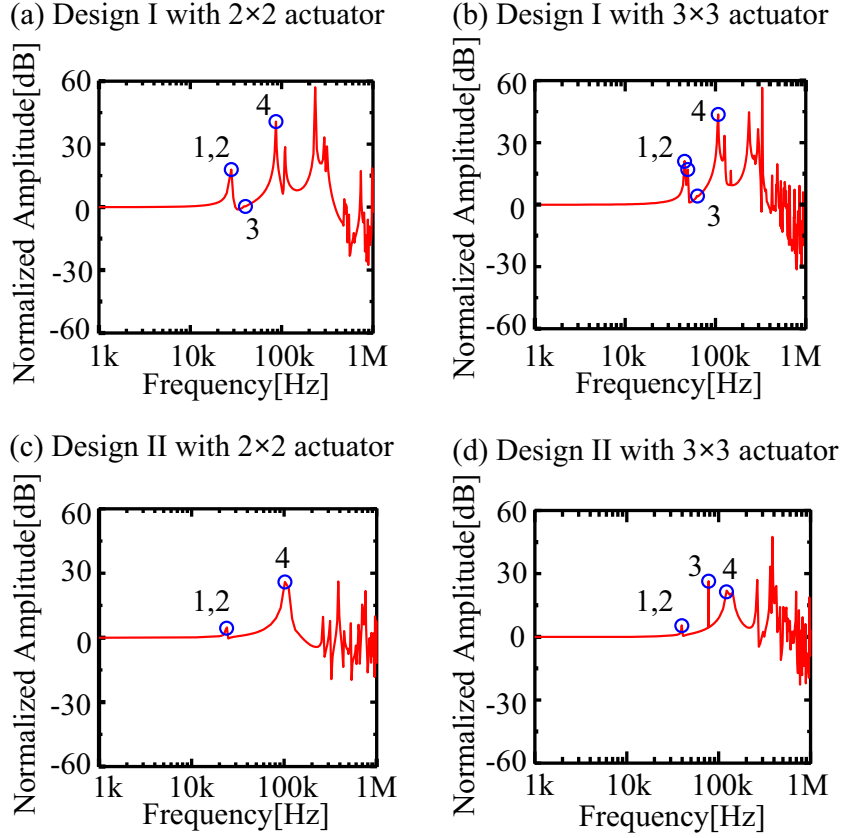


Figure 3.7: Frequency responses of the  $Z$  scanners with different cantilever holding mechanisms obtained by FEA.

the actuator. This should enhance the magnitude of the swinging vibration. These results suggest that Design II with a  $3 \times 3$  actuator should give the best performance among these designs.

## Experiments

Based on the analysis presented above, we have developed a  $Z$  tip scanner with Design II and a  $3 \times 3$  actuator. Figure 3.9(a) shows frequency response of the developed  $Z$  tip scanner. The amplitude curve shows a broad peak from 40 kHz to 130 kHz. This frequency range agrees with the frequencies of Modes 1–4 shown in Figs. 3.7(d) although they are not separately observed.

Figure 3.9(b) shows frequency response of the tip-sample distance regulation measured by contact-mode AFM with AC240 cantilever. The feedback gains are adjusted such that the bandwidth is maximized. The amplitude curve shows that  $-3$  dB bandwidth of the feedback regulation is  $\sim 6$  kHz. This is sufficient for performing high-speed AFM imaging at a few seconds per frame as demonstrated below. Figure 3.9(c) shows frequency response of the tip-sample distance regulation measured by

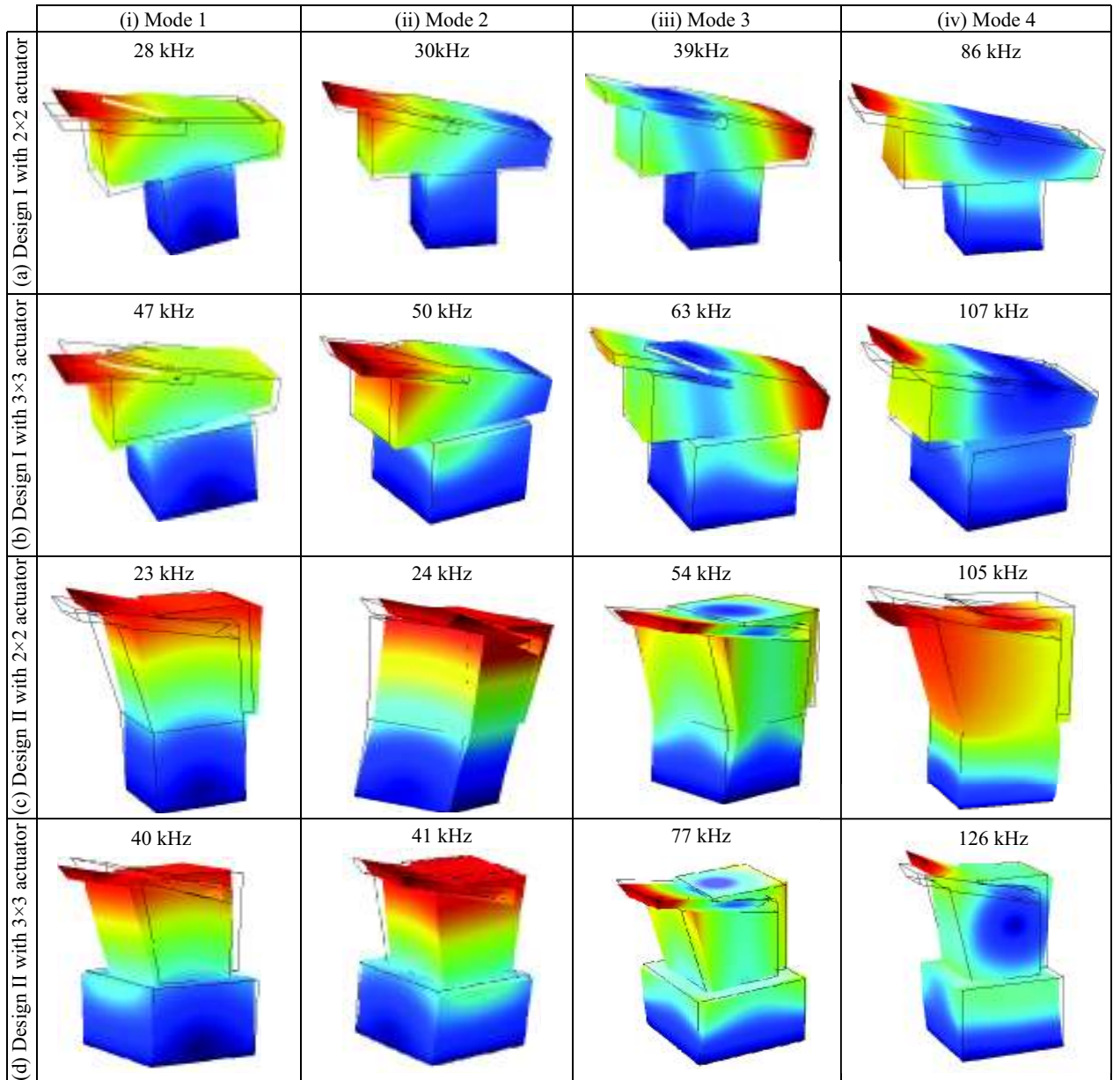


Figure 3.8: Vibration modes of the  $Z$  tip scanners with different cantilever holding mechanisms obtained by FEA.

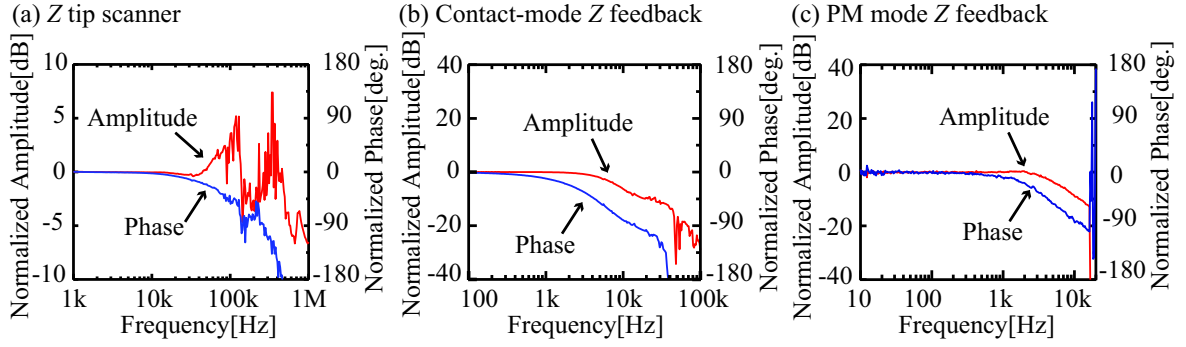


Figure 3.9: Frequency response of (a) the developed Z tip scanner; (b) Z feedback regulation measured in contact-mode AFM ;(c) Z feedback regulation measured in PM mode AFM.

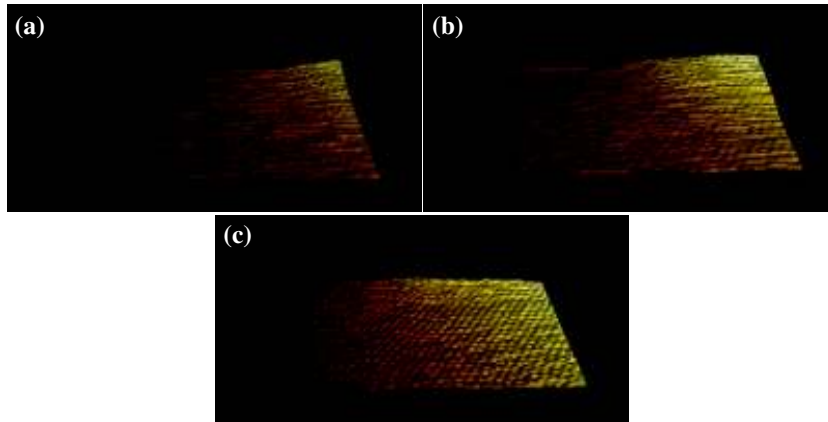


Figure 3.10: Snapshots of 44 successive contact-mode AFM images of calcite crystal dissolution process in water. (a) 0 s. (b) 40 s. (c) 80 s. Scan size:  $20 \times 10 \text{ nm}^2$ . Scan rate: 50 Hz. Imaging speed: 2 s/frame. Pixel size:  $200 \times 100 \text{ pix}^2$ . Tip velocity:  $4 \text{ }\mu\text{m/s}$ .  $f_{cr} = 5\text{--}8 \text{ kHz}$ .

PM-AFM. In this experiment we used phase detector system with AC55 cantilever. In this condition, by  $-5 \text{ dB}$  Amplitude the bandwidth of feedback is  $\sim 4.3 \text{ kHz}$ .

Figures 3.10 3.12 and shows snapshots of successive AFM images of calcite crystal dissolution process. The imaging was performed at 2 s/frame in water using contact-mode AFM. In spite of the fast scanning speed, the images show atomic-scale contrasts separated by  $\sim 0.5 \text{ nm}$ . The images also show that the movement of the upper terrace edge from the top right to the bottom left of the image.

The step edge in the image does not appear to be atomically sharp. This is probably due to the averaging of the interactions from several atoms. Such a nanoscale averaging often takes place in contact-mode AFM imaging.

Although we performed imaging in water, calcite crystal dissolution is observed. This is because the imaging was performed in an open liquid cell. Calcite is sparingly

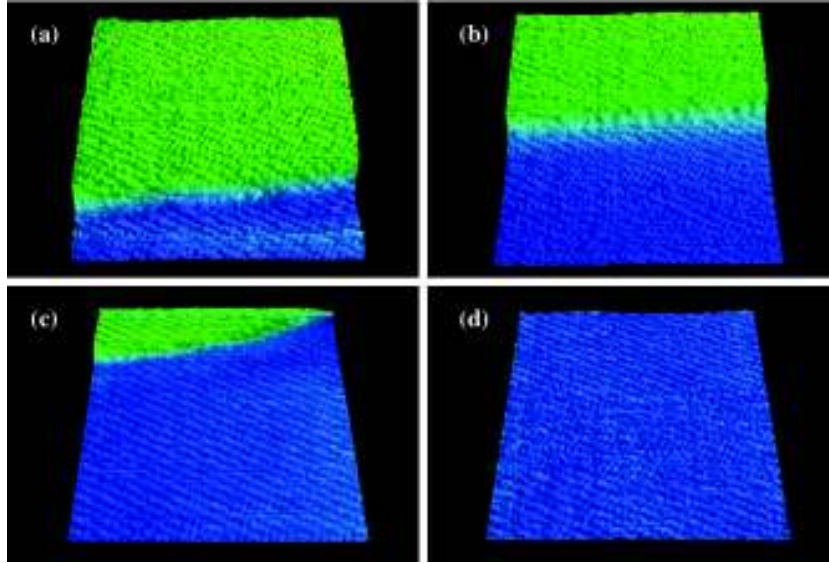


Figure 3.11: Snapshots of successive PM-AFM images of calcite crystal dissolution process in water. (a) 0 s. (b) 20 s. (c) 32 s. (d) 40 s. Scan size:  $20 \times 20 \text{ nm}^2$ . Scan rate: 250 Hz. Imaging speed: 2 s/frame. Pixel size:  $500 \times 500 \text{ pix}^2$ . Tip velocity:  $10 \mu\text{m/s}$ .

soluble in water. Thus, immediately after the immersion into water, dissolution process takes place and the imaging solution is soon saturated with the dissolved calcite. As water evaporates, the solution becomes supersaturated. In this way, we can observe crystal dissolution process at a relatively slow rate.

The atomic-scale corrugation period is 0.5–0.8 nm while the tip velocity was  $4 \mu\text{m/s}$ . Thus, frequency ( $f_{\text{cr}}$ ) of the corrugations that tip-sample distance regulation should follow is 4–8 kHz. This is close to the feedback bandwidth estimated from the frequency response curve shown in Fig. 3.9(b). The result demonstrates that the developed scanner is applicable to atomic-scale high-speed AFM imaging in liquid.

Figure 3.11 shows snapshots of successive PM-AFM images of calcite crystal dissolution process. In spite of the fast scanning speed (2 s/frame), the images show atomic-scale contrasts with a periodicity of  $\sim 0.5 \text{ nm}$ . The images also show that the movement of a step edge from the top to the bottom of the image. The atomically sharp step edge is visualized in the images, which demonstrates the true atomic resolution of the PM-AFM imaging. The result demonstrates that the developed scanner is applicable to atomic-scale high-speed AFM imaging in liquid.

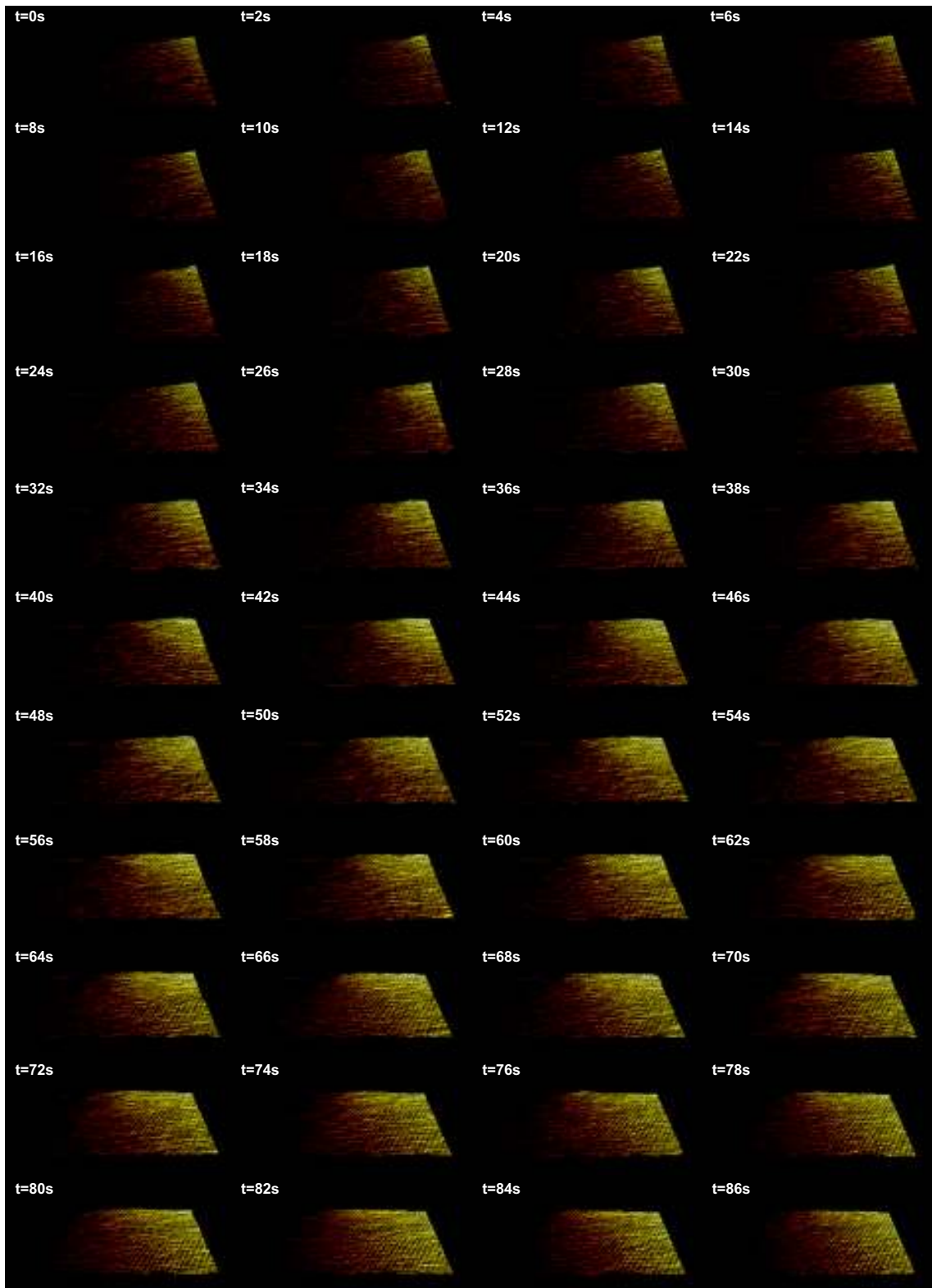


Figure 3.12: Snapshots of 44 successive contact-mode AFM images of calcite crystal dissolution process in water. Scan size:  $20 \times 10 \text{ nm}^2$ . Scan rate: 50 Hz. Imaging speed: 2 s/frame. Pixel size:  $200 \times 100 \text{ pix}^2$ . Tip velocity:  $4 \mu\text{m/s}$ .  $f_{\text{cr}} = 5\text{--}8 \text{ kHz}$ .

## 3.3 Counterbalance Z tip scanner

### 3.3.1 Basic design

One of the methods to improve the performance of Z scanner is counterbalance structure. In figure 3.17 we present setup of counterbalance structure. In this structure we placed same piezo material on the both side of the plate accurately. We did this experiment with different kind of the piezo and study the relationship between the kind of the piezo with performance of the structure. Also, The effect of the thickness of the plate on the performance of counterbalance system was discussed. Alignment of the piezo on the plate surface is very important. The small miss alignment of piezo was significant affect on the performance of counterbalance structure. Piezo are attached by glue on the plate. We used support plates and very heavy plates to control of the displacement and vibration of the main plate. The gape between the heavy plates should be as small as possible to avoid the vibration effect of the main plate on the performance of the counterbalance structure. Displacement of the piezo was measured by hetero-dyne laser displacement sensor (ST-3761, IWATSU).

### 3.3.2 Experimental detail

FEA software (COMSOL Multiphysics ,COMSOL) was used for theoretical analysis of resonance frequency and vibration modes of scanner. In simulation ,we define Young Modulus of 193 GPa ,Poisson ratio of 0.25 and density of 8030 kg/m<sup>3</sup> as a mechanical properties of scanner body that made of SS316L. As a stack piezo modeling we used density of 7500 kg/m<sup>3</sup>. Coupling and elasticity of them were determined by measuring the displacement and resonance frequency of piezo actuator fixed to a large body. Frequency resonance of developed scanner was measured by frequency response analyzer (FRA5097,NF). Displacement of Z counterbalance scanner was mapped by vibration of cantilever body fixed on the cantilever stage and using a hetero-dyne laser displacement sensor (ST-3761, IWATSU).

### 3.3.3 Simulation of Counterbalance Z tip scanner

Figure 3.17 shows schematic model of counterbalance z tip scanner . In this model we have 1 mm thickness plate in which pair of stack piezo by dimension of 3x3x2mm<sup>3</sup> was displaced concurrently by glue in opposite direction in precised way and counterbalanced. Cantilever stage mounted on the top of each piezo and fixed by glue. Cantilever supports by U shape plates that fixed by 2 screw to main body .All the metal parts are made by SS316L stainless steel. We check the efficiency of counterbalance by different thickness of plate and based on the height limitation and

performance of counterbalance system we decided to use 1 mm thickness plate. Furthermore, in order to balance the cantilever weight, a dummy mass is placed at the opposite end of the Z tip scanner.

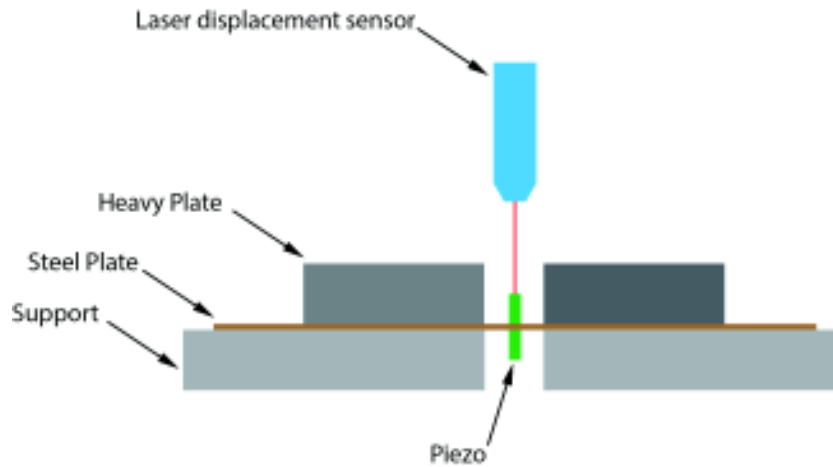


Figure 3.13: Schematic setup for checking counterbalance effect with changing the position of piezo and thickness of plate

### 3.3.4 Effect of changing the plate thickness on the performance of the counterbalance structure

we measure the performance of counterbalance structure by different plate thickness and study the effect of plate thickness on the performance. In figure 3.14, we measured the performance of the piezo with and without counterbalance structure system with 1mm, 2mm, 3mm and 5mm thickness plates. In any thickness using of the counterbalance system improves the performance. This improvement was happen not only in amplitude but also in phase curve. In frequency response curve without using the counterbalance system there are some vibration whereas by using the counterbalance system the vibration decreases. In both with and without counterbalance the resonance frequency is around 200kHz. By using the counterbalance system the phase curve became stable and the phase delay is decreases. Figure 3.14 shows that counterbalance system has good efficiency on the performance till 3mm plate thickness. In 5mm plate thickness the efficiency of counterbalance system is negligible. Although in comparing the amplitude, 1mm thickness plate has lower amplitude around 16dB but resonance frequency is same for all cases and its around 200kHz. In this study, all frequency resonances were measured by frequency response analyzer (FRA5097, NF) and displacements were mapped by using a hetero-dyne laser displacement sensor (ST-3761, IWATSU).

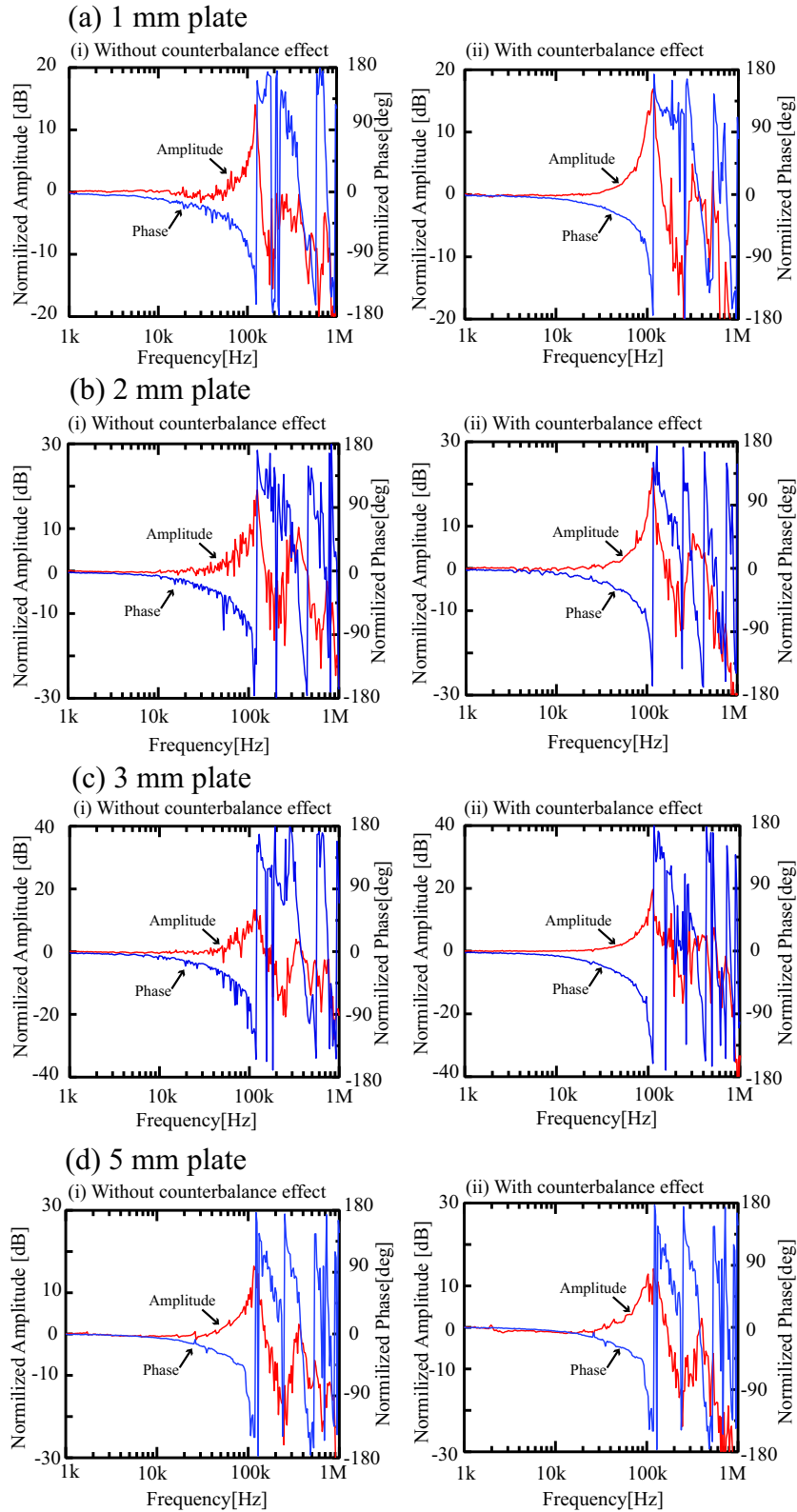


Figure 3.14: Effect of changing the plate thickness on the performance of the counterbalance structure with  $5 \times 3 \times 2 \text{ mm}^3$  piezo in which planed on the center of the plate; (a)1mm palte; (b)2mm plate; (c)3mm palte; (d)5mm plate.

### 3.3.5 Effect of changing the type of piezo on the performance of the counterbalance structure

In this section ,we want to study the relationship between kind of the piezo with the performance of counterbalance system. In the effect of the thickness of plate on the performance, 1mm thickness plate has low amplitude in resonance frequency. On the other hand ,based on the height limitation, 1mm thickness plate has useability on our  $Z$  scanner. So, we used 1mm thickness plate as a main plate during this experiment. In this study, we attached 3 different kind of piezo( $2 \times 2 \times 2mm^3$ ,  $3 \times 3 \times 2mm^3$  and  $2 \times 3 \times 5mm^3$ ) on the 1mm thickness plate and study of piezo effect on the performance. In  $2 \times 2 \times 2 mm^3$  and  $3 \times 3 \times 2mm^3$  piezo resonance frequency are around 230kHz and 280kHz respectively but in  $2 \times 3 \times 5 mm^3$  is around 120kHz. In  $2 \times 2 \times 2 mm^3$  and  $3 \times 3 \times 2mm^3$  piezo phase delay reaches to  $180^\circ$  around 240kHz whereas in  $2 \times 3 \times 5 mm^3$  its around 110kHz. In  $2 \times 2 \times 2 mm^3$  piezo, there are some vibration on phase delay curve but  $3 \times 3 \times 2mm^3$  has stable manner. There are some vibration on the  $3 \times 3 \times 2mm^3$  piezo amplitude curves in which related to the small misalignment of the piezo on attachment on the plate. In this study, all frequency resonances were measured by frequency response analyzer (FRA5097,NF) and displacements were mapped by using a hetero-dyne laser displacement sensor (ST-3761, IWATSU).

### 3.3.6 Effect of changing the piezo position on the performance of the counterbalance structure

Figure 3.16 shows the simulation result of effect of changing piezo position in the center or edge of 1 mm plate on the performance of the counterbalance structure scanner. In both cases first vibration mode happens in  $\sim 40$  kHz. While the resonance frequency on the center and edge are in  $\sim 120$  kHz and  $\sim 190$  kHz respectively. In total the trace of both arrangement are same.

### 3.3.7 Asymmetric actuating system

In asymmetric structure the vibration transfer from piezo to the base is negligible. This property can suggest an idea in the mind to use for  $Z$  scanner. Asymmetric actuating structure consist of 2 piezo in which attached in one side to each other . On of the piezos has duty of actuating the system and other one is used for counterbalancing the system. Main idea of this system comes from this point that mass center of the whole system during the actuation be stable and move. By this idea transferred vibration of actuating to the base will be as less as possible. In figure 3.21 the schematic setup of piezo was introduced. A pair of piezo attached to

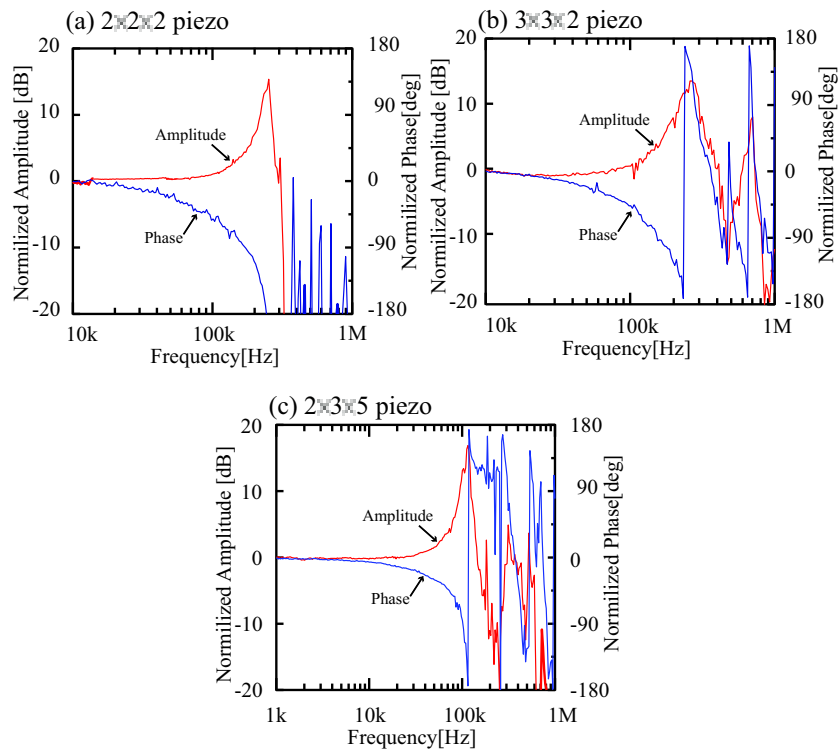


Figure 3.15: Effect of changing the type of piezo on the performance of the counterbalance structure with 1 mm plate in which piezos placed on the center of the plate

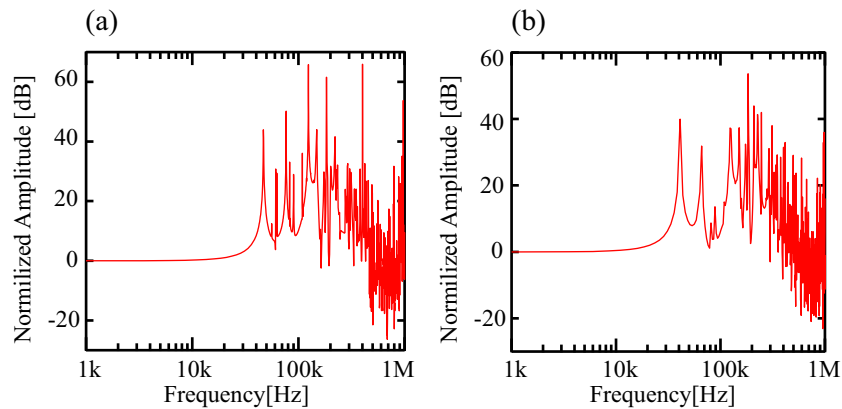


Figure 3.16: Effect of changing the piezo position on the performance of the counterbalance structure with 1 mm plate; piezo attached at the (a)Center and (b)Edge of plate

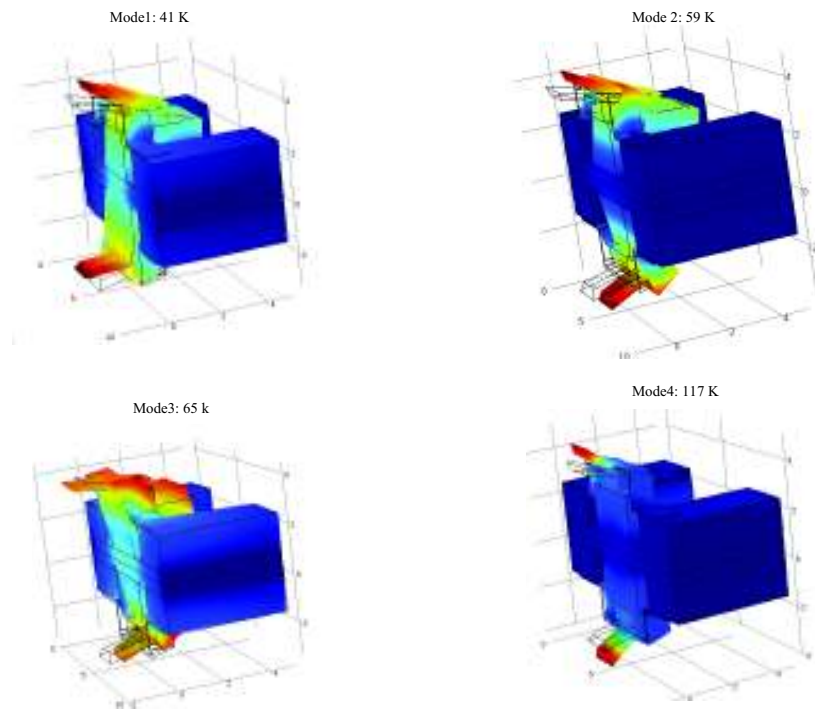


Figure 3.17: Simulation result of counterbalance structure at the edge of the 1 mm plate and its first 4 modes

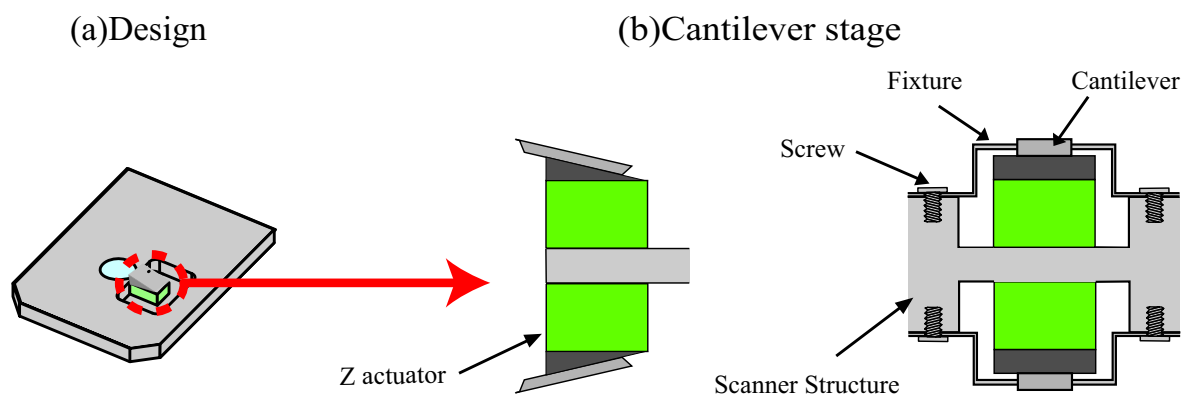


Figure 3.18: Schematic of perpendicular arrangement of counterbalance  $Z$  tip scanner; (a)Design (b)Cantilever stage.

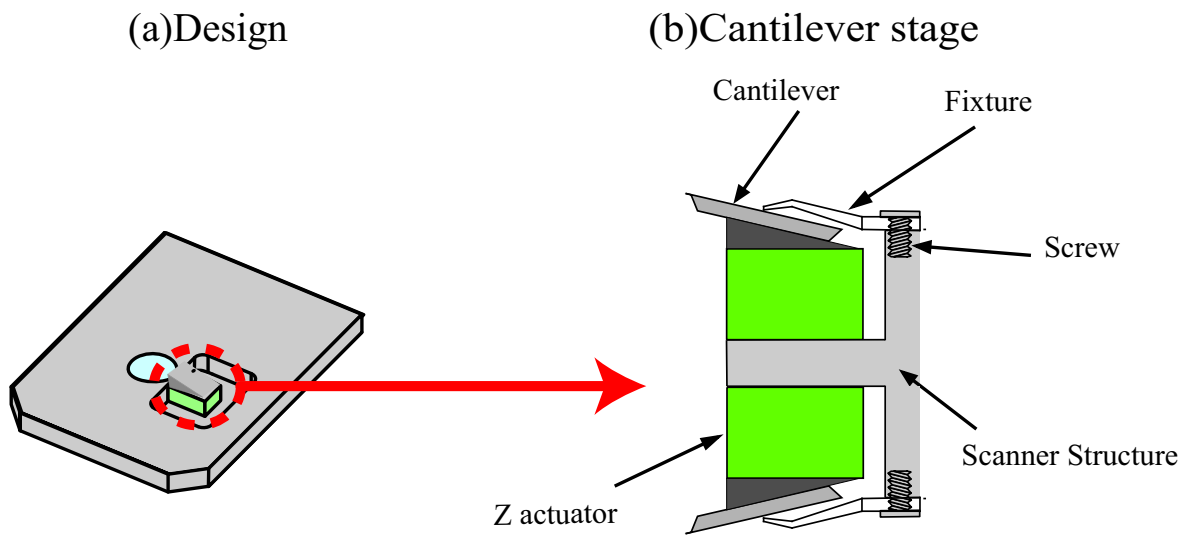


Figure 3.19: Schematic of parallel arrangement of counterbalance  $Z$  tip scanner; (a) Design (b) Cantilever stage.

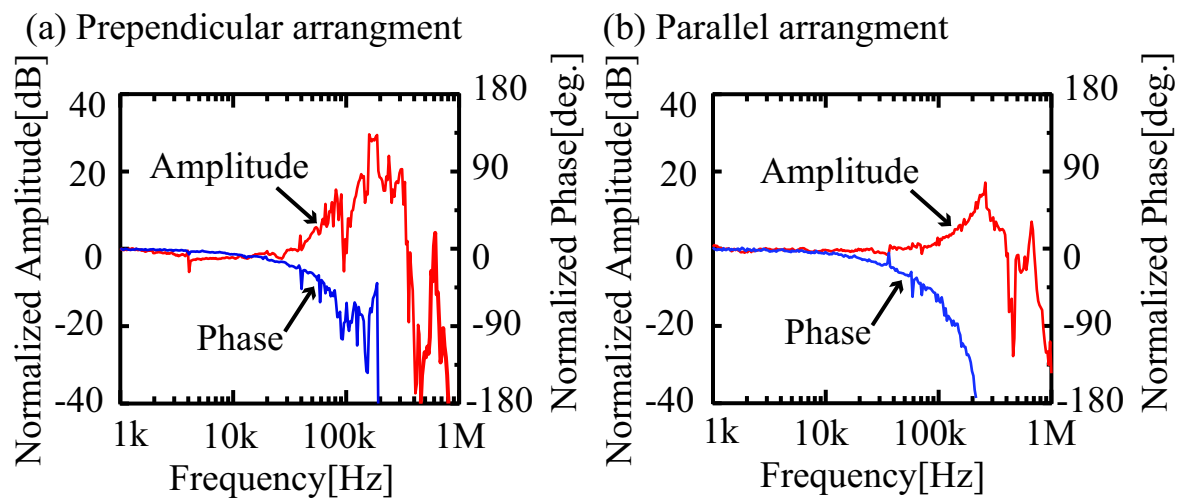


Figure 3.20: Performance of the counterbalance  $Z$  tip scanner (a) Perpendicular arrangement (b) Parallel arrangement

the each other while the top of actuator 1 is used for generating the displacement, the bottom of the piezo is firmly fix to the base. In figure 3.21(a) mass center of every piezo(green point) and total mass center(red point)was represented. While the piezo 2 is actuating the pizo 1 is used to contract(or extend) for compensating synchronous to keep mass center pf whole structure motionless. As the same piezos are used for this purpose, so the applied voltage for actuating should be different with each other. There is calculation for finding the relationship between applied voltages to piezos. Based on the calculation;  $V_1 = -\frac{V_2}{3}$ .  $V_1$  and  $V_2$  represent applied voltages for piezo 1 and piezo 2 respectively. In figure 3.22we simulate the  $2 \times 2 \times 2mm^3$  piezo that attached to the end of cantilever beam. Cantilever beam dimension is  $50 \times 5 \times 1mm^3$ . The vibration amplitude of beam end monitored. Ten first vibration modes are demonstrated in figure 3.22. Figure 3.23 shows the effect of this system on the suppressing the vibration during the actuating. Amplitude values through without(red line) and with(blue line) using the asymmetric actuating system was displayed. Its clearly obvious that by using this system amplitude of vibration modes decreased significantly on order of magnitude. It shows that this system has good efficiency for damping the vibration.

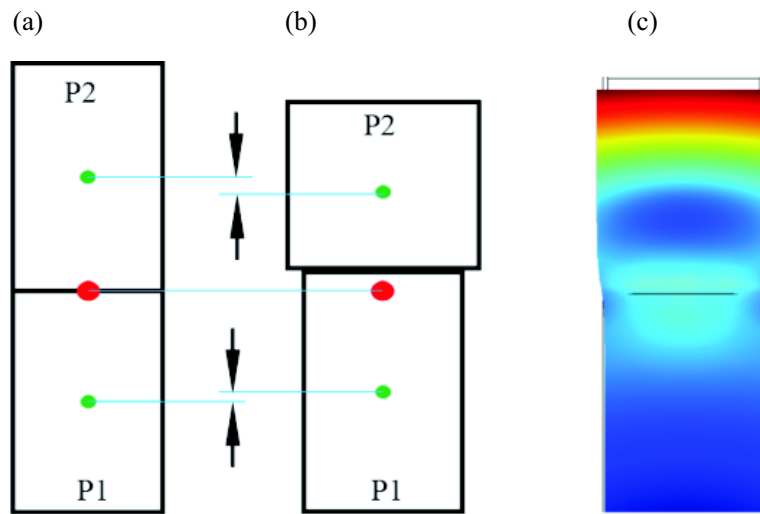


Figure 3.21: Asymmetric actuating system (a)Simplified theoretical model (undeformed) ; (b)Simplified theoretical model (deformed) ; (c) Finite element model

### 3.4 Summary

In this study, we have compared the performance of high-speed  $Z$  tip scanners with a screw cantilever holding mechanism. The investigated designs are different in the actuator size and the screw arrangement (Fig. 3.2). We have investigated frequency

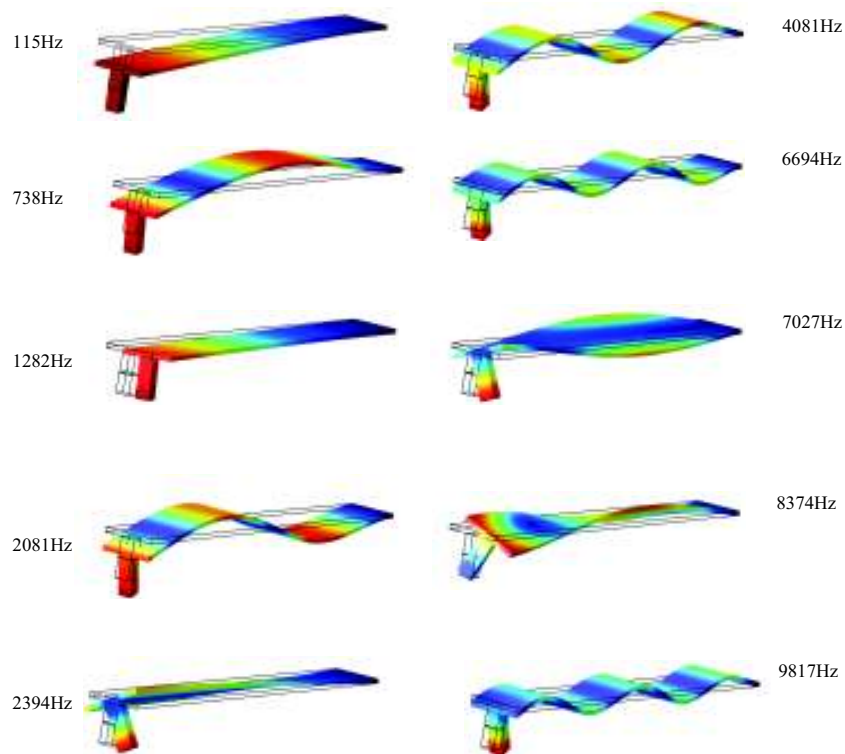


Figure 3.22: Asymmetric actuating system vibration modes

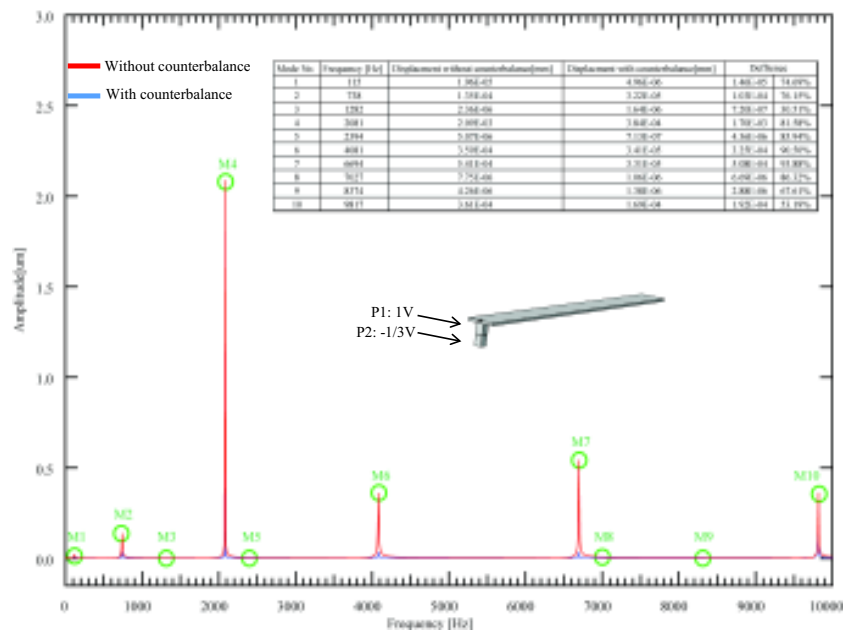


Figure 3.23: Simulation of performance of asymmetric actuating system and damping the amplitudes

responses and vibration modes of these scanners by FEA (Figs. 3.7 and 3.8). The results reveal that the vertical screw arrangement with a larger actuator should give the best performance. Based on this design, we have developed a  $Z$  tip scanner and measured its performance. The frequency response of the developed scanner shows a broad peak from 40 kHz to 130 kHz as expected from the FEA results. The frequency response of the tip-sample distance regulation shows  $-3$  dB bandwidth of  $\sim 6$  kHz. Finally, we have demonstrated high-speed atomic-resolution imaging of calcite crystal dissolution process using the developed scanner. The result shows that the developed scanner is applicable to atomic-resolution imaging at a few seconds per frame in liquid.

# Bibliography

- [1] G. Binnig, C. F. Quate, and Ch. Gerber. *Phys. Rev. Lett.*, 56:930–933, 1986.
- [2] T. Ando, N. Kodera, E. Takai, D. Maruyama, K. Saito, and A. Toda. *Proc. Natl. Acad. Sci. USA*, 98:12468, 2001.
- [3] A. D. L. Humphris, M. J. Miles, and J. K. Hobbs. *Appl. Phys. Lett.*, 86:034106, 2005.
- [4] J. H. Kindt, G. E. Fantner, J. A. Cutroni, and P. K. Hansma. *Ultramicroscopy*, 100:259, 2004.
- [5] G. E. Fantner, G. Schitter, J. H. Kindt, T. Ivanov, K. Ivanova, R. Patel, N. Holten-Andresen, J. Adams, P. J. Thurner, I. W. Rangelow, and P. K. Hansma. *Ultramicroscopy*, 106:881, 2006.
- [6] K. Miyata, S. Usho, S. Yamada, S. Furuya, K. Yoshida, H. Asakawa, and T. Fukuma. *Rev. Sci. Instrum.*, 84:043705, 2013.
- [7] G. Schitter, P. J. Thurner, and P. K. Hansma. *Mechatronics*, 18:282, 2008.
- [8] I. S. Bozchalooi, K. Youcef-Toumi, D. J. Burns, and G. E. Fantner. *Rev. Sci. Instrum.*, 82:113712, 2011.
- [9] C. Braunsmann and T. E. Schäffer. *Nanotechnology*, 21:225705, 2010.
- [10] F. C. Tabak, E. C. M. Disseldorp, G. H. Wortel, A. J. Katan, M. B. S. Hesselberth, T. H. Oosterkamp, J. W. M. Frenken, and W. M. van Spengen. *Ultramicroscopy*, 110:599, 2010.
- [11] T. Fukuma, H. Okazaki, N. Kodera, T. Uchihashi, and T. Ando. *Appl. Phys. Lett.*, 92:243119, 2008.
- [12] T. Ando, T. Uchihashi, and T. Fukuma. *Prog. Surf. Sci.*, 83:337, 2008.
- [13] Y. K. Yong, S. O. R. Moheimani, B. J. Kenton, and K. K. Leang. *Rev. Sci. Instrum.*, 83:121101, 2012.

- [14] G. T. Paloczi, B. L. Smith, P. K. Hansma, D. A. Walters, and M. A. Wendman. *Appl. Phys. Lett.*, 73:1658, 1998.
- [15] N. Sanz, J. K. Hobbs, and M. J. Miles. *Langmuir*, 20:5989, 2004.
- [16] N. Kodera, D. Yamamoto, R. Ishikawa, and T. Ando. *Nature*, 468:72, 2010.
- [17] T. Uchihashi, R. Iino, T. Ando, and H. Noji. *Science*, 333:755, 2011.
- [18] K. Miyata, H. Asakawa, and T. Fukuma. *Appl. Phys. Lett.*, 103:203104, 2013.
- [19] T. Fukuma, M. Kimura, K. Kobayashi, K. Matsushige, and H. Yamada. *Rev. Sci. Instrum.*, 76:053704, 2005.
- [20] T. Fukuma and S. P. Jarvis. *Rev. Sci. Instrum.*, 77:043701, 2006.
- [21] T. Fukuma. *Rev. Sci. Instrum.*, 80:023707, 2009.

# Chapter 4

## Capasitive sensor

### 4.1 Introduction

Atomic force microscopy (AFM) has a wide growing application in different fields of science as a metrological AFM so accuracy is a main parameter in the scanning system.<sup>1-3</sup> Atomic force microscopy consist of the mechanical and electrical components. Every components has it own properties. During the imaging some phenomena such as drift, creeping, non linearity of mechanical and electrical components and hysteresis may affect accuracy of the AFM image. For example, in commercial AFM drift may vary from 1 to 10 nm/s. So, long range study of samples face with very big problem. In fact, there are not enough research in this fields. Metrological AFM could be mentioned a probe in a high accuracy precision positioning known as a sub atomic measuring machine (SAMM).<sup>4</sup> Lang range scanning stage<sup>5,6</sup> was developed by using maglov linear motors. In this scanning stage linear motors was used to position an oil-floated platen in 6 degree of freedom with range of 25 mm 25 mm 0.1 mm. The purpose of this this experiment was demonstrating the stage motion errors from scanning probe microscopy (STM). Nonetheless, it was not successful experiment. The great measurements have been achieved applying a metrological confocal microscope by Dr. Robert Hocken and Dr. Chunhai Wang<sup>7</sup> These data are demonstrated sub nano meter resolution (1 nm repeatability) in the order of 30 nm accuracy. Also the precise motion control needs an accurate scan and position the tip at sub nanometer scale. To achieve high accuracy in AFM, the system scales should be calibrated. on the other hand, developing of the metrological AFM was done by some researchers.<sup>1-3,8</sup> They introduced prototype of SAMM AFM with reimbursing of relationship between drive voltage and head displacement. In fact, piezo actuator is one of the best candidate for this purpose.<sup>9</sup> Moreover, charging control,<sup>10</sup> capacitor insertion,<sup>11</sup> post-processing technique<sup>12</sup> and feed forward control<sup>13</sup> are applicable to remove undesired displacement of AFM head. Although, these

methods do not have direct affect on the error but they can limited the unwanted displacements. Furthermore, using of separate single axes piezo actuator in hoight with lateral stage for horizontal motion in 2 axes may improve avoiding nonliterary of the axes cross talk.<sup>14,15</sup> Also, capacitance sensor at the prob tip was monitored for displacment estimation.<sup>16-18</sup> So, I aim to find solution to this problem. By having a wide research and checking the possible ways, I found that I can use crystal oscillator as a part of capacitive sensor to detect amount of unwanted displacement. I introduced capacitive sensor system and still working on it to develop and use in XY scanner.

## 4.2 Theory

Figure4.1 is the schematic of capacitive detection system in which by changing of the lever deflection the capacitance of lever and reference plate will be change and displacement of the lever can be calculated. We want to detect the displacement of lever by measuring the change of the capacitance.It is obvious that if the system has higher Q-factor the sensitivity will be higher.By excitation of the lever in its resonance frequency,any changes in the capacitive will cause to shift the frequency curve.

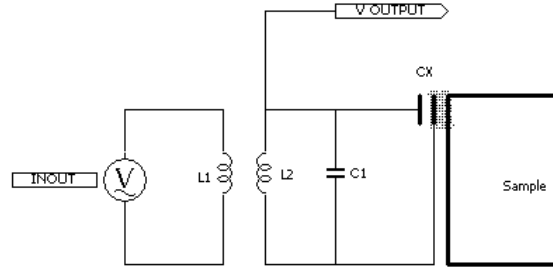


Figure 4.1: Schematic of Capacitance Detection System

Based on the Lorentzian curve ,the voltage across tuned circuit,as a function of frequency is given by :

$$V = \frac{V_0}{\sqrt{1 + 4Q^2\Delta f^2/f_0^2}} \quad (4.1)$$

Where  $\Delta f = |f - f_0|$ , and  $V_0$  is the voltage at the resonance frequency ,  $f_0$  is resonance frequency and  $Q$  is the quality factor of the system.

For LC circuite we have

$$f_0 = \frac{1}{2\pi\sqrt{LC}} \quad (4.2)$$

where  $Q$  is the quality factor and  $L$  is the inductance. By derivation of this equation we can get:

$$\frac{d_f}{d_c} = \frac{1}{2\pi} \frac{-L}{2} (LC)^{-\frac{3}{2}} \quad (4.3)$$

on the other hand ,we have  $(LC)^{-\frac{1}{2}} = 2\pi f$

So,by combining this two equations we will reach to:

$$\frac{d_f}{d_c} = \frac{1}{2\pi} \frac{-L}{2} (LC)^{-1} \times 2\pi f \quad (4.4)$$

by simplifying we have

$$\frac{d_f}{d_c} = -\frac{2\pi f L}{4\pi LC} \quad (4.5)$$

and;

$$\frac{d_f}{d_c} = -\frac{f}{2C} \quad (4.6)$$

So,

$$\frac{d_f}{d_c} = -\gamma \frac{f}{C}$$

where  $\gamma = -\frac{1}{2}$

in the schematic circuit of capacitive detection system by replacing the displacement between sample and lever as a capacitance we can simplify the circuit and calculate the impedance as below. Figure 4.2 is schematic of capacitance detection system.

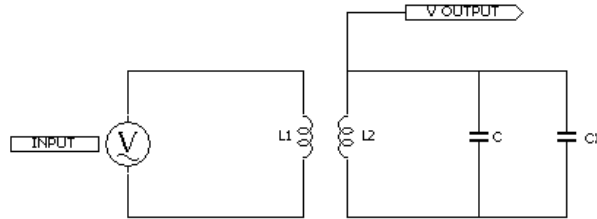


Figure 4.2: Circuit of capacitive Detection system

We can simplify the transformer with below circuit (Figure 4.3).  
the impedances are :

$$Z_3 = j\omega(L_2 - M) + \frac{1}{j\omega C_1} + \frac{1}{j\omega C_x} \quad (4.8)$$

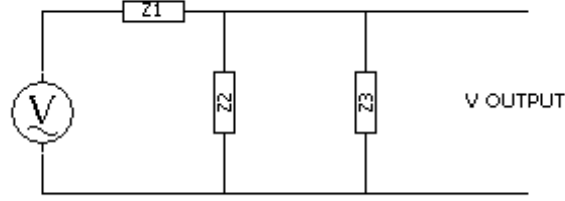


Figure 4.3: Equivalent circuit of the circuit of capacitive detection system

$$Z_1 = L_1 - M \quad (4.9)$$

$$Z_2 = M \quad (4.10)$$

where the  $L_1$  and  $L_2$  are the inductance of solenoid and  $M$  is the internal impedance of the solenoids.  $C_1$  and  $C_x$  are the capacitance of system. Based on the above figures and equations, relation between input and output is:

$$V_o = \frac{Z_2 || Z_3}{Z_1 + Z_2 || Z_3} V_i \quad (4.11)$$

$V_o$  and  $V_i$  show the output and input voltage respectively. By inserting the value of  $Z_1$ ,  $Z_2$  and  $Z_3$  in above equation we have :

$$\frac{V_o}{V_i} = \frac{1}{\frac{L_1}{M} + \frac{L_1 - M}{L_2 - M - \frac{1}{w^2(C + C_x)}}} \quad (4.12)$$

In the resonance frequency we can write:

$$w = w_0 \quad (4.13)$$

So,

$$w_0 = \frac{1}{\sqrt{(L_2 - M)(C_x + C_1)}} \quad (4.14)$$

By changing the capacitance the resonance frequency will be shift and this shift cause the change on the voltage. So, for determining the sensitivity of the circuit based on the derivation of  $\frac{dV}{df}$  and  $\frac{df}{dC}$  we can write:

$$\delta V = \frac{dV}{df} \frac{df}{dC} \delta C \quad (4.15)$$

Palmer in 1982 define the equation  $\frac{dV}{df} = \alpha \frac{V_0}{B}$  The bandwidth (B) of the circuit is obtained from

$$B = 2|f_{3dB} - f_0| \quad (4.16)$$

where  $f_{3dB}$  is that frequency for which the amplitude decreases by a factor of  $\sqrt{2}$  from its maximum value, or the power decreases by  $3dB$ .  $Q$  is related to the bandwidth  $B$  by

$$Q = \frac{f_0}{B} \quad (4.17)$$

coefficient  $\alpha$  for the  $f = f_{6dB}$  is equal to  $\frac{\sqrt{3}}{4}$ .

So, we can write :

$$\delta V = \gamma \frac{f}{C} \alpha \frac{V_0}{B} \delta C \quad (4.18)$$

Based on the equation ,by increasing the resonance frequency or using the smaller capacitance the sensitivity will be increase.  $C$  is combination of the  $C_1$  and  $C_x$  in which they are in parallel with each other. Then;

$$C = C_1 + C_x \quad (4.19)$$

on the other hand;

$$C_x = \epsilon_0 \frac{wl}{z} \quad (4.20)$$

where  $\epsilon_0$  is the permittivity of free space,  $l$  and  $w$  are the length and width of each of the two plates, and  $z$  is their separation. Assume now that the lever vibrates around its equilibrium position,  $z_0$ ,

$$z = z_0 + A \sin(\Omega t) \quad (4.21)$$

$$\frac{1}{z} = \frac{1}{z_0} \left( 1 + \frac{A}{z_0} \sin(\Omega t) \right) \quad (4.22)$$

$$\frac{1}{z} = \frac{1}{z_0} \frac{1}{1 + \frac{A}{z_0} \sin(\Omega t)} \quad (4.23)$$

$$\frac{1}{z} = \frac{1}{z_0} \left( 1 + \frac{A}{z_0} \sin(\Omega t) \right)^{-1} \quad (4.24)$$

Based on the tailor series;

$$\frac{1}{z} = \frac{1}{z_0} \left[ 1 - \frac{A}{z_0} \sin(\Omega t) \right] \quad (4.25)$$

So;

$$C_x = \epsilon_0 \frac{wl}{z} \quad (4.26)$$

$$C_x = \epsilon_0 \frac{wl}{z_0} \left[ 1 - \frac{A}{z_0} \sin(\Omega t) \right] \quad (4.27)$$

while;

$$C_x = C_{x_0} + \delta C_x \quad (4.28)$$

$$C_{x_0} = \epsilon_0 \frac{wl}{z_0} \quad (4.29)$$

Then;

$$\delta C_l = \epsilon_0 \frac{wl}{z_0^2} A \sin(\Omega t) \quad (4.30)$$

in conclusion;

$$\delta V = \alpha \gamma \frac{V_0 f}{BC} \epsilon_0 \frac{wl}{z_0^2} A \sin(\omega t) \quad (4.31)$$

$$\beta = \alpha \gamma \frac{V_0 f}{C B} \epsilon_0 \frac{wl}{z_0^2} \quad (4.32)$$

$$\beta = \alpha \gamma f B \frac{1}{z_0} \quad (4.33)$$

$\beta$  is sensitivity of capacitive detection system. It means that for having high sensitivity ,we need high  $Q$  factor and operating high frequency. To maximize the sensitivity , the f.Q should be maximized.

### 4.3 Experiment

Based on the theory of capacitive detection sensor ,we design the circuit as figure 4.4.

and as a  $C_x$ , we make the capacitance by micrometer. Instead of the parallel plates of capacitance in one side there is  $2 \times 2 \times 2$  metal piece that has thread hole for wiring on the top of piezo device and on the other hand the micrometer spindle used (Figure 4.5).

In current version of scanner ,we use separate type of  $Z$  tip scanner and  $XY$  scanner. Piezo actuator are used in concurrent arrangement in  $X$  and  $Y$  axis. I aim to replace one of the piezo actuator in every axis with capacitive sensor. My proposed capacitive sensor consist of 2 metal plates in which separated by insulator

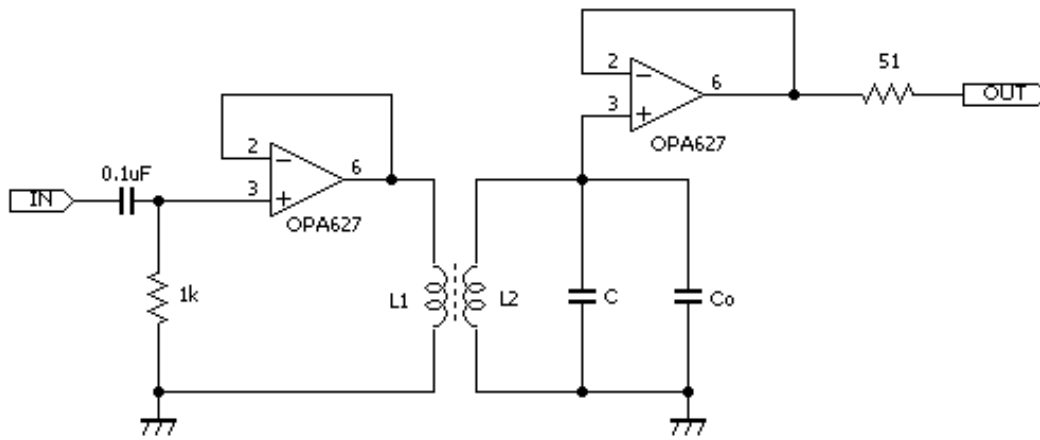


Figure 4.4: First experimental circuit for detection of effect of changing capacitance on the output

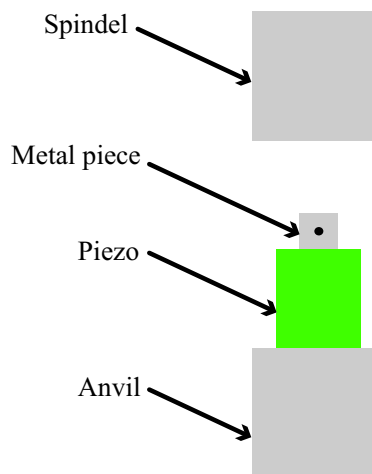


Figure 4.5: Using of the micrometer anvil and spindle instead of the capacitance plates and changing the distance of those to check of capacitance changes and effect of this changment on the output

from each other with several micrometer thickness. One of the metal plates attaches to the sbody by glue and other one connected to the crustal oscillator for detecting the displacement changes(Figure 4.6). At the back side of the movable metal plates, frequency detection circuit was placed to transfer the frequency shift as a output to the PLL.

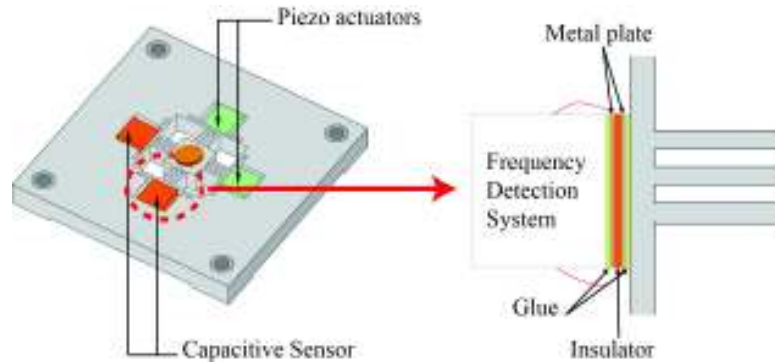


Figure 4.6: Using the capacitance detection sensor on the *XY* scanner

I used crystal oscillator by nominal peak frequency equal to 10 MHz and measure the peak frequency of circuit with different values of capacitance load range from 10 pF to 100 pF in seri arrangement(Table 4.1).

The results show that by increasing the capacitance load the peak frequency will be decrease. This decrement has linear relationship with capacitance load. I plot the function of the capacitance load(Figure 4.7). The red line shows the original values point by point respectively. Blue line is a linearized values. The difference between red and blue lines is negligible. So, I can conclude that frequency shift as capacitance load has linear relationship.

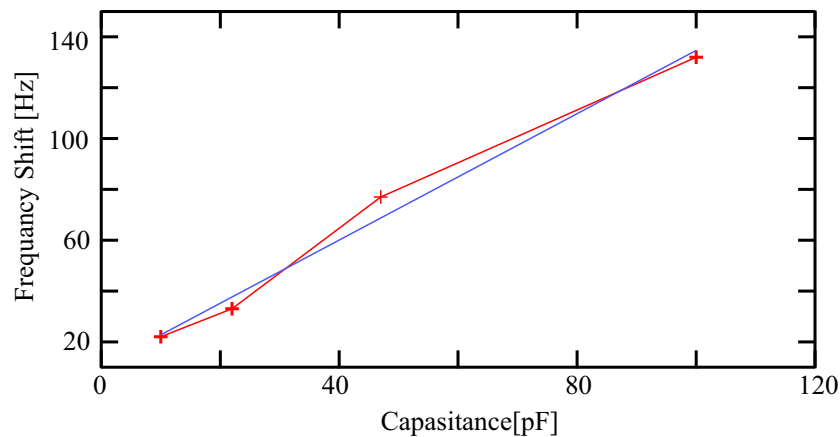


Figure 4.7: Estimation of the sensitivity of the capacitive sensor system based on the Frequency shift vs capacitance curveby nominal 10 MHz crystal oscillator

Table 4.1: Estimation of the sensitivity of the capacitive sensor system based on the Frequency shift vs capacitance curve

Capacitance[pF]	Peak Frequency[MHz]	Frequency Shift[Hz]
Open	9.998661	—
10	9.998638	22
22	9.998628	33
47	9.998584	77
100	9.998529	132

Figure 4.8 shows the affect of capacitance load on the frequency peak. Capacitance changes from 2.2 pF to 100 pF that connected in the seri and parallel arrangement with 2 MHz crystal oscillator. In figure 4.8(a) amplitude vs frequency were plotted in both of seri and parallel arrangement. As it is obvious in 2 MHz we have very sharp peak with high Q factor. In the figure 4.8(b) phase vs frequency were plotted. Figure 4.8(c)and (d) show resonance frequency and Q factor as a function of capacitance loads. In seri arrangement except of 10 pF capacitance load by increasing the capacitance load the resonance frequency and phase peak will be decrease while in parallel arrangement we dont have exception. In seri arrangement Q factor is a 42500 from 2.2 pF to 10 pF while from 22 pF to 100 pF it changes to about 43500. In 44 pF it is about 42500. In parallel arrangment Q factor is about 62500 in the range of 2.2 pF to 10 pF while it switch to 64500 in range of 22 pF to 100 pF.

To have atomic resolution image the signal to noise ratio should be very high.It means that, our system must insulated from noise sources. In using of the crystal oscillator to have a better result we have to use crystal oscillator with higher resonance frequency. This high resonance frequency in order of several MHz may create noise in our system. So, we have to decrease the frequency less than 5 MHz. For this porpuse we have 2 alternative;using of the local oscillator with low pass filter and PLL (figure 4.9(a))or voltage control oscillator with loop filter(Figure 4.9(b)).

In figure 4.10 ,frequency shift and resonance frequency as a function of capacitance was plotted. I found that if crystal oscillator with 100 MHz nominal resonance frequency was use in seri with the different capacitance load,the shifted resonance is stable between 3 pF to 10 pF. In this range it has a second order shape curve in which has good agreement with the real condition. So, based on the stable area capacitance ,we can calculate and optimize the capacitive sensor dimension and insulator material. For having a wid3e range of stable capacitance area, it is possible to examine other kinds of crystal oscillator . If the lower resonance frequency crystal oscillator was use in order of few 10 MHz ,the frequency down convertor circuit is

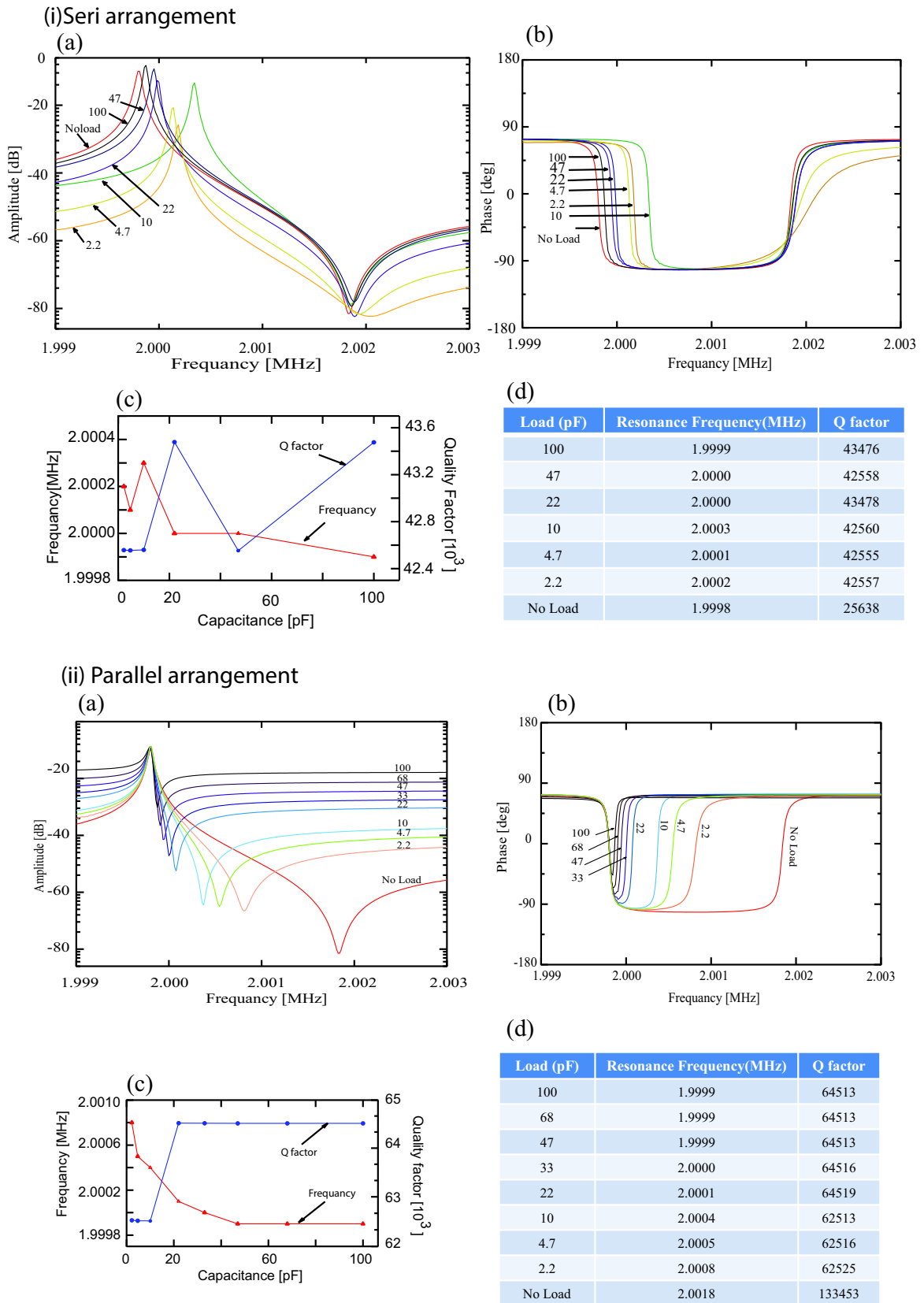


Figure 4.8: Using of the external capacitance in (i)seri arrangement (ii)parallel of internal capacitance of the capacitive sensor system

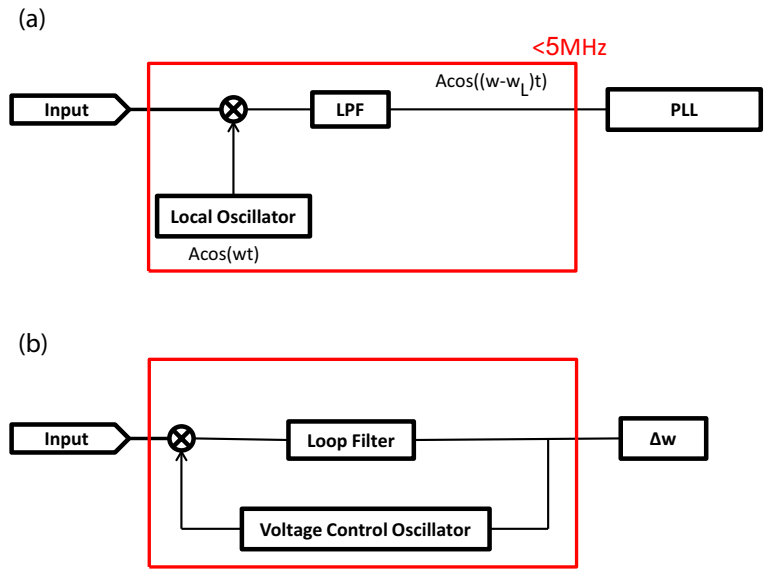


Figure 4.9: Frequency detection system

not needed.

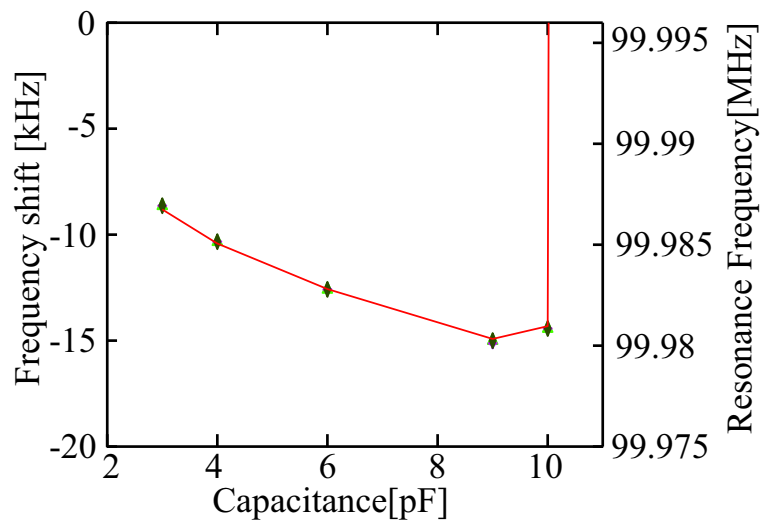


Figure 4.10: Acceptable range of capacitance for capacitive sensor with 100 MHz resonance frequency

# Bibliography

- [1] Stein AJ. *A metrological atomic force microscope. Masters thesis. Cambridge, MA: Massachusetts Institute of Technology, 2002.*
- [2] Mazzeo AM. *Accurate capacitive metrology for atomic force microscopy. Masters thesis. Cambridge, MA: Massachusetts Institute of Technology, 2005.*
- [3] Mazzeo AM, Stein AJ, Hocken RJ, Trumper DL *In Proceedings of ASPE 20th annual meeting*, vol. 37, 2005.
- [4] Hocken RJ, Trumper DL, Wang C. *Ann CIRP*,50(1):3736, 2001.
- [5] Holmes ML. *Analysis and design of a long range scanning stage. PhD thesis. Charlotte, NC: University of North Carolina at Charlotte, 1998.*
- [6] Holmes ML, Hocken RJ, Trumper DL. *Prec. Eng.*,24(3):191209,2000.
- [7] Hocken R, Wang C. *Personal communication*, 2002.
- [8] Binnig G, Quate CF, Gerber Ch. *Phys Rev Lett*, 56(9):9303, 1986.
- [9] *Digital Instruments, Veeco Metrology Group. Scanning probe microscopy training notebook*, Ver. 3.0, 2000.
- [10] Newcomb CV, Flinn I. Improving the linearity of piezoelectric ceramic actuators *Electron Lett*, 18(11):4424,1982.
- [11] Kaizuka H. *Rev Sci Instrum*, 60(10):311922, 1989. [13] .
- [12] Jorgensen JF, Carneiro K, Madsen LL, Conradsen K *J Vac Sci Technol B*, 12(3):17024,1994.
- [13] Schitter G, Schimmer A. *IEEE Trans Control Syst Technol*, 12(3):44954,2004.
- [14] *AFM automated AFM/SPM for 200mm wafers: advanced scan system*. ,[http://www.parkafm.com/products/industrial/xe\\_200/description/scan systems/](http://www.parkafm.com/products/industrial/xe_200/description/scan_systems/)[accessed 14 January 2008].

- [15] Kwon J, Hong J, Kim YS, Lee DY, Lee K, Lee S *Rev Sci Instrum*, 74(10):437883, 2003.
- [16] Bhikkaji B, Ratnama M, Moheimani SOR. *Sens Actuators A*,135:70012,2007.
- [17] Dixson RG, Koning R, Fu J, Vorburger TV, Renegar TB *Proc SPIE*, 3998:3628,2000.
- [18] Jusko O, Zhao X,Wolff H,Wilkening G. *Rev Sci Instrum*, 65(8):25148,1994.

# Chapter 5

## Stability and reproducibility improvement of atomic force microscopy in liquid

### 5.1 Introduction

One of the main superiority of atomic force microscopy (AFM)<sup>1</sup> is a unique capability of scanning insulating samples, as well as conductive ones, in liquid with nano scale (atomic) resolution. This ability provides subnanometer studies on variety of mineral<sup>2-4</sup> and organic samples.<sup>5-11</sup> Metal surfaces are investigated typically by this system.<sup>13</sup> Traditionally for scanning such these materials in liquid with sub nanometer resolution contact mode AFM has been used in spite of its limitations in application range.<sup>2,6</sup>

For instance friction forces caused by probe tip made difficulties to image isolated molecules bound to substrate due to weak van der waals forces. Particularly operating AFM modes could provide true atomic resolution scanning is limited. Despite of its limitations contact modes support non periodic atomic scale features often averaged out in an obtained image.

Recently dynamic mode AFM achieved remarkable improvements in liquid environments. Atomic-scale measurements by dynamic-mode AFM have traditionally been performed only in vacuum using frequency modulation AFM (FM-AFM).<sup>14-16</sup>

In 2005, Fukuma et al. enabled operation of FM-AFM in liquid with true atomic resolution.<sup>3</sup> One of the main improvements of AFM was reduction of cantilever oscillation amplitude (A: peak-to-zero value) to less than 0.5 nm. Such small amplitudes improve operation sensitivity to a short range forces like friction and capillary which are playing the major roles to create an atomic scale contrasts.<sup>15,16</sup>

The efficiency of the small amplitude operation in both phase modulation and amplitude one was revealed.<sup>19,20</sup> Another technique supported high resolution imag-

ing proposed as bimodal AFM.<sup>21</sup> Bimodal AFM cantilever oscillates in two different frequencies simultaneously corresponding to the first and second vibration modes. This method creates two extra data sources of second mode amplitude and phase.

Second mode amplitude oscillation is normally fixed at small value so oscillation amplitude and phase images of the second vibration mode provide the atomic scale contrasts.<sup>10</sup> These operation technique advancements have significantly enhanced the spatial resolution of dynamic mode AFM. Additionally, recent developments of novel ultra thin cantilevers end in remarkable improvements in force sensitivity of dynamic mode AFM.<sup>9,22</sup>

So these two advancements, specific resolution and force sensitivity, seem enough to provide atomic resolution of dynamic mode AFM. However stability and reproducibility of these methods arent adequate for practical experiments.

The obtained scanning image contrast, usually changes overall one frame scan even when scanning applied over a standard sample like cleaved mica layer. Besides, atomic scale contrasts in one image is not repeated in another one necessarily.

Such these weaknesses like instabilities and uncertain reproducibility block systematic research on interfacial phenomena. These troubles derive from instability and poor reproducibility of the tip apex situations. A suitable solution method is a tip cleaning when scanning is done in vacuum for instance in FM-AFM by ion beam sputtering.

For liquid environment scanning, the condition is a little different somehow the cleaned tip should enter to an aqueous surface through the air so keeping the clean tip apex, during the oscillation, seems difficult. Previous studies demonstrate that surface treatment methods using plasma, UV/O<sub>3</sub>, piranha solution (mixture of sulfuric acid ( $H_2SO_4$ ) and hydrogen peroxide ( $H_2O_2$ ) to solve and clean organic contamination) are enhanced at least for nanoscale measurements.<sup>23-25</sup>

This research is going to propose an enhanced tip cleanliness and hydrophilicity effects on AFM measurements. However it couldnt generally conclude that these methods are also effective to atomic scale AFM measurements specially where atom to atom interactions predominantly play a major contributed role in image contrast.

The influence of various tip treatment methods, for sub nano scale scanning and force measurements in liquid environments, is investigated during the following research. The examined methods contain silicon (Si) coating, Ar plasma, Ar sputtering and UV/O<sub>3</sub> cleaning steps. The results show the best method from performance aspect in atomic scale AFM measurements.

Additionally the tip surface properties before and after treatments by X ray photoelectron spectroscopy (XPS) and contact angle measurements (CA) are compared and probed. The variety of methods with different performance and basis are

studied and the cleaning mechanism is clarified.

## 5.2 Experimental details

### 5.2.1 Tip treatment methods

In this study Si coating cantilever with backside Au layer coating (PPP-NCHAuD, Nanoworld) is used. The nominal cantilever spring constant ( $k$ ) is 42 N/m with typical resonance frequency and Q factor in liquid are 140 KHz and 8, respectively. The nominal tip apex radius ( $R_t$ ) is less than 8 nm. Silicon coating step is applied on the tip by dc sputter coater (K575XD, Emitech). Silicon deposited layer was set at 30 nm. This thickness is chosen to assure the tip completely covered and protected by silicon thin film. In Ar plasma cleaning step, plasma cleaner from Sanyu Electronics (SC-701) has been used. The examination shows that Ar plasma cleaning with ordinary operation conditions can seriously damage the cantilever surface. Thus, the bias voltage and the inlet gas pressure have been adjusted just as high as required for the plasma remaining. Also the cantilever is covered by tantalum (Ta) plate to suppress the electric field applied over its surface. These conditions make the cleaning damage negligible. In the Ar sputtering method, an ion source from SPECS (IQE 11/35) is applied by custom built vacuum chamber. In this operation the cantilever plays the substrate role placed in 5 cm distance of ion gun. The initial base pressure of chamber before sputtering was  $5 \times 10^{-6}$  pa. Ar gas was injected into the chamber to raise the pressure to  $1.3 \times 10^{-4}$  pa value. The sputtering operation was done for 5 min with acceleration voltage of 0.6 kV. In UV/O<sub>3</sub> cleaning step, UV/O<sub>3</sub> cleaner from BioForce Nanoscience (ProCleaner Plus) was used. The cantilever was placed on a piece of large quartz crystal processed in about 5 min. furthermore processing significantly results in a rise of tip radius ( $R_t$ ) as the following section discussed. After sputtering process, the cantilever immediately was immersed into water to discharge for a few seconds. This immersion avoided the cantilever contaminant absorption during the moving through the air. In previous studies,<sup>23,25-27</sup> tip treatment and cleaning methods was done by acidic solution of piranha which has a successful effect on organic contaminations. Prior experiments show that acidic solution can damage Au backside coating of the cantilever. Despite there must be an effective safe cleaning method to eliminate surface contamination, it didnt find in the preliminary experiments. So the following is going to compare some of the major dry processing operations have been used for tip treatments.

## 5.2.2 AFM measurements

In this study, nano scale measurements were done by custom-made FM-AFM with an ultra noise cantilever deflection sensor.<sup>28-30</sup> Also a commercially available AFM controller (ARC2, Asylum Research) was used for controlling the AFM and recording data. The cantilever was oscillated at its resonance frequency in an operating phase-locked loop (PLL) circuit (OC4, SPECS) which is also used for detecting frequency shifting ( $\Delta f$ ) of the cantilever resonance. The FM-AFM is a non contact operating mode of imaging performed with a constant frequency shifting ( $\Delta f$ ). To evaluate the effect of the tip treatments, atomic-scale imaging and force measurements on a cleaved mica surface in phosphate buffered saline (PBS) cleaning solution was examined. This model system generally has been used for demonstrating and comparing the ability of atomic resolution imaging in various dynamic mode AFM techniques.<sup>3,19,20</sup> To evaluate the reproducibility parameter, three experiments for each tip treatment methods with three new cantilevers for each of them, were performed. The following is going to describe the experimental procedure of one of these experiments. After tip treatment, the cleaned tip immediately immersed to an imaging solution. After a tip approach is applied on a cleaved mica surface, 10 frames imaging with typical conditions for atomic resolution FM-AFM imaging in liquid were taken with the following conditions: (scan size:  $8 \times 8 \text{ nm}^2$ , tip velocity: 223 nm/s, cantilever oscillation amplitude (A): 0.25 nm, frequency shift ( $\Delta f$ ): 800 Hz). After the imaging, 10 frequency shift curves for hydration force measurements were measured by FM-AFM with the following typical conditions. (Tip velocity: 1 nm/s, sample rate: 1 kHz, measurement bandwidth (B): 10 Hz, A: 0.1 nm). After collecting these curves, another 10 curves were drawn while amplitude range of changing was between 0.1 to 0.25 nm. This amplitude value in the same is used for the imaging so the measured  $\Delta f$  curves and its slope estimation made a tip-sample distance regulation during the imaging. During the imaging and force measurements all the parameters remains fix. Therefore, the obtained data may not be obtained with the optimal conditions. However, the data are definitely independent of operator's experimental expert.

## 5.2.3 Other evaluation methods

Scanning electron microscopy (SEM) imaging was operated with high resolution field emission SEM of Elionix (ERA-8000FE). The scanning acceleration voltage and working distance were set at 15 kV and 11 mm. it should be mention that the cantilevers imaged by SEM were not used for AFM measurements once again. Especially all the AFM experiments were done just after the tip cleaning methods

without any SEM imaging.

Additionally XPS measurements were operated by Sigma Probe (Thermo VG Scientific). This measurement instrument has the minimum beam spot diameter of  $15 \mu m$ , which is much larger than tip apex. The much larger beam spot diameter the simpler measurements. Hence the measurements on the cantilever base were done with a beam spot diameter of  $400 \mu m$ , which is the maximum size for this instrument. CA measurements were performed by DM-301 (Kyowa). The amount of  $2 \mu l$  milli-Q droplet water was used for the measurements. The results demonstrate that the surface area of the cantilever base is too small. Thus, the cantilevers integrated in a Si wafer have been chosen and purchased (PPP-NCHAuD-W, Nanoworld) and the measurements performed on the silicon wafer surface.

## 5.3 Results and Discussions

### 5.3.1 SEM imaging

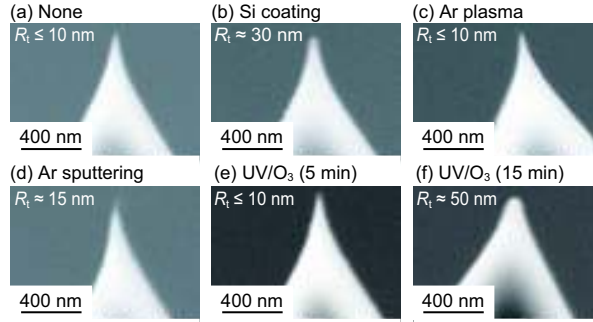


Figure 5.1: SEM images of the tips before and after the tip treatments.

Figure 5.1 shows images of tips comparison before and after treatments. The  $R_t$  smaller than  $10 \text{ nm}$  couldnt be estimated precisely because of the SEM resolution limitation. The SEM image in fig 5.1(a) reveals that  $R_t$  is less than  $10 \text{ nm}$  before the treatment. Tip sharpness was remained preserved even after Ar plasma and UV/O<sub>3</sub> cleaning as shown in figures 5.1(c) and (e), respectively. The silicon coating and argon sputtering made the tip radius rise to  $30 \text{ nm}$  (figure 5.1(b)) and  $15 \text{ nm}$  (figure 5.1(d)), respectively. This thickness raise may make difficulties for nanoscale measurements where surface nanoscale corrugations should be precisely measured. In contrary such slight increase of tip radius hardly effects on the atomic-scale image contrasts or short-range force profiles, which is supporting by the experimental data adding later. The experiment shows that a long term UV/O<sub>3</sub> cleaning makes a sharp rise in  $R_t$ . For example 15 min UV/O<sub>3</sub> cleaning, increases the  $R_t$  to  $50 \text{ nm}$  as

it shown in figure 5.1(f) which is much larger than its thickness after 5 min cleaning (figure 5.1(e)). This sharp change probably happen due to strong oxidation begins after 5 minutes UV irradiation. Because of this rapid change, the same Rt size reproduction seems difficult. To deal with this problem, and security of the tip thickness reproducibility, the cleaning time was set up to 5 min.

### 5.3.2 Atomic-resolution imaging

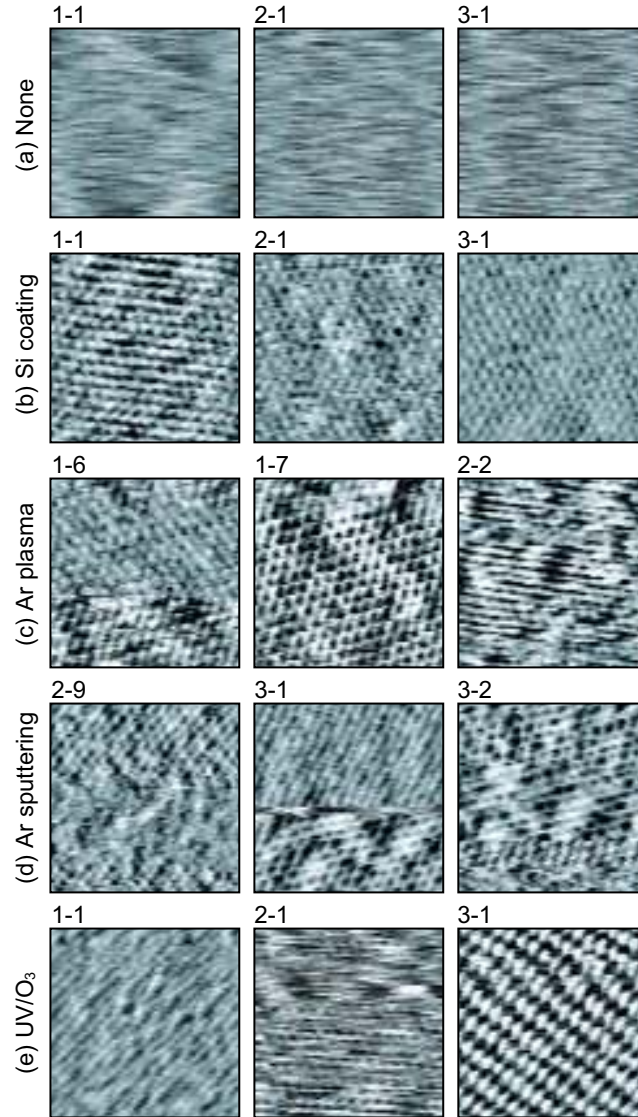


Figure 5.2: FM-AFM images of a cleaved mica surface obtained in PBS solution. (a) None. (b) Si coating. (c) Ar plasma. (d) Ar sputtering. (e) UV/O<sub>3</sub>. The numbers  $n$ - $m$  indicated in each image shows that the image corresponds to the  $m$ -th image obtained in the  $n$ -th experiment. Scan size:  $8 \times 8 \text{ nm}^2$ . Tip velocity: 223 nm/s.  $A = 0.25 \text{ nm}$ .  $\Delta f = 800 \text{ Hz}$ .

FM-AFM imaging of a cleaved mica surface in PBS solution with different tip

treatment methods was performed. As explained before for each tip treatment methods three experiments were done while 10 images were taken from each of them. Therefore, 150 images were obtained totally in this test). Figure 5.2 shows some of the example images randomly however, all of them are shown in figure 5.3.

Without a tip treatment, obtaining image with atomic resolution is hardly possible. (Figure 5.2(a)) In contrary, with every tip treatment methods, an atomic resolution image have been obtained from the first scan of the tip approaching. Since the apex of the as-purchased tip is covered by different contaminations, achieving atomic resolution imaging in liquid is impossible. These contaminations should be removed by tip treatment methods, to create an atomic resolution imaging. For the silicon coating method, the images always show a similar atomic-scale contrast. for example the first scan images of the three experiments show similar contrasts (figure 5.2(b)). However the images obtained by the other methods usually show a discontinuous contrast change due to tip altering (figure 5.2(c)-(e)). Additionally this is clear that, the atomic scale contrasts observed in one test are different from those in the other tests (figure 5.2(c)-(e)). The results significantly proved that the tip apex condition after treatments is not stable and reproducible. Thus, as an outcome, it could be suggested that, silicon coating supplies the best quality and reproducibility in an atomic-resolution imaging.

### 5.3.3 $\Delta f$ curve measurements

To study and probe the influence of the tip treatments on the force curve measurements, 10  $\Delta f$  curves with  $A0.1nm$  just after the 10 frame imaging were measured. This applied amplitude is a typical value for hydration force measurements. Since for each treatment methods, three experiments were done so 150 graphs achieved totally (figure 5.5).

Figure 5.4 shows the graphs obtained in one of the three experiments. The graphs obtained by tests without the tip treatment show the long range repulsive forces (figure 5.4(a)). The tip treatments before experiments discard the influence of long range interacting forces so visualize an oscillatory hydration force profile (figures 5.4(b)-(e)). The results demonstrates that tip apex contaminations produce long range repulsive forces which is prevent exact measurements of short range force interactions. This problem could be solved by each tip treatment approach of this research. By comparing the 10 curves achieved in one experiment (figure 5.4), some variations in the  $\Delta f$  profiles for each treatment methods were detectable. Such variations can be caused not only by the tip altering but also by its drifting so the atomic-scale site is dependent of the force profile. For the Ar plasma, Ar sputtering

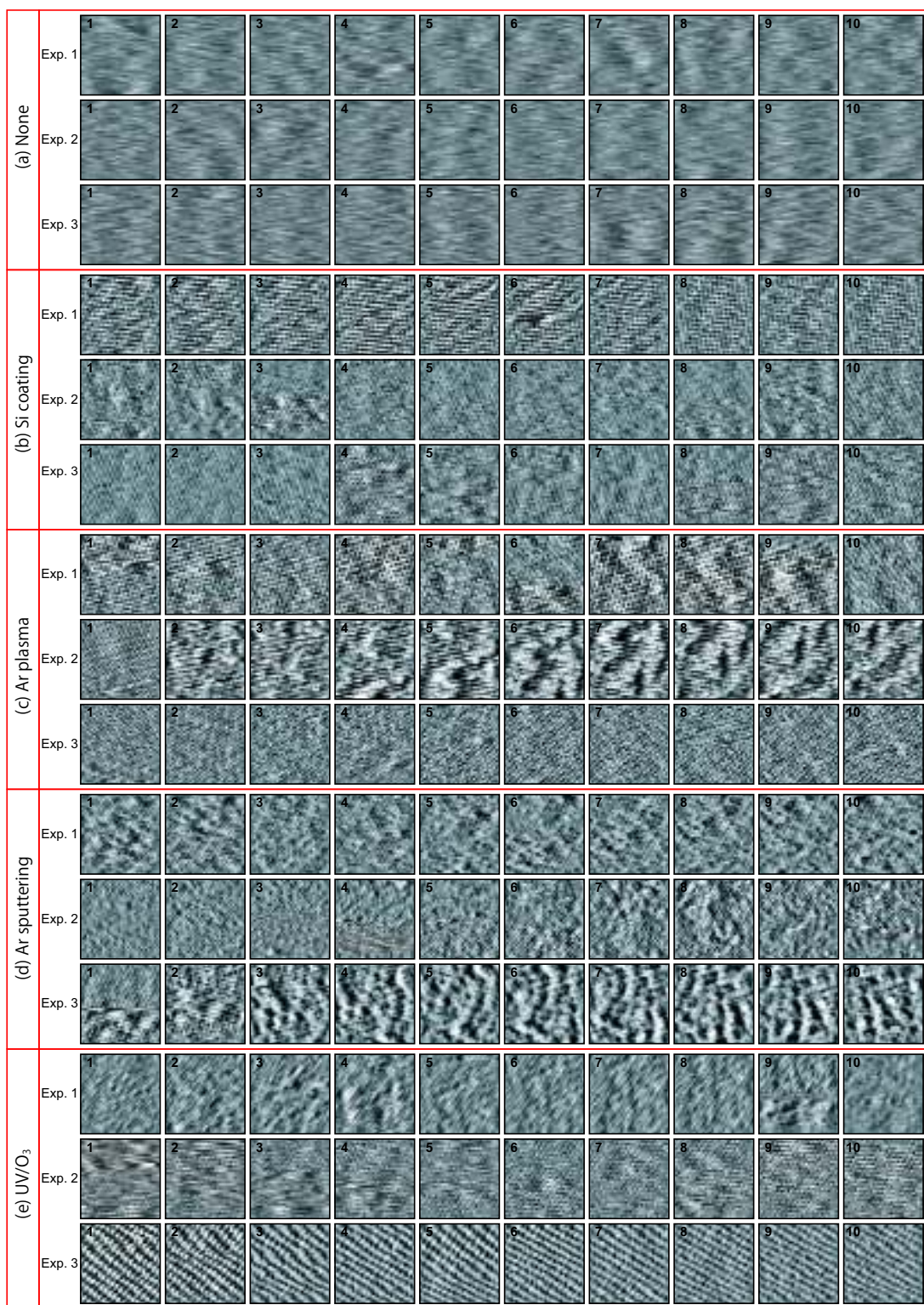


Figure 5.3: FM-AFM images of mica in PBS solution ( $8 \times 8 \text{ nm}^2, \Delta f = 800 \text{ Hz}, A = 0.25 \text{ nm}$ )

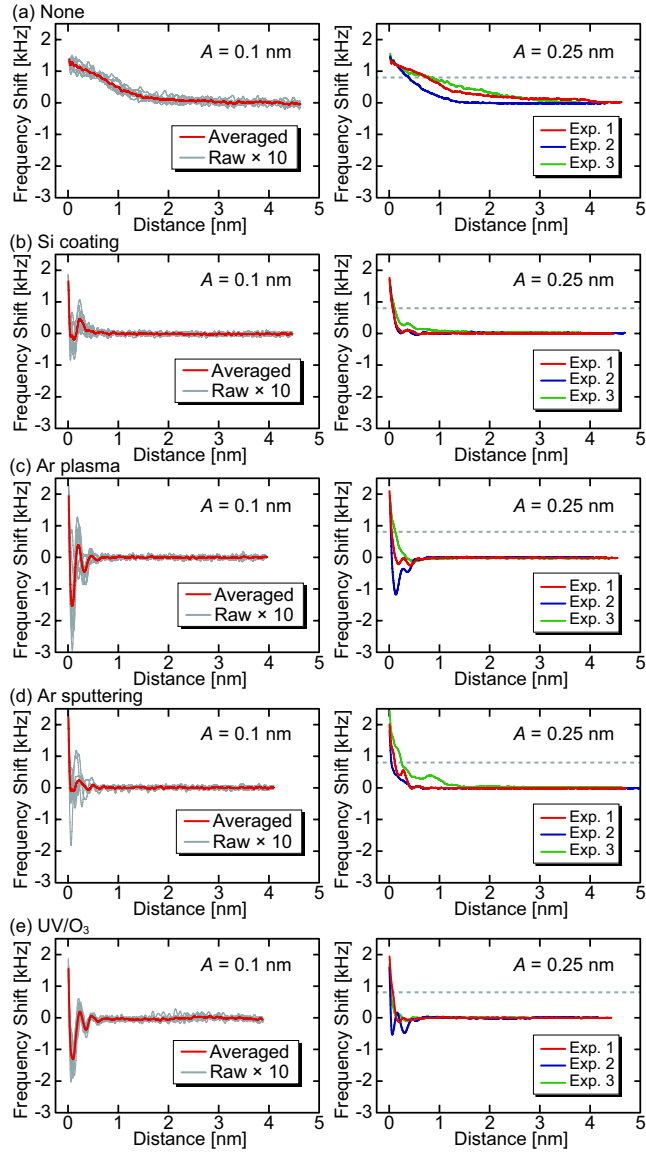


Figure 5.4:  $\Delta f$  versus distance curves measured on a cleaved mica surface in PBS solution. (a) None. (b) Si coating. (c) Ar plasma. (d) Ar sputtering. (e) UV/O<sub>3</sub>. Tip velocity: 1 nm/s. Sample rate: 1 kHz.  $B = 10$  Hz. For the curves obtained with  $A \approx 0.1$  nm, we show raw data of 10 curves and their average. For those obtained with  $A \approx 0.25$  nm, we show the averaged curves over 10 curves obtained in the individual experiment. The dotted lines indicate the  $\Delta f$  setpoint value used for the imaging experiments (figure 5.2).

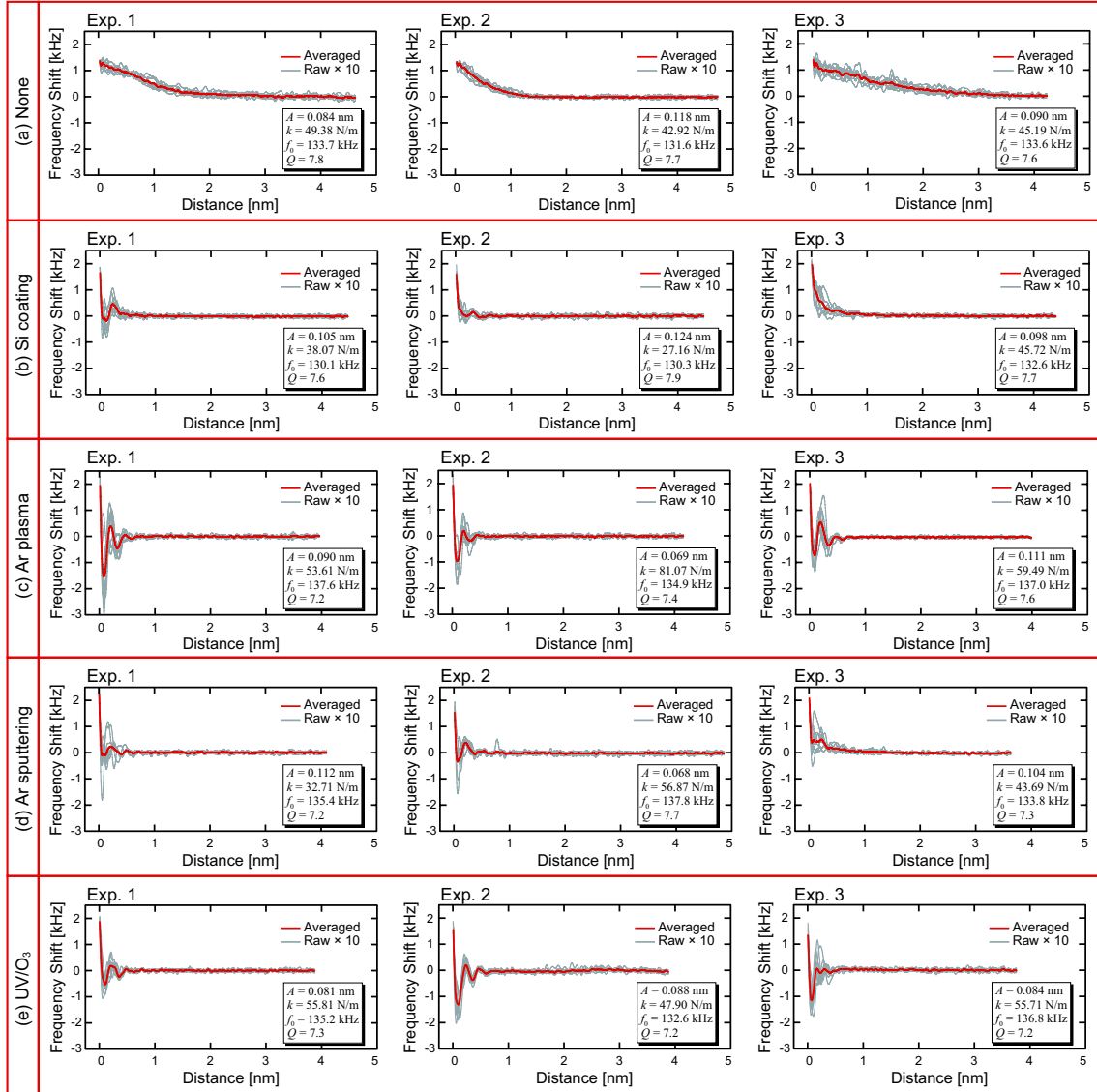


Figure 5.5:  $\Delta f$  versus distance curves measured in PBS solution ( $A_{0.1}$  nm). For each experiment, raw data of 10 curves is indicated by the gray lines while the average of them by the red line.

and UV/O<sub>3</sub> cleaning, the curves occasionally show a strong attractive force near the sample surface. Such an adhesion forces are barely seen in silicon coating tip curves. Another tip results show the similar behavior (figure 5.5). The adhesion forces make nanoscale scratch and change in tip geometry which can justify the contrasts altering during the scanning after the tip treatments (figure 5.2). To analyze the  $f$  profiles (figure 5.4) and the images relationship, 10  $f$  curves with  $A_0 : 25nm$  were measured. Applying amplitude is the same as used before for the imaging experiments (figure 5.2). As there are three experiments for each treatment, 150 curves obtained totally. (Figure 5.6).

The averages graphs are reached from the three different experiments are shown in figure 5.4. It could be declare that, in each tip treatment methods, the variation between 10 graphs of one experiment become more negligible by increasing the amplitude. (Figure 5.6). One of the probable reasons could justify this effect is sensitivity reduction to the short range force that is in charge for the atomic-scale site dependence of the force profile. Another probable reason is a raised restoring force ( $kA$ ) which may prevent an atomic scale tip crash caused by the strong attractive force near the surface. The averaged curved achieved by three different experiments are clearly varies except those achieved by silicon coating tips (Figure 5.4). Therefore the results demonstrate that silicon coating in tip treatments has a significant positive effect in reproducibility of force curve measurements. This conclusion is consistent with the one obtained by the imaging experiments.

Table 5.1: The slopes [kHz/nm] of the  $\Delta f$  versus distance curves shown in figure 5.4 ( $A \approx 0.25$  nm) at  $\Delta f = 800$  Hz. This  $\Delta f$  corresponds to the setpoint used for the tip-sample distance regulation during the imaging. The error range corresponds to the standard deviation of the slope values.

Exp.	None	Si coating	Ar plasma	Ar sputtering	UV/O <sub>3</sub>
1	-0.76±0.19	-13.7±3.42	-22.6±11.9	-13.3±3.7	-59.3±16.9
2	-1.53±0.25	-11.1±1.32	-53.1±16.4	-17.7±10.3	-14.3±3.3
3	-0.98±0.67	-7.67±1.48	-10.7±2.29	-10.0±3.9	-40.1±21.4

To declare a quantitative discussion on the relationship between the imaging and the  $\Delta f$  curves, the slope of the  $\Delta f$  curves at  $\Delta f = 800$  Hz (the dotted lines in figure 5.4) were analyzed. The tip-sample distance regulation normally occurs at repulsive force term of the  $\Delta f$  curves. Thus, the graphs incline around the  $\Delta f$  setpoint (800 Hz in this experiment) critically effects on the vertical resolution ( $\delta z$ ) obtained in the scanning. Table 5.1 proposes an average and standard deviation (SD) of the slope values briefly. The results show that the curve incline without tip treatment is one order of magnitude smaller than those values with the tip treatment methods.

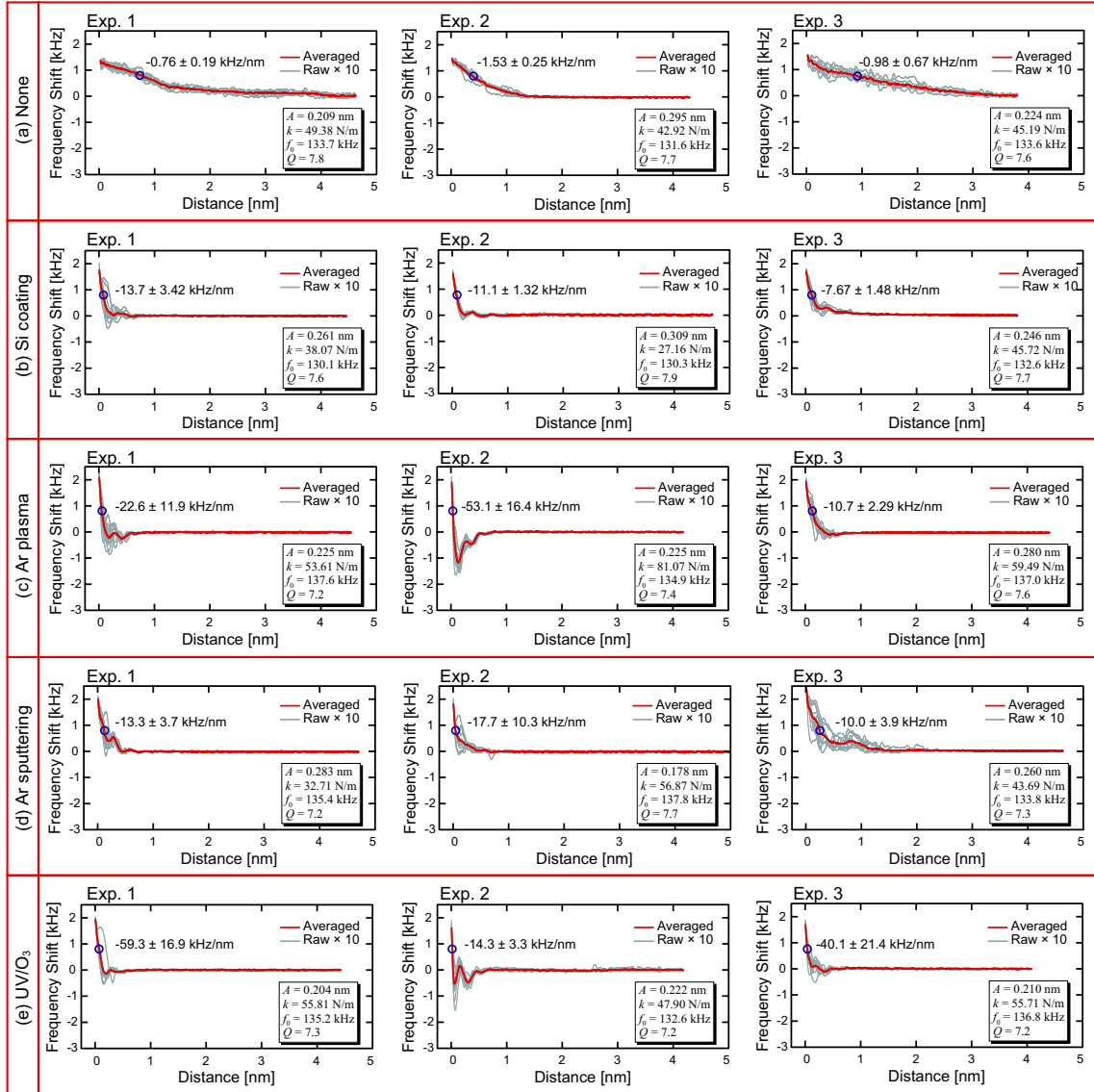


Figure 5.6:  $\Delta f$  versus distance curves measured in PBS solution ( $A$  0.25 nm). For each experiment, raw data of 10 curves is indicated by the gray lines while the average of them by the red line. The blue circles are indicated at  $\Delta f = 800$  Hz, which correspond to the set point value used for the imaging experiments

The  $\Delta f$  noise ( $\delta f$ ) is determined by the thermal vibration of a cantilever is given by<sup>14</sup>

$$\delta f = \sqrt{\frac{k_B T f_0 B}{\pi k Q A^2}}, \quad (5.1)$$

where  $k_B$  and  $T$  denote Boltzmann's constant and temperature, respectively.

The experimental conditions applied in this study are  $\delta f = 30$  Hz at  $B = 100$  Hz. By assuming the constant incline of  $|\partial(\Delta f)/\partial z|$ ,  $\delta z$  is given by:

$$\delta z = \frac{\delta f}{|\partial(\Delta f)/\partial z|}. \quad (5.2)$$

Exact atomic resolution AFM scanning normally needs  $\delta z$  of  $\sim 10$  pm. to satisfy this condition the  $\Delta f$  curve incline should be more than 3 kHz/nm. Based on the table 1 data, the incline values refer to methods without tip treatments are always smaller than this value while the incline values of tip treatment methods are larger than it. These results are the same as concluded by imaging experiments (figure 5.2). A long-range repulsive force measured in liquid is often explained by an electric double layer force.<sup>31</sup> Since in this case the PBS solution containing 150 mM NaCl is used, it is not probably convincingly. The  $\Delta f$  curves refer to methods without tip treatments show much noises than those achieved by tip treatments even from far tip position. (Figure 5.4). This is reproducible with different tips (Figures 5.5 and 5.6). Since the cantilever is the same type for all the experiments,  $\Delta f$  curves noise could not be happened due to the thermal vibration of cantilever. The results declare that the tip contaminated by thin film of soft contaminant so its fluctuation and deformation leads to a rise of a long-range repulsive force. The average slope values obtained by the silicon coating tip show the lower variation than the others (Table 5.1). This is also true for the slope values SD. These results are also proved silicon coating method supplies the best reproducibility and stability in the force curve measurements.

### 5.3.4 Origin of the fouling resistance

The results achieved by the imaging and the force curve measurements propose influence study of the tip cleaning stability through the air transfer. To recognize the base of the fouling resistance, XPS measurements on the cantilever base before and after the tip treatments were done. From the achieved wide-range XPS spectra (figure 5.7), compositional surface ratio is estimated (Table 5.2) The c content is significantly decreased however it isn't totally eliminate by the tip treatments. The results demonstrate that, although hydrocarbon compounds removed by the

Table 5.2: Compositional ratio (Unit: %) of the cantilever base surface before and after the tip treatments estimated from the wide-range XPS spectra (figure 5.7).

Element	None	Si coating	Ar plasma	Ar sputtering	UV/O <sub>3</sub>
C	31	11	17	8	8
O	27	36	50	47	47
Si	40	52	28	44	43
Others	2	1	5	1	2

first cleaning process, these contaminations adsorbed on the surface during the tip transfer process. In the meanwhile, the O content is significantly raised by the tip treatments. As the results show, silicon surface is oxidized by tip treatments which is improve hydrophilicity surface effect.

According to these results, a model to explain the origin of the fouling resistance is suggested (Figure 5.8). Before the tip treatments, the tip surface is covered by an organic molecule contaminant (figure 5.8(a)). Thus, the surface should be almost hydrophobic. After the tip treatments the hydrophobic film eliminated from the tip and the surface begins to oxidize and enhance hidrophilicity effect so the tip should be wet by water even during the tip transfer through the air (figure 5.8(b)). Although he high affinity to water molecules probably decrease organic contaminant adsorption, it couldnt totally prevent them. When the tip immersed to aqueous environments, the hydrophobic affect of unsaturated surface leads to the strong stable hydration bonds at the interface. This fact ends in the reject of adsorbed organic molecules. The influence of the tip treatments during transfer through the air is explained by this model.

### 5.3.5 Origin of the improved stability and reproducibility

Silicon coating tips show the best stability and reproducibility in both the imaging and force measurements than the other methods. To discover the main basis of this excellence, Si2p XPS spectra were analyzed on a cantilever base before and after tip treatment methods (Figure 5.9). Si2p spectra show different peak positions depending on the Si oxidation state ( $n_{Si}$ ) as indicated by the dotted lines in figure 5.9. Before the tip treatments, the spectrum shows two peaks at  $n_{Si} = 0$  and 3–4. So the siface silicon atoms are mostly fully oxidized to become SiO<sub>2</sub>. Based on the literature,<sup>23,32–34</sup> the tip contaminant compounds typically come from poly(dimethylsiloxane) (PDMS) which is found in cantilever storage boxes. Since the surface is covered by contamination film, some of the Si2p signals probably come from Si atoms of adsorbed PDMS fragments. After the silicon coating, the spectrum

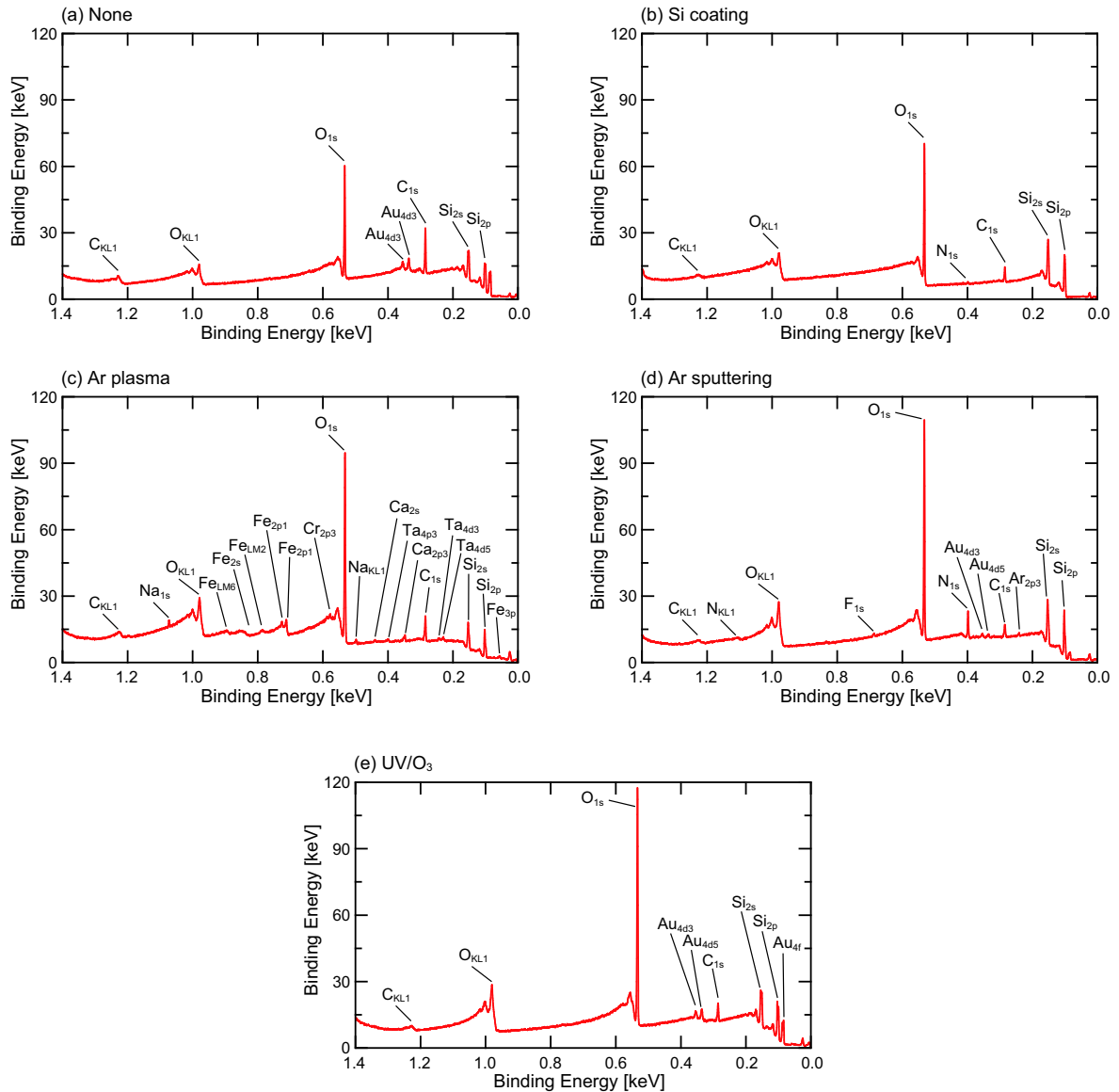


Figure 5.7: Wide-range XPS spectra measured on a cantilever base

shows a broad peak at  $n_{Si} = 1-3$ . So the surface Si atoms are partially oxidized. For AFM experiments, the tip is immersed in an aqueous solution so an unsaturated surface must be fully oxidized at last. In contrary, those obtained by the other treatment methods show two peaks at  $n_{Si} = 0$  and 4. In these cases silicon atoms are fully oxidized by dry process. So it is concluded that surface oxidation states is notably independent of aqueous solution immersion.

To satisfy the previous claim, CA measurements on a Si wafer with and without surface treatments were done (figure 5.10). The measurements were done before and after 10 min pure water immersion of the Si wafer. Without a tip treatments, the surface shows a large CA ( $88^\circ$ ) declaring its high hydrophilicity effect. The CA

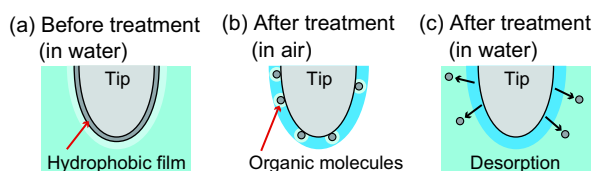


Figure 5.8: Schematic models to explain the origin of the fouling resistance of the cleaned tip surface.

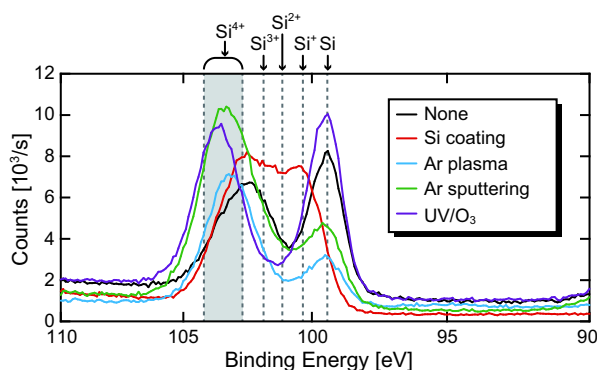


Figure 5.9: Si2p XPS spectra measured on a cantilever base before and after the tip treatments.

parameter doesn't change significantly by water immersion. So the results prove that the surface is contaminated by a hydrophobic film before the tip treatment. (Figure 5.10(a)). After silicon coating the surface shows almost high CA ( $60.9^\circ$ ) however this value is remarkably decreased to  $31.5^\circ$  by water immersion. In the meanwhile, the surface processed by the other methods show a smaller CA changing. These results satisfy this claim that the surface is oxidized by the wet process in Si coating while it is oxidized by the dry one in the other methods.

It is concluded that Si surface oxidized by a wet process provides a better quality stability and reproducibility in the atomic-scale AFM measurements than the ones oxidized by the dry process. One of the possible models can declare this variation is proposed (figure 5.11). According to the previous infrared spectroscopy research,<sup>35</sup> a wet oxidation of surface Si atoms occurs in an aqueous solution of H and OH ions come from water dissociative adsorption (figure 5.11(a)). This should create local spots where strong hydration bonds formed thus the hydration bonds under the tip apex seems hopefully stable. In contrary, the dry oxidation mechanism is not consisting of any active mechanism. This surface are mostly contains SiO<sub>2</sub> compounds without any strong hydration sites under the tip apex. (Figure 5.11(b)). This difference can satisfy the instabilities and poor reproducibility of the atomic-scale AFM measurements. The PBS solution used in this study consist of various ions such as

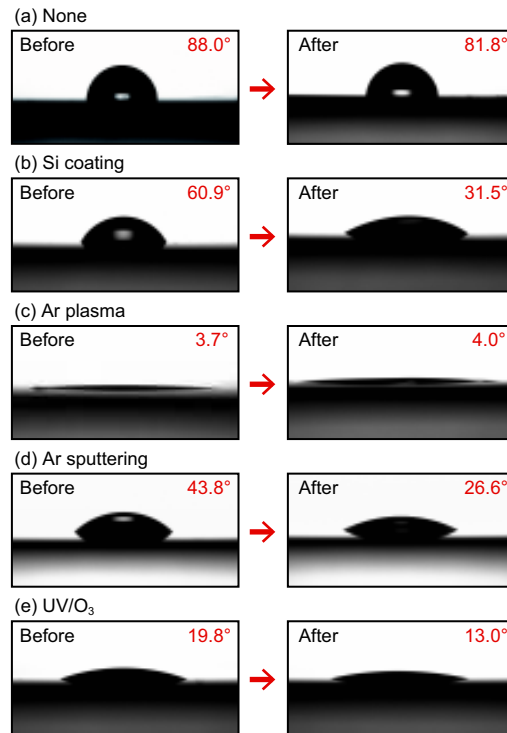


Figure 5.10: CAs of a  $2 \mu\text{l}$  water droplet on a Si wafer with and without the surface treatments. (a) None. (b) Si coating. (c) Ar plasma. (d) Ar sputtering. (e) UV/O<sub>3</sub>. Measurements were performed before and after 10 min immersion of the wafer in pure water.

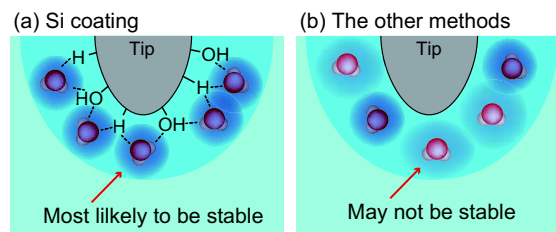


Figure 5.11: Schematic models showing hydration structures formed on a tip prepared by (a) the Si coating and (b) the other methods.

$Na^+$ ,  $K^+$ ,  $Cl^-$  and  $PO_4^{3-}$  These ions probably effect on the imaging resolution and stability. Actually getting a high resolution image of three-dimensional hydration structures in water is much tougher than the same imaging in electrolyte solution. This indicates that strong hydration bonds both on the tip and sample surface may be fixed. In this case, a satisfied explanation of the stabilization mechanism couldnt propose. Detailed explained of ion influence should need another systematic study AFM resolution and stability in variety of solutions. In this research the experiments in an aqueous solution is investigated. At last the best stable AFM measurements require not only stable tip structures but also stable hydration structures on the tip apex proposed. As this conclusion seems reasonable even by putting solvation” instead of hydration, the similar discussion probably can be made for AFM measurements in other solutions. Obviously the influence intensity of the tip treatment methods should be significantly dependent on the solvent and the tip chemistry. Additionally, it may be more difficult to discard the tip contaminations during the air transferring as the solvent molecules are not generally contained in ambient air. Silicon coating have been used normally. More stable tip could tolerate for more than typical experimental time (about 3 to 5 hours) is proposed. Thus the stability seems sufficient for most applications. One of the main parameter enhanced this ability is chemical functionalization of the tip apex which may be one of the bright ways to create strong stable hydration sites. Since in this case, the tip apex must have a nanoscale protrusion such as single molecule supported by adjacent ones. If an applicable reproducibility approach of such a tip found, it may satisfy the better stability than the current method.

## 5.4 Summary

In recent years, one of the main major improvements of Atomic force microscopy in aqueous environments has been achieving high atomic scale resolution in various interfacial phenomena studies. During these analysis, instabilities and poor data reproducibility made systematic studies impossible. To solve this problem, the effect of various tip treatment methods for atomic scale imaging and force measurements in liquid environments have been investigated during the following research. The tested methods, examined in Si coating, Ar plasma, Ar sputtering and UV/O3 cleaning tips. The experiments demonstrated that, all of these methods provide remarkable progress in both the imaging and force measurement even though the tip oscillates through the air. Among these methods silicon coating tips provide the best stability and reproducibility in the measurements. To recognize anti-fouling effect basis of the cleaned tip surface and the comparison of different cleaning meth-

ods, the tip surface characteristics have been investigated by x-ray photoelectron spectroscopy and contact angle measurements. The results show that the contaminations adsorbed on the tip during oscillation through the air should be discarded from the tip surface by aqueous solution immersion which is because of the enhanced hydrophilicity by the tip treatments. The prepared silicon coated tip is oxidized by aqueous solution immersion and water absorption. This oxidation creates local spots where stable hydration structures are formed. In other methods there is no active mechanism to create these local hydration sites. Basically these hydration structures are not steady under the tip apex. These results demonstrate the desirable tip characteristics atomic scale AFM in aqueous measurements creates a new guideline for further improvements of the tip treatment methods.

# Bibliography

- [1] G. Binnig, C. F. Quate, and Ch. Gerber. *Phys. Rev. Lett.*, 56:930, 1986.
- [2] F. Ohnesorge and G. Binnig. *Science*, 260:1451, 1993.
- [3] T. Fukuma, K. Kobayashi, K. Matsushige, and H. Yamada. *Appl. Phys. Lett.*, 87:034101, 2005.
- [4] B. W. Hoogenboom, H. J. Hug, Y. Pellmont, S. Martin, P. L. T. M. Frederix, D. Fotiadis, and A. Engel. *Appl. Phys. Lett.*, 88:193109, 2006.
- [5] K. Suzuki, N. Oyabu, K. Kobayashi, K. Matsushige, and H. Yamada. *Appl. Phys. Express*, 4:125102, 2011.
- [6] D. J. Muller, F. A. Schabert, G. Buldt, and A. Engel. 68:1681, 1995.
- [7] K. H. Sheikh and S. P. Jarvis. *J. Am. Chem. Soc.*, 133:18296, 2011.
- [8] H. Asakawa, S. Yoshioka, K. Nishimura, and T. Fukuma. *ACS NANO*, 6:9013, 2012.
- [9] C. Leung, A. Bestembayeva, R. Thorogate, J. Stinson, A. Pyne, C. Marcovich, J. Yang, U. Drechsler, M. Despont, T. Jankowski, M. Tschope, and B. W. Hoogenboom. *Nano Lett.*, 12:3846, 2012.
- [10] E. T. Herruzo, H. Asakawa, T. Fukuma, and R. Garcia. *Nanoscale*, 5:2678, 2013.
- [11] S. Ido, K. Kimura, N. Oyabu, K. Kobayashi, M. Tsukada, K. Matsushige, and H. Yamada. *ACS NANO*, 7:1817, 2013.
- [12] S. Ido, H. Kimiya, K. Kobayashi, H. Kominami, K. Matsushige, and H. Yamada. *Nat. Mater.*, 13:264, 2014.
- [13] F. Hausen, J. A. Zimmet, and R. Bennewitz. *Surf. Sci.*, 607:20, 2013.
- [14] T. R. Albrecht, P. Grutter, D. Horne, and D. Ruger. *J. Appl. Phys.*, 69:668, 1991.

- [15] S. Morita, R. Wiesendanger, and E. Meyer, editors. *Noncontact Atomic Force Microscopy(Nanoscience and Technology)*, Springer Verlag, 2002.
- [16] F. J. Giessibl. *Rev. Mod. Phys.*, 75:949, 2003.
- [17] F. J. Giessibl, H. Bielefeldt, S. Hembacher, and J. Mannhart. *Appl. Surf. Sci.*, 140:352, 1999.
- [18] F. J. Giessibl. *Appl. Phys. Lett.*, 76:1470, 2000.
- [19] T. Fukuma, J. I. Kilpatrick, and S. P. Jarvis. *Rev. Sci. Instrum.*,77:123703, 2006.
- [20] K. Votchovsky, J. J. Kuna, S. A. Contera, E. Tosatti, and F. Stellacci. *Nat. Nanotech.*, 5:401, 2010.
- [21] T. R. Roderiguez and R. Garcia. *Appl. Phys. Lett.*, 84:449, 2004.
- [22] T. Fukuma, K. Onishi, N. Kobayashi, A. Matsuki, and H. Asakawa. *Nanotechnology*, 23:135706, 2012.
- [23] L. Sirghi, O. Kylin, D. Gilliland, G. Ceccone, and F. Rossi. *J. Phys. Chem. B*, 110:25975, 2006.
- [24] M. Fujihira, Y. Okabe, Y. Tani, M. Furugori, and U. Akiba. *Ultramicroscopy*, 82:181, 2000.
- [25] X. Feng, B. D. Kieviet, J. Song, P. M. Schn, and G. J. Vancso. *Appl. Surf. Sci.*, 292:107, 2014.
- [26] S. Patil, G. Matei, A. Oral, and P. M. Hoffmann. *Langmuir*, 22:6485, 2006.
- [27] S. H. Khan, G. Matei, S. Patil, and P. M. Hoffmann. *Phys. Rev. Lett.*, 105:106101, 2010.
- [28] T. Fukuma, M. Kimura, K. Kobayashi, K. Matsushige, and H. Yamada. *Rev. Sci. Instrum.*, 76:053704, 2005.
- [29] T. Fukuma and S. P. Jarvis. *Rev. Sci. Instrum.*, 77:043701, 2006.
- [30] T. Fukuma. *Rev. Sci. Instrum.*, 80:023707, 2009.
- [31] D. J. Muller, D. Fotiadis, S. Scheuring, S. A. Muller, and A. Engel., 76:1101, 1999.

- [32] Y.-S. Lo, N. D. Huefner, W. S. Chan, P. Dryden, B. Hagenhoff, and Jr. T. P. Beebe. *Langmuir*, 15:6522, 1999.
- [33] E. Bonaccorso and G. Gillies. *Langmuir*, 20:11824, 2004.
- [34] B. M. Borkent, F. Mugele S. Beer, and D. Lohse. *Langmuir*, 26:260, 2009.
- [35] Y. Enta, D. Shoji, M. Shinohara, M. Suemitsu, M. Niwano, N. Miyamoto, Y. Azuma, and H. Kato. *Jpn. J. Appl. Phys.*, 38S1:253, 1999.

# Chapter 6

## Conclusions

Nanotechnology plays important roles in our life in everything ranging from clothes to medicine. There are lots of things that benefits our life based on the possibilities of nanotechnology. So, to have enough information about nano world, we need to have equipment with ability of displaying in nano scale. Nanotechnology and nanoengineering needs detection, visualization, calibration and manipulation in molecular scale. For this purpose, we need accurate microscope. In first section of this research ,I introduces different kind of accurate microscopy methods with those advantage and disadvantage shortly. Atomic force microscopy (AFM) is one of the representative nano scale and nondestructive imaging tools. AFM can be operated in liquid as well as in air and vacuum. It can be used to image wide range of materials from insulating materials to conductive ones. Owing of these unique capabilities, AFM has been used for various applications and considered to be suitable for direct imaging of interfacial phenomena with nano scale resolution. Imaging of dynamic process at solid/liquid interfaces requires high-speed operation of AFM. Although researchers made lots of efforts in this regards and developed the components, but still it needs more punctuation. In first part of this study, I develop a high-speed  $Z$  tip scanner.  $Z$  tip scanner is one of the most important components of the AFM in high-speed imaging. I propose high-speed  $Z$  tip scanner with precisely machined cantilever holding mechanism.

In this study, we have compared the performance of high-speed  $Z$  tip scanners with a screw cantilever holding mechanism. The investigated designs are different in the actuator size and the screw arrangement. I have investigated frequency responses and vibration modes of these scanners by FEA. The results reveal that the vertical screw arrangement with a larger actuator should give the best performance. Based on this design, I have developed a  $Z$  tip scanner

and measured its performance. The frequency response of the developed scanner shows a broad peak from 40 kHz to 130 kHz as expected from the FEA results. The frequency response of the tip-sample distance regulation shows  $-3$  dB bandwidth of  $\sim 6$  kHz. Finally, we have demonstrated high-speed atomic-resolution imaging of calcite crystal dissolution process using the developed scanner. The result shows that the developed scanner is applicable to atomic-resolution imaging at a few seconds per frame in liquid. In addition, I found more development by proposing the counterbalance mechanism as a  $Z$  tip scanner. The simulation results show that we can get better results with using of this  $Z$  tip scanner. On the other hand, during the imaging some phenomena such as creeping, non-linearity of the mechanical and electrical components and hysteresis may affect accuracy of the AFM. In fact, there are not enough researches in this regards. So, I aim to find solution to this problem. By having a wide research and checking the possible ways, I found that I can use crystal oscillator as a part of capacitive sensor to detect amount of unwanted displacement. I introduced capacitive sensor system and still working on it to develop and use in XY scanner. In addition, sometimes during the one image we may lose atomic-scale contrasts or with the same condition cannot get atomic-resolution images. It means that our imaging is not under stable and reproducible conditions. One of the main reasons for it is tip conditions. Tip may have some contaminations on its surface. It may have also chemical or mechanical instabilities. So, I was focused on the improvement of the stability of AFM as a next task. I worked on the tip preparation process to have stable and reproducible imaging. This work opens a view of systematic study in this regards. In this research, the influence of various tip treatment methods in an atomic scale AFM scanning and force measurements are probed in aqueous environments. To discover the relationship between AFM measurements and surface characteristics, XPS and CA measurements before and after the tip treatments were performed in several conditional situations. The following is going to sum up the obtained major results. Although the tips transfer through the air, all the treatment methods significantly enhanced both imaging and force measurements. The tip treatment methods, besides surface contaminant elimination, improved hydrophilicity influence by surface oxidation. In spite of organic contaminants adsorbed on the tip through the air transferring, they distracted from the surface by being immersed to a hydrophobic aqueous environments. This unsaturated surface oxidation in aqueous environments enhanced the tip treatment quality, stability and reproducibility. Among all of tested methods silicon coated tip supplies the best stability and reproducibility in the atomic-scale AFM measurements.

The silicon coating tip surface is fully oxidized by solution immersion. Wet oxidation creates local spots of hydration bonds strongly formed under the tip apex. However in other methods, there is no hydration site or active chemical mechanism to support tip stability. So unexpectedly hydration sites under the tip apex are not stable. The desirable tip properties for atomic scale AFM measurements in liquid environments are proposed. First and foremost, the tip should have hydrophobic characteristics to remain clean during air transfer. Secondly the tip and environment chemical structure could improve the system stability supported by strong hydration bonding during measurements. Though silicon coating tip is proposed and tested as the best choice among the others, there may be other applicable methods with more stability and performance. The desirable tip properties discovered in this study should serve as a guideline to further efforts on enhanced tip treatment methods. The improved stability and reproducibility clearly advanced atomic studies of interfacial phenomena with AFM measurements.

In conclusion, the proposed Z tip scanner significantly improves imaging speed with true atomic resolution. Moreover, I introduced displacement sensor to advance the accuracy of the AFM. Furthermore, study on the tip preparation process provides a guideline for future improvement of the stability and reproducibility in AFM measurements.

## List of Acronyms

AFM	atomic force microscopy
AM	amplitude modulation
PLL	phase-locked loop
SPM	scanning probe microscopy
STM	scanning tunneling microscopy
XPS	X-ray photoelectron spectroscopy
FM	frequency modulation
TEM	transmission electron microscopy
SEM	scanning tunneling microscopy
CNT	carbon nanotubes
SWNT	single wall nanotubes
MWNT	multi walled nanotubes
LL-AFM	Light lever sensors atomic force microscopy
MEMS	micro electro mechanical system
LFM	lateral force microscopy
HVAMP	high voltage amplifier
FEA	finite element analysis
PBS	Phosphate Buffer Saline
CA	contact angle
SD	standard deviation

## Publications

1. S.M.R. Akrami, H. Nakayachi, T. Watanabe-Nakayama, H. Asakawa and T. Fukuma, "Significant improvements in stability and reproducibility of atomic-scale atomic force microscopy in liquid ", *Nanotechnology*, 25 (2014) 455701 (8pp).
2. S.M.R. Akrami, K. Miyata, H. Asakawa and T. Fukuma, "High-Speed Atomic Force Microscopy with Atomic-Scale Resolution Using Separate-Type XY and Z Scanners with Screw Cantilever Holding Mechanism ", *Proceedings of the 5<sup>th</sup> International Conference on Nanostructures (ICNS5)*, EPP065,962-964(3pp).
3. S.M.R. Akrami, K. Miyata, H. Asakawa and T. Fukuma, "High-speed Z tip scanner with screw cantilever holding mechanism for atomic-resolution atomic force microscopy in liquid ", *Review of scientific Instruments*.....(3pp).

## Presentation

1. S.M.R. Akrami, K. Miyata, H. Asakawa and T. Fukuma, "High-speed Z Tip Scanner with Screw Cantilever Holding Mechanism in atomic force microscopy", The 21<sup>st</sup> International Colloquium on Scanning Probe Microscopy, Tsukuba, Japan (November, 2013).
2. S.M.R. Akrami, K. Miyata, H. Asakawa and T. Fukuma, "High-Speed Atomic Force Microscopy with Atomic-Scale Resolution Using Separate-Type XY and Z Scanners with Screw Cantilever Holding Mechanism", The 5<sup>th</sup> International Conference on Nanostructures, Kish Island, Iran (March, 2014).
3. S.M.R. Akrami, H. Asakawa and T. Fukuma, "High-speed Z Tip Scanner with Screw Cantilever Holding Mechanism for Atomic-resolution Atomic Force Microscopy in Liquid", The 17<sup>th</sup> International Conference on non-contact Atomic Force Microscopy, Tsukuba, Japan (August, 2014).

## Acknowledgment

None other than my advisor, Professor Takeshi Fukuma, can top the list of people I would like to take the opportunity here to thank. He accepted me into his environment and guided me through with his unlimited patience and energy. His support, guidance, and advice have been invaluable and deserve a special recognition. Thank you for your continuous support and advice throughout the past years. It has been an extremely educational and rewarding experience. I have enjoyed the enthusiasm and energy that you have brought towards all aspects of my life at Kanazawa University. I have enjoyed working with you tremendously and I hope we will continue to do so for years to come.

I am also very grateful to my dear professor in the Bio Nano AFM laboratory; Dr. Asakawa. It has been a privilege to have him participated in this important part of my life's work. You have been sources of inspiration and support in various stages of my dissertation. Without your suggestions, timely advice, and comprehensive understanding of various aspects of my problems, my work would not have taken this shape and direction. I would like also to thank committee members of this dissertation: Prof. Takeshi Fukuma, Prof. Shigeru Yamamoto, Prof. Kenji Satou, Prof. Norio Tokuda and Prof. Noriyuki Kodera from Kanazawa University for their critical reading and helpful argue.

Thanks are also to Iranian Ministry of Science and technology for providing the financial support during my study in Kanazawa University. My admiration and gratitude go out to my family for supporting my study and encouragement throughout my life. I am grateful for their unfailing love and support that has been very rewarding. I attribute my success to their reassuring love and sacrifice. Thanks are also to Professor Masakatsu Miyajima and Dr. Abdolhossein Fallahi for introducing me to Professor Fukuma and supporting me during my studies in Kanazawa University.